Ore Geology Reviews 88 (2017) 565–618

Contents lists available at ScienceDirect

Ore Geology Reviews

journal homepage: www.elsevier.com/locate/oregeo

Gold mineralization in the Jiangnan Orogenic Belt of South China: Geological, geochemical and geochronological characteristics, ore deposit-type and geodynamic setting

Deru Xu [a,b,*], Teng Deng [a,b,c], Guoxiang Chi [b], Zhilin Wang [d], Fenghui Zou [a,c], Junling Zhang [a], Shaohao Zou [a,c]

[a] Key Laboratory of Mineral and Metallogeny, Guangzhou Institute of Geochemistry, Chinese Academy of Sciences, Guangzhou 510640, China
[b] Department of Geology, University of Regina, Regina S4S 0A2, Canada
[c] University of Chinese Academy of Sciences, Beijing 10049, China
[d] Key Laboratory of Metallogenic Prediction of Nonferrous Metals and Geological Environment Monitoring, Ministry of Education, School of Geosciences and Info-Physics, Central South University, Changsha 410083, China

ARTICLE INFO

Article history:
Received 26 June 2016
Received in revised form 3 February 2017
Accepted 6 February 2017
Available online 12 February 2017

Keywords:
Au (-polymetallic) deposits
Jiangnan Orogenic Belt (JOB)
Basin-and-Range like province
Intracontinental reactivation-type
South China

ABSTRACT

Located in the southeastern margin of the Yangtze Block and generally interpreted as the Neoproterozoic collisional product of the Yangtze with the Cathaysia Blocks of South China, the Jiangnan Orogenic Belt (JOB) contains a number of gold (Au) (-polymetallic) ore deposits and mineral showings, mostly hosted by Neoproterozoic low-grade metamorphic volcaniclastic and sedimentary rocks. The mineralization styles mainly include auriferous quartz veins and disseminated mineralization in altered mylonite and cataclasite that are developed along shear zones, fracture zones and inter- or intra-formational fault zones closely related to regional folding and shearing deformation. Three gold mineralizing epochs are recognized in the JOB. The ca. 423–397 Ma mineralization was associated with the early Paleozoic tectonothermal event(s), which induced widespread emplacement of Silurian S-type granites, low-grade metamorphism and enrichment of gold in the Neoproterozoic rocks (i.e., forming Au source beds). The second Au mineralization epoch, occurring at ca. 176–170 Ma (Jurassic), was related to the subduction of the Paleo-Pacific plate beneath the South China continental margin. The third and most important Au mineralization epoch took place at ca. 144–130 Ma (early Cretaceous), when a Basin-and-Range tectonic pattern was developed, characterized by NE–NNE-trending strike-slip faults, granitic domes and metamorphic core complexes (MCC), and basins filled with red bed lithologies. C, H, O, He-Ar, S and Pb isotopic and fluid-inclusion data suggest that the ore fluids were predominantly metamorphic and/or magmatic, with variable input of mantle-derived fluids and the progressive involvement of meteoric waters in the later stages of mineralization. Ore materials were mostly contributed by the Neoproterozoic source beds, plus a possible contribution from mantle- or magma-derived components. The Au (-polymetallic) deposits in the JOB, particularly those formed in the early Cretaceous, share many geological and geochemical features with the orogenic-type and Carlin-type deposits. In the context of tectonic evolution of South China, the gold mineralization in the JOB may be considered an "intracontinental reactivation type", characterized by synchronous development of Au–polymetallic mineralization, reactivation of stuctures developed in Neoproterozoic metamorphic rocks, and widespread granite emplacement in the late Mesozoic.

1. Introduction

With the reputation for abundant W–Sn-polymetallic mineral deposits associated with the Yanshanian (Jurassic and Cretaceous) granites, South China also contains significant amounts of gold resources. One of the most important gold producers in South China is the Jiangnan Orogenic Belt (JOB), having a total reserve of more than 970 t Au (Zhao, 2001; Chen et al., 2008; Li et al., 2009; Fu et al., 2011; Gu et al., 2012; Ni et al., 2015; Wang et al., 2015; Liu et al., 2016; Wen et al., 2016). The JOB, also called the Jiangnan Paleo-Island Arc, Jiangnan Oldland or Jiangnan Paleo-Uplift in the Chinese literature (Huang, 1945; Ren, 1991), is a Neoproterozoic collisional zone situated between the Yangtze Block to

* Corresponding author at: .Key Laboratory of Mineral and Metallogeny, Guangzhou Institute of Geochemistry, Chinese Academy of Sciences, Guangzhou 510640, China.
E-mail address: xuderu@gig.ac.cn (D. Xu).

http://dx.doi.org/10.1016/j.oregeorev.2017.02.004
0169-1368/

the northwest and the Cathaysia Block to the southeast (Fig. 1a). This orogen is characterized not only by widespread outcrops of Neoproterozoic low-grade metamorphic volcaniclastic and sedimentary rocks with typical turbidite sequences, but also by occurrences of abundant granites with the Neoproterozoic to Cretaceous ages (Fig. 1b). A variety of mineral deposits are developed in the JOB, including hydrothermal Au, Au–Sb and Au–Sb–W deposits mainly hosted in Neoproterozoic successions, porphyry- and/or skarn-type Cu–Au–Pb–Zn deposits and W–(Cu) deposits associated with Mesozoic granitoids, and Cu–Ni sulfide deposits related to mafic/ultramafic rocks. These ore-hosting assemblages are significantly different from those in neighboring tectonic units. The Cathaysia Block to the southeast is characterized by abundant granite-related W–Sn–Bi–Mo–Nb–Ta–REE and U deposits, porphyry and epithermal Cu–Au–Mo–Pb–Zn deposits and volcanogenic massive sulfide deposits, whereas the Yangtze Block to the northwest is

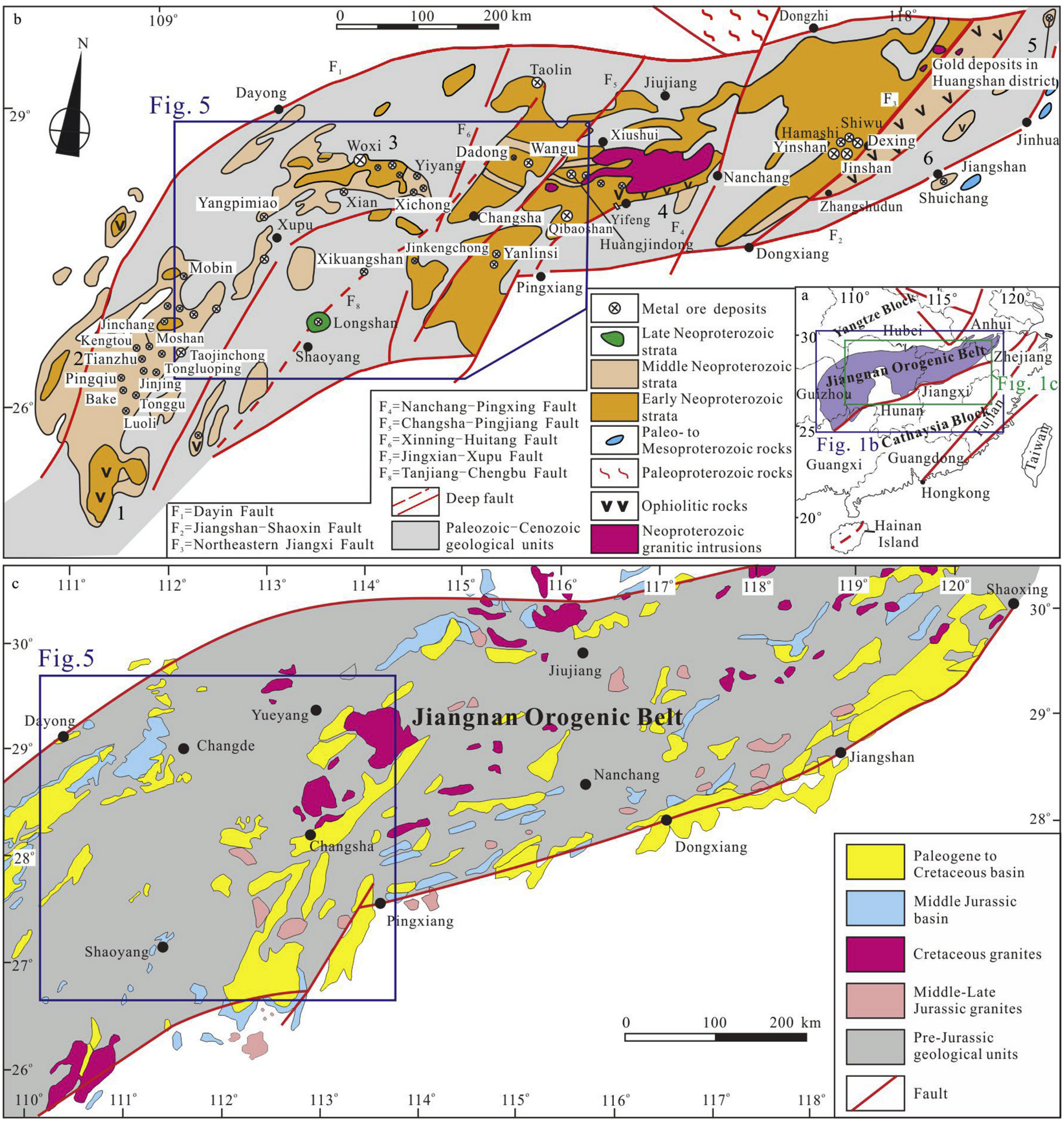

Fig. 1. (a) Simplified map of South China showing the tectonic relationship between the Yangtze and the Cathaysia Blocks, and the distribution of the Neoproterozoic rocks in the southeastern margin of the Yangtze Block, modified after Chen and Jahn (1998); (b) Simplified map showing the structures, Proterozoic successions, magmatic rocks and ore deposits in the Jiangnan Orogenic Belt (JOB), South China, modified after Shu et al. (1995); (c) Simplified map showing the Jurassic–Cenozoic successions and granites in the JOB, South China, modified after Shu et al. (2009) and Zhou et al. (2006). The shaded area in the Fig. 1a represents the JOB. Numbers 1, 2, 3, 4, 5 and 6 in the Fig. b respectively are the northern Guangxi Province, southeastern Guizhou Province, Hunan Province, northern Jiangxi province, eastern Zhejiang Province and Huaiyu (Zhejiang) region.

characterized by development of Carlin-type Au deposits, stratabound-type PGE and Fe deposits, Mississippi Vally- or sedimentary exhalative (SEDEX)-type Pb–Zn deposits and flood basalt-hosted Cu deposits (Hua et al., 2003; Zaw et al., 2007; Pirajno et al., 2009; Mao et al., 2011a, 2013a; Deng and Wang, 2016).

In the last three decades, numerous stratigraphical, structural, petrological, mineralogical, geochemical and geochronological studies have been carried out on the Au (-polymetallic) deposits in the JOB, and various genetic models have been proposed. Based on the fact that most of the Au (-polymetallic) deposits in the JOB are hosted by Neoproterozoic volcaniclastic and sedimentary rocks, many researchers concluded that the ore-forming materials were derived from the Neoproterozoic successions, and then were remobilized and enriched by later large-scale circulation of fluids from various sources (metamorphic water, meteoric water, magmatic water, and/or their mixtures) infiltrating through the host rocks (Luo, 1990; Liu et al., 1991; Ma and Liu, 1991; Zhu and Fan, 1991; Ji et al., 1994a,b; Ye et al., 1994; Chen and Xu, 1996; Hua et al., 2002; Zeng et al., 2002a, b; Li et al., 2003a, 2007a; Mao et al., 2005; Lu et al., 2006; Tian et al., 2011; He et al., 2015; Pan et al., 2015). A synsedimentary exhalative mineralization model was put forward for some Au (-polymetallic) deposits in the JOB (e.g., the Woxi W–Sb–Au deposit in western Hunan Province and the Jinshan Au deposit in northeastern Jiangxi Province; Zhang, 1985; Liu et al., 2005a; Gu et al., 2007). Nevertheless, some other researchers emphasized the importance of magmatic intrusions for mineralization, and suggested that the ore metals were mainly derived from the Mesozoic to Cenozoic or older felsic-, mafic- and/or intermediate-basic intrusive rocks (Li, 1990; Wang et al., 1993; Liu and Wu, 1993; Luo, 1996; Mao et al., 2013a; Cao et al., 2015a, b; Zhang et al., 2015). Integrating the data and genetic interpretations in previous studies, Mao and Li (1997), Mao et al. (2002), He et al. (2004) and Peng and Frei (2004) proposed that the Au (-polymetallic) deposits in the JOB are related both to the Neoproterozoic host rocks (as source rocks) and to the emplacement of late Mesozoic granites. Furthermore, the link of the Au (-polymetallic) mineralization in the JOB with a number of orogenies, for example the Neoproterozoic orogeny (Zhao et al., 2013a; Deng and Wang, 2016), the early Paleozoic orogeny (Ni et al., 2015; Zhu and Peng, 2015), the late Mesozoic orogeny (He et al., 2004), and multistage orogenies (Pirajno and Bagas, 2002), was also emphasized.

This paper is an overview on Au (-polymetallic) mineralization in the JOB and its association with the tectonic settings, host rocks and magmatism, with an aim to place the genesis of the Au (-polymetallic) deposits in a plate-tectonic and geodynamic framework. After the summaries of the geological characteristics of representative Au (-polymetallic) deposits in the JOB, an integrated analysis of the geochemical data including S, Pb, C–O, H–O and He–Ar isotopes, fluid inclusions and geochronological data is carried out, to constrain the sources of the ore-forming fluids and materials and the mineralization ages. Finally, a model emphasizing the intracontinental reactivation nature of the Au mineralization in the JOB is proposed.

2. Geological setting

South China consists of the Yangtze Block in the northwest and the Cathaysia Block in the southeast (Fig. 1a). The JOB, spanning several provinces including northwestern Zhejiang, southern Anhui, western, northern and northeastern Jiangxi, majority of Hunan, northern Guangxi and southeastern Guizhou, is generally regarded as the southeastern margin of the Yangtze Block. It is bounded to the southeast by the Jiangshan–Shaoxin deep fault zone and to the northwest by the Dayin fault zone (Fig. 1b). This ENE–NNE-trending orogen, with a length of approximately 1,500 km and a width of about 500 km, has been interpreted as the collisional result of the Yangtze with the Cathaysia Blocks during the assembly of the Rodinia Supercontinent from the late Mesoproterozoic to early Neoproterozoic (Li et al., 2002, 2008a; Greentree et al., 2006; Li et al., 2009). However, the exact age and nature of the collision and its relationship to the Grevillian orogeny have been in debate (Shu and Charvet, 1996; Zhou et al., 2002; Zheng et al., 2007, 2008; Zhou et al., 2009; Shu et al., 2011; Wang et al., 2012a; Zhao and Cawood, 2012; Zhao, 2015).

The JOB mainly consists of Neoproterozoic low-grade metamorphic volcaniclastic and sedimentary rocks, which widely outcrop along an NE–SW-trending arcuate belt convex to the northwest, striking E–W at the eastern part and NNE at the western part (Fig. 1). Cretaceous terrigenous gravelly sandstones and conglomerates of red color are developed in a few NE–NNE-trending continental basins in the JOB. To the northeast of the JOB, Paleo- to Mesoproterozoic rocks consisting of volcaniclastic rocks and gneisses with amphibolite to granulite facies metamorphism (Fig. 1b), are dispersed over the Cathaysia Block adjacent to the JOB. The Proterozoic Lengjiaxi Group in Hunan Province and its equivalents (i.e., the Fanjingshan Group in Guizhou Province, Sibao Group in Guangxi Province, Shuangqiaoshan Group in Jiangxi Province, and Chencai Group in Zhejiang Province), which were previously interpreted as having Mesoproterozoic ages, have been confirmed to be early Neoproterozoic sediments (ca. 970–825 Ma), using SHRIMP and LA–ICPMS zircon U–Pb dating (Gao et al., 2010, 2012, 2014; Wang and Zhou, 2012; Meng, 2014 and references therein; Yao et al., 2014; Qin et al., 2015; Zhang, 2015 and references therein; Yang et al., 2015). The Banxi Group in Hunan Province and its equivalents (i.e., Xiaojiang Group in Guizhou Province, Danzhou Group in Guangxi Province, Xiushui Group in Jiangxi Province, Shangxi Group in Anhui Province and Shuangxiwu Group in Zhejiang Province), which overlie the early Neoproterozoic successions, have a middle Neoproterozoic age of ca. 820–750 Ma (Zhang, 2015). Two ophiolite belts in southern Anhui Province and northeastern Jiangxi Province were tectonically emplaced within the Neoproterozoic groups along the southeastern margin of the Yangtze Block (Zhao and Cawood, 2012). An angular unconformity occurs between the early Neoproterozoic and the overlying middle Neoproterozoic successions, likely corresponding to the Neoproterozoic collision between the Yangtze and Cathaysia Blocks (Zhao, 2015).

The JOB is characterized by the Basin-and-Range tectonic style at the late Mesozoic, which is delineated by a series of NE- to NNE-trending uplifts, extensional basins, and metamorphic core complexes (MCC) bounded by strike-slip faults (Fu et al., 1999; Shu and Wang, 2006; Li and Li, 2007). This tectonic style has been interpreted as a result of the subduction and subsequent rollback of the Paleo-Pacific plate beneath the Eurasian continent (Zhou et al., 2006; Zhu et al., 2014). Although the exact time for the initiation of the subduction has been in debate, varying from the middle Permian to middle Jurassic (Zhou et al., 2006; Li and Li, 2007), most Chinese researchers agree that the subduction began at ca. 180 Ma and subsequently the South China Block (SCB) was under a compressional setting during ca. 180–160 Ma (Dong et al., 2007; Mao et al., 2011a, 2013a; Mao et al., 2014). After ca. 160 Ma, the rollback of the subducted Paleo-Pacific plate probably initiated the late Mesozoic tectonic transformation of the SCB from compression to extension, as revealed by the development of a series of NE–NNE-trending strike-slip faults (Fu et al., 1999) and the widespread occurrence of A–type granites of ca. 160 Ma in the Nanling region of South China (Jiang et al., 2006, 2009; Li et al., 2007b,c; Jiang et al., 2008; Zhu et al., 2008). The overall extension after ca. 160 Ma is supported by paleomagnetism, large-scale volcanism and a series of rift basins during the early Cretaceous in eastern China (e.g., Mao et al., 2013a). The occurrence of several mafic intrusions of ≤ ca. 135 Ma in northeastern Hunan Province of the JOB also confirmed the extensional setting (Jia et al., 2004). The Basin-and-Range structural pattern comprising extensional basins and granitic domes, and their marginal strike-slip faults in the JOB (Fig. 2) is similar to that of western North America, which formed in an extensional tectonic setting (Cline et al., 2005; Muntean et al., 2011).

Granites in the JOB were dominantly emplaced into the Neoproterozoic successions, with the main intrusive ages varying from the early to late Neoproterozoic (ca. 835–730 Ma), the early Paleozoic (ca. 540–390 Ma), the early Mesozoic (ca. 250–205 Ma), to the late Mesozoic (ca. 180–120 Ma), as dated by zircon SHRIMP, LA–ICPMS and SIMS U–Pb methods (Li, 1999; Li et al., 2003b; Wang et al., 2004; Wang et al., 2006; Li et al., 2008a; Wang, 2012; Wang et al., 2013a and references therein; Zhou et al., 2012a; Zhao et al., 2013b; Liu et al., 2012; Wang et al., 2015; Zhu et al., 2014; Xiang et al., 2015; Chen et al., 2016; this study). Most of these granites were regarded as the S-type and formed by the partial melting of the Neoproterozoic and/or older rocks, with variable contributions from other younger sources (Chen and Jahn, 1998; Peng et al., 2004; Li et al., 2005a; Wang et al., 2006; Xu et al., 2006, 2009; Wang, 2012).

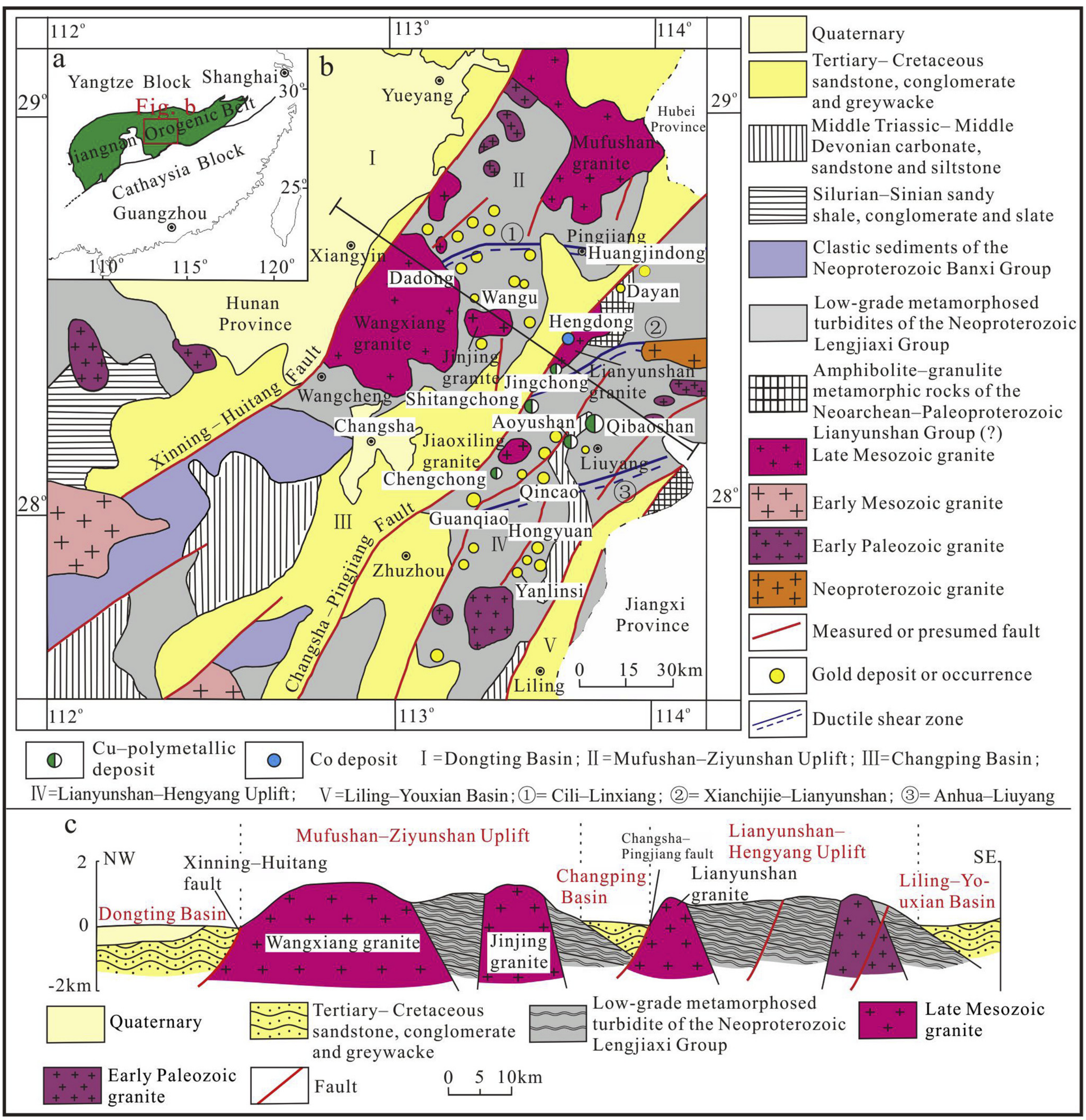

Fig. 2. (a) Simplified map of South China; (b) Basin-and-Range tectonic pattern and associated magmatic rocks and ore deposits in northeastern Hunan Province, South China (modified after Xu et al., 2009); (c) NW-trending cross section showing the Basin-and-Range tectonic style.

3. Geological characteristics of Au (-polymetallic) mineralization in the JOB

The JOB contains more than 250 Au (-polymetallic) deposits and occurrences. The representative deposits include the Huangshan Au deposit in northwestern Zhejiang Province, the Jinshan Au deposit in northeastern Jiangxi Province, the Huangjindong, Wangu, Yanlinsi and Mobin Au-Sb deposits, and Woxi Au–Sb–W deposit in Hunan Province, and the Pingqiu, Tonggu, Jinjing and Jintou Au deposits in southeastern Guizhou Province (Fig. 1b). In addition to these Au (-polymetallic) deposits, there are many other intrusion-related deposits in the JOB that contain significant Au resources. For example, the world-class Dexing porphyry Cu–Mo–Au deposit and the Yinshan hydrothermal Ag–Cu-polymetallic deposit closely associated with the Mesozoic volcanic and subvolcanic rocks in Jiangxi Province, which are about 5–10 km away from the Jinshan Au deposit (Fig. 1b), contain 215 t Au and 107 t Au, respectively (Wang et al., 2013a; Liu et al., 2016). Thus, the JOB has become an important Au metallogenic belt in South China with a total reserve of >970 t Au (mined and estimated).

The main geological characteristics of the representative Au (-polymetallic) deposits in the JOB are summarized in Appendix A1. These Au (-polymetallic) deposits and occurrences in the JOB are generally associated with shear structures, with the mineralization styles including auriferous quartz veins and disseminations in altered mylonite, cataclasite and structural breccia. The Au mineralization occurs along a group of subsidiary WSW–EW–ENE-, NW–WNW- and/or NE–NNE-trending shear zones, fracture zones, and inter- or intraformational detachment fault zones, which are closely related to a series of regional anticlinoria and synclinoria (Appendix A1). Although some Au (-polymetallic) deposits and occurrences occur surrounding Mesozoic plutons (Fig. 2), magmatic intrusions are generally absent in most of the mining districts except for a few mafic, felsic and intermediate-basic dikes (Appendix A1). Alteration zones consisting of proximal and intensive silicification, pyritic, arsenopyritic sericitic, chloritic and carbonate alterations and distal and weak silicification, sericitic and chloritic alterations, are developed around these Au (-polymetallic) deposits. The ore mineral assemblages are characterized by pyrite + native gold + arsenopyrite ± scheelite ± galena ± sphalerite ± chalcopyrite, and the gangue mineral association by quartz + calcite + sericite + chlorite ± albite ± ankerite (Appendix A1). Field and petrographic observations generally reveal a two- to four-stage mineral paragenesis in these ore deposits: 1) quartz + pyrite ± calcite; 2) auriferous scheelite + pyrite + quartz or sulfide + Fe–Mg carbonate; 3) sulfide + native gold + quartz; and 4) quartz ± calcite (Appendix A1). However, there are some differences in ore geology from one deposit to another in the JOB, which are likely due to differences in local geological setting including host rocks, magmatism, mineralization ages and ore-forming physicochemical conditions (Appendix A1). The geological characteristics of representative Au (-polymetallic) deposits are described as follows.

3.1. Au mineralization in northwestern Zhejiang Province

In northwestern Zhejiang Province, more than thirty Au deposits and mineral showings, represented by the Huangshan, Fengshuilin, Miaoxiafan, Dagaowu, Xinsheng, Jiangcun, Tongshuling, Mali, Meidian, Heshan, Pingshui, Zhongao, Zhupuao, Shiqi, Qicun and Kuzhijian deposits, occur within the hanging wall of the NE-trending Jiangshan–Shaoxin deep fault zone (Fig. 3a; Li, 1990; Tong, 2014; Ni et al., 2015). The deposits are hosted either by the early Neoproterozoic Chencai Group, comprising gneiss, schist, granulite, amphibolite, marble and quartzite of amphibolite-facies metamorphism, or by the ca. 844–808 Ma (Ye et al., 2007; Wang et al., 2012b) intrusive complex consisting of pyroxene diorite, quartz diorite and diorite, and associated mafic to ultramafic rocks. These host rocks are generally subjected to intensive ductile shearing and mylonitization, resulting in a series of tectonites composed of sericite–chlorite phyllonite, chlorite–sericite phyllonite, sericite–quartz phyllonite, and minor mylonite. Au mineralization generally occurs in the subsidiary NE-, NW- or ENE-trending phyllonite sub-zones within the NE-trending Tongshulin–Huangshan ductile shear zone (Li, 1990; Tong, 2014), and commonly has a positive correlation with the intensity of alterations including silicification, pyritic and sericitic alterations (Ye et al., 1994). Minor Indosinian to Yanshanian (ca. 230–123 Ma, K–Ar method) felsic to mafic dikes such as diabase, felsite porphyry and lamprophre, which have close spatial relationship with Au mineralization, are present within the fracture zones in most of the mineralization areas (Ye et al., 1993; Chen and Xu, 1996). Ye et al. (1993) and Chen and Xu (1996) suggested a two-stage mineralization process for the Au deposits in northwestern Zhejiang Province. The early stage produced the auriferous quartz veins composed of ore minerals including pyrite, native gold (with sizes of 0.03–0.06 mm), chalcopyrite, sphalerite, calaverite and electrum, whereas the late stage yielded Au-bearing quartz veinlets and stockworks comprising pyrite, invisible native gold and silver, chalcopyrite, sphalerite and electrum. A three-stage mineralization process was also proposed for Au mineralization in northwestern Zhejiang Province (Ye et al., 1994): 1) quartz + sulfide + native gold, 2) quartz + invisible native silver + sulfide + electrum, and 3) quartz + calcite stages, from early to late. Minor coloradoite, cinnabar, orpiment and fluorite were locally observed in some of the deposits (Ye et al., 1994).

The Huangshan deposit (Appendix A1 and Fig. 3b) has a measured reserve of about 30 t Au, with an average grade of 9 g/t Au. This deposit is hosted within the Huangshan quartz dioritic intrusive complex which has a fault contact with the Chencai Group to the southeast of the mining district. Au orebodies generally occur within the subsidiary NE-trending phyllonite sub-zones (Tong, 2014). The ores mainly occur in quartz veins, with subordinate auriferous phyllonite. The auriferous quartz veins are characterized by lenticular ribbon structures marked by white and dark-grey quartz which shows undulatory extinction and sub-grain microstructures (Ni et al., 2015), suggesting strong ductile-shearing. Pyrite is the predominant (accounting for 98%) ore minerals, with minor chalcopyrite, galena and sphalerite. Native gold, which has a fineness of 950 and grain size of 0.002–0.13 mm (Ni et al., 2015), is the main auriferous mineral, with minor calaverite, petzite and auriferous coloradoite. Quartz is the main gangue mineral, with subordinate sericite, calcite, ankerite, aphrizite and chlorite. The Au mineralization is associated with silicification, pyritic, sericitic, chloritic, epidotic, tourmalitic, ankeritic and carbonate alterations (Ni et al., 2015).

3.2. Au mineralization in northeastern Jiangxi Province

Au deposits in northeastern Jiangxi Province mainly include the Jinshan, Xijiang, Wanjiawu, Dabeiwu, Hamashi, Shangshan and Hujiajian deposits. These deposits share similar ore geological characteristics (see Appendix A1), and we take the Jinshan deposit as an example, as described below.

With a measured reserve of more than 300 t Au, the Jinshan Au deposit occurs in the hanging wall of the regional NE-trending Jiangxi deep-fault zone corresponding to the Neoproterozoic collision between the Jiuling and Huaiyu terrenes (Shu et al., 1995; Wu et al., 2006). The ENE-trending Jinshan ductile shear zones dip to NW or NE at an angle of 5°–35°. Bounded by both

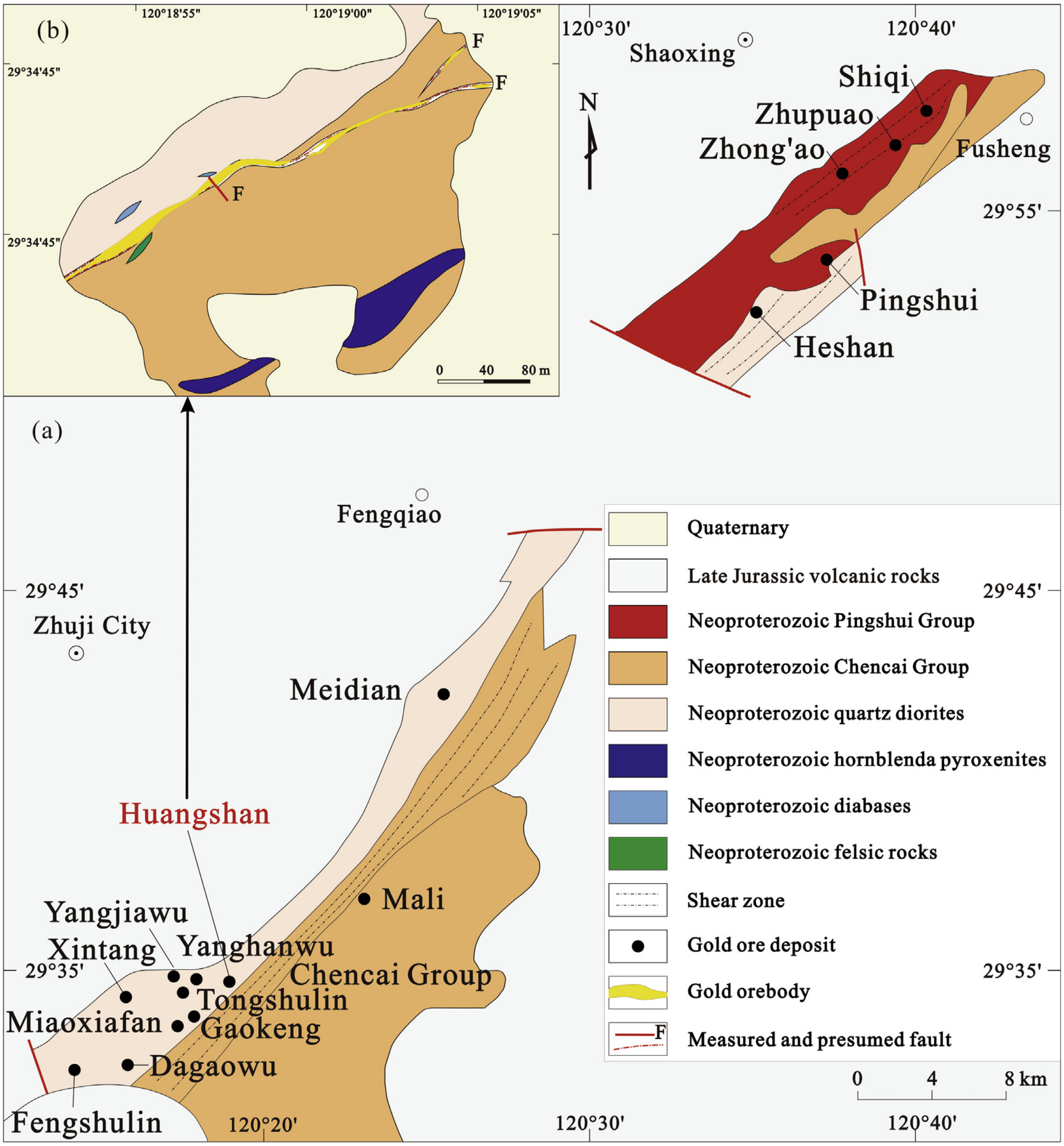

Fig. 3. (a) Spatial distribution of the gold deposits in Zhejiang Province; (b) Geologic map of the Huangshan gold deposit (modified from Ni et al., 2015).

the NNE-trending Bashiyuan–Tongchang strike-slip faults and the Jiangguang–Fujiawu strike-slip fault, this ore-hosting Jinshan shear zone has a length of more than 6 km along strike, a width of 120–700 m, and an extension of more than 1.8 km along the dip. This deposit is hosted by the early Neoproterozoic Shuangqiaoshan Group, a suite of low-grade metamorphic volcaniclastic rocks composed of slate, phyllite, metamorphic crystal-fragment tuff and greywacke, intercalated with andesitic basalt (Fig. 4a). Four tectonite sub-zones (i.e., carbonaceous phyllonite, ultramylonite–mylonite, mylonite and mylonized host rock zones) have been recognized within the Jinshan ductile shear zone, from the center to the margin. With stratiform, stratiform-like and lenticular shapes, the orebodies mainly occur in mylonites and ultramylonites with similar attitudes to the host rocks (Fig. 4b). Minor diabase and pyroxene diorite dikes sporadically appear in the Jinshan mining district, with the zircon SHRIMP U–Pb age of ca. 154 Ma (Zhou et al., 2012b).

Three distinct alteration zones (i.e., quartz + albite + ankerite + pyrite, quartz + sericite + dolomite (ankerite), and sericite + chlorite + calcite zones) from center to margin of the ductile shear zone have been identified (Li et al., 2007a, 2010a). Among them, the quartz + albite + ankerite + pyrite zone with widths ranging from several meters to about 50 m is endowed with high-grade (locally in excess of 1600 g/t Au) ores. The main ore modes consist of auriferous mylonites and quartz veins, with the Au grades of 4 to 20 g/t and 10 to 900 g/t, respectively. The disseminated pyrite-bearing mylonite ores around the laminated Au-bearing quartz veins contain 75% of the Au reserve (Li et al., 2010a). The high-grade Au ores also contain greater abundance of base-metal sulfides than the low-grade ones (Li et al., 2010a). Besides the presence of albite, the Jinshan deposit shares similar ore and gangue minerals to those in northeastern Hunan Province (see the description, below). With the fineness of 954–970 (Wei, 1995), the fine-grained, xenomorphic native gold is present as disseminations or as

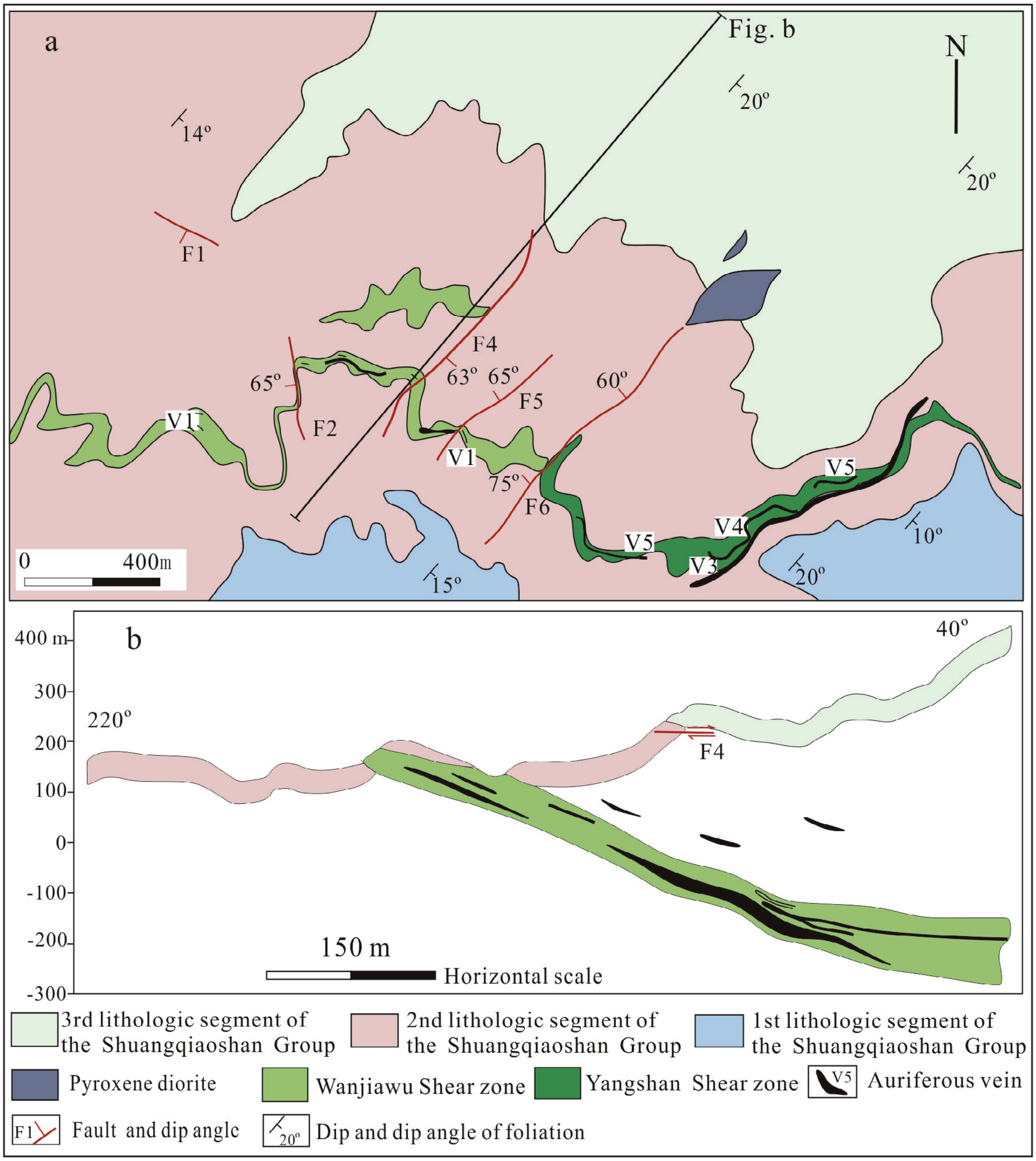

Fig. 4. Simplified geologic map (a) and a cross section (b) of the Jinshan deposit in northeastern Jiangxi Province, modified after Zhao et al. (2013a).

micro-veinlets within pyrite and quartz intergrown with chalcopyrite, galena and tetrahedrite (Mao et al., 2011b). Pyrite as the most important Au-hosting mineral, typically represents more than 90% of the sulfides which occupy less than 1% of the ores. The altered mylonite ores show two stages of Au mineralization (i.e., native gold + quartz + sulfide and quartz + calcite) from early to late (Liu et al., 2005b), whereas the Au quartz veins were formed in three stages: pyrite + quartz, native gold + quartz + sulfide + sericite + chlorite + calcite (the main mineralization stage), and chlorite + calcite + quartz (Zhao et al., 2013a). A later-stage hydrothermal reworking that formed thin quartz–pyrite veins has also been recognized in the Jinshan mining district (Liu et al., 2005a, b).

3.3. Gold mineralization in Hunan Province

Based on their relationships to the host rocks, intrusions, ore-controlling structures, ore- and gangue minerals, and ore metal associations (Appendix A1), the Au (-polymetallic) deposits and mineral showings in Hunan Province are roughly subdivided into three regions (i.e., the northeastern, northwestern and southwestern regions) (Fig. 5).

3.3.1. Au mineralization in northeastern Hunan Province

Separated from the northwestern Hunan Province by the regional NE–NNE-trending Xinning–Huitang fault (Figs. 1, 2 and 5), the northeastern Hunan Province contains about 125 Au (-polymetallic) deposits and occurrences, with the Wangu, Huangjindong and Yanlinsi deposits (Fig. 2 and Appendix A1) as the representatives. They are hosted by the slates of the Lengjiaxi Group, and regionally controlled by both the approximately EW-trending overthrust-ductile shear zones and the NE–NNE-trending strike-slip faults (Fig. 2). Various structural styles including folds, faults and shear zones are well-developed in the mining districts (Liu et al., 1997), but the orebodies are mainly located in

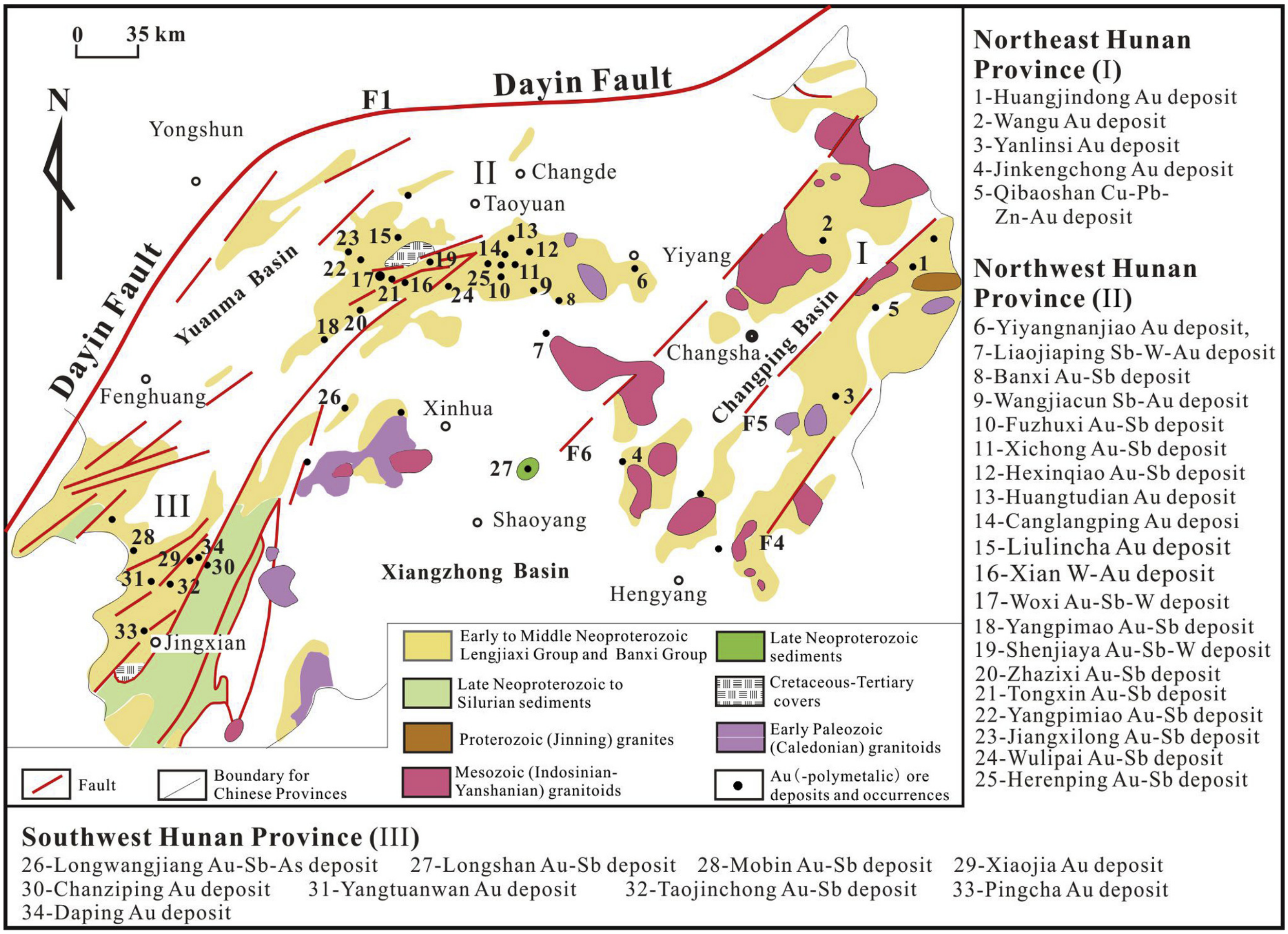

Fig. 5. Sketch map showing the structural and magmatic geology, and Au (-polymetallic) ore deposits and occurrences hosted by the Neoproterozoic rocks in Hunan Province, South China (modified after Ma and Liu, 1991). F1, F4, F5 and F6 can be found in the Fig. 1b.

the NW- to WNW- or NE-trending inter- and intraformational fracture zones (Appendix A1). These fracture zones (1–10 m wide) consist of altered cataclasites, structural breccias and quartz veins, corresponding to three mineralization styles (i.e., auriferous cataclasite, auriferous structural breccia, and auriferous quartz veins). Quartz is the most abundant gangue mineral, typically making up to 85–95% of the veins, and calcite is another common gangue mineral. Ore minerals include pyrite, arsenopyrite, stibnite, galena, sphalerite and chalcopyrite, with subordinate scheelite. Gold minerals are dominated by native gold, with some invisible gold contained in sulfides such as arsenopyrite, pyrite, chalcopyrite, and galena. Gold grades in the ore veins are generally positively correlated with the abundances of arsenopyrite and pyrite.

The large Wangu deposit contains a total reserve of 85 t Au with grades ranging from 3 g/t to 73 g/t (avg. 6.8 g/t) Au (Appendix A1). The main ore types are auriferous quartz veins and auriferous altered cataclasite, with minor auriferous altered structural breccia, which are hosted by the (W)NW-trending intraformational fracture zones (Fig. 6). These fracture zones are crosscut by the NE–NNE-trending strike-slip faults, leading to an equidistant distribution of the orebodies. Field and thin-section observations suggest a four-stage Au mineralization for the Wangu deposit: 1) quartz + calcite, 2) quartz + pyrite + arsenopyrite, 3) sulfide + native gold + quartz, and 4) quartz + calcite from early to late stages.

Another large deposit in this region is the Huangjindong deposit, with a total reserve of about 80 t Au and grades of 4–10 g/t Au. Despite of a similar ore geology to the Wangu deposit, the Huangjindong deposit is related to a series of WNW- to nearly EW-trending overturned anticlines and synclines, and associated inter- or intraformational shear fracture zones (Figs. 7a–c). In return, these folds and fracture zones are crosscut by NNE-trending faults. Locally, the WNW- to EW-trending fracture zones form a group of X-type conjugate transtensional joints in a cross section (Fig. 7c). Four stages of Au mineralization including 1) quartz + pyrite + calcite, 2) auriferous scheelite + pyrite + quartz, 3) sulfide (pyrite, arsenopyrite) + native gold (with the fineness between 963 and 998) + quartz, and 4) quartz + calcite, from early to late, were recognized for the Huangjindong deposit (Luo, 1988).

The Yanlinsi deposit (Appendix A1) has a total reserve of about 50 t Au, with variable grades from 0.6 g/t to 24.7 g/t Au. Different from both the Wangu and Huangjindong deposits, the Yanlinsi deposit contains two groups of auriferous quartz veins, i.e., a group of veins present within the NE-trending cleavage (brittle–ductile) zones with widths ranging from dozens of cm to dozens of m and lengths from 100 m to >1 km, and a group of veins occurring within the NW-trending ductile shear zones with widths ranging from 50 m to 150 m and lengths of more than 1.5 km (Fig. 8; Huang et al., 2012). A concealed pluton of Mesozoic age is inferred to underlie the mining district to account for the extensive thermal-contact metamorphic aureoles within the Lengjiaxi Group (Liu and Wu, 1993). Felsic to mafic dikes of the late Cretaceous age in the district (Fig. 8c) are unfoliated, and clearly crosscut the

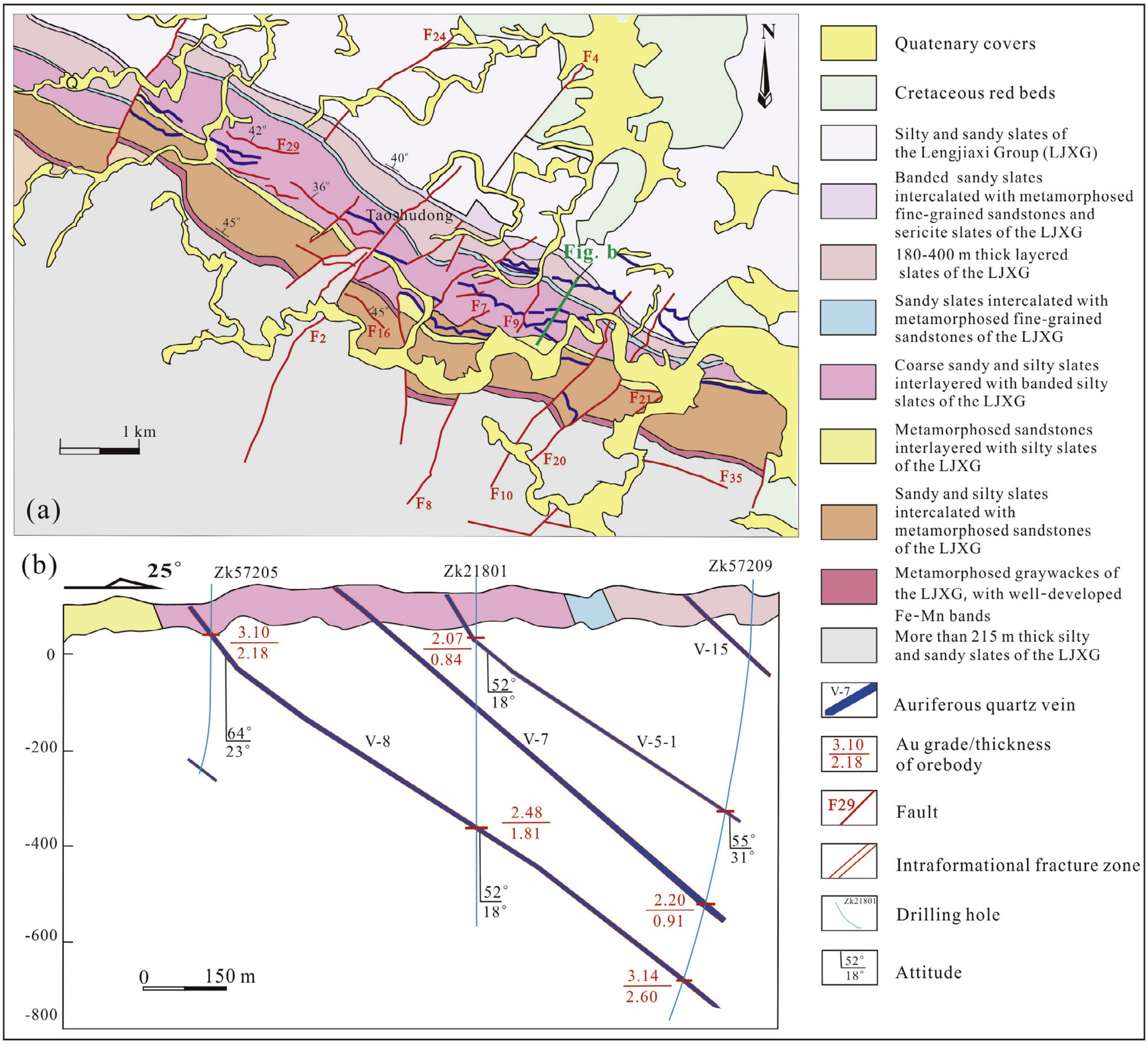

Fig. 6. (a) Geological map of the Wangu gold deposit (modified after Mao et al., 2002); (b) A cross section showing ore geological features and related host rocks of the deposit.

foliated mineralized host rocks and ore veins, indicating that they postdate the deformation of the host rocks and mineralization.

3.3.2. Au mineralization in northwestern Hunan proivnce

The northwestern Hunan region contains about one hundred Au, Au–Sb and Au–Sb–W deposits and mineral showings (Fig. 5). Most are hosted by purple red slates interbedded with sandy slates and sandstones of the middle Neoproterozoic Banxi Group, except for the Xichong and Yiyangnanjiao deposits hosted by the volcaniclastic and sedimentary (carbonate) rocks of the early Neoproterozoic Lengjiaxi Group, and the Liaojiaping deposit hosted by the Lower Cambrian shales (Luo, 1994a). Although most deposits in this region are far away from granitic plutons, a few seem to be spatially and temporally associated with the Mesozoic granitic porphyry dykes (i.e., the Liaojiaping, Banxi, Xichong and Fuzhuxi deposits) (Luo, 1994; Luo, 1994; HRGI, 1995).

As the most important deposit in the region, the Woxi Au–Sb–W deposit (Appendix A1) has a total proven reserve of 40 t Au with a grade of 13.0 g/t, 1.67 Mt Sb with a grade of 6.45%, and 250,000 t WO_3 with a grade of 0.47% (Luo et al., 1996). The regional EW-trending Woxi brittle-ductile shear fault, with a length of 20 km and a width of 10–30 m, and dipping 25° to N, cuts through the entire mining district and controls the W–Sb–Au mineralization (Fig. 9a). The mineralization style in the Woxi deposit is dominated by auriferous quartz veins, which are sheeted and parallel to the bedding, and networks of veins and veinlets at the footwall of the Woxi fault. The orebodies are controlled by a series of inter- or intraformational fracture zones associated with multiple anticlines and synclines (Fig. 9). The main ore minerals include scheelite, wolframite, stibnite, native gold (with the fineness of 976 to 997) and pyrite, with minor arsenopyrite, sphalerite, galena, chalcopyrite, and cinnabar. Au–Sb–W mineralization is closely associated with silicification, pyritic and sericitic alterations, whereas chloritic and carbonate alterations are developed peripheral to the main ore veins and/or in places where these veins thin out. Based on previous studies on mineral paragenesis (Liu et al., 1994b; Peng

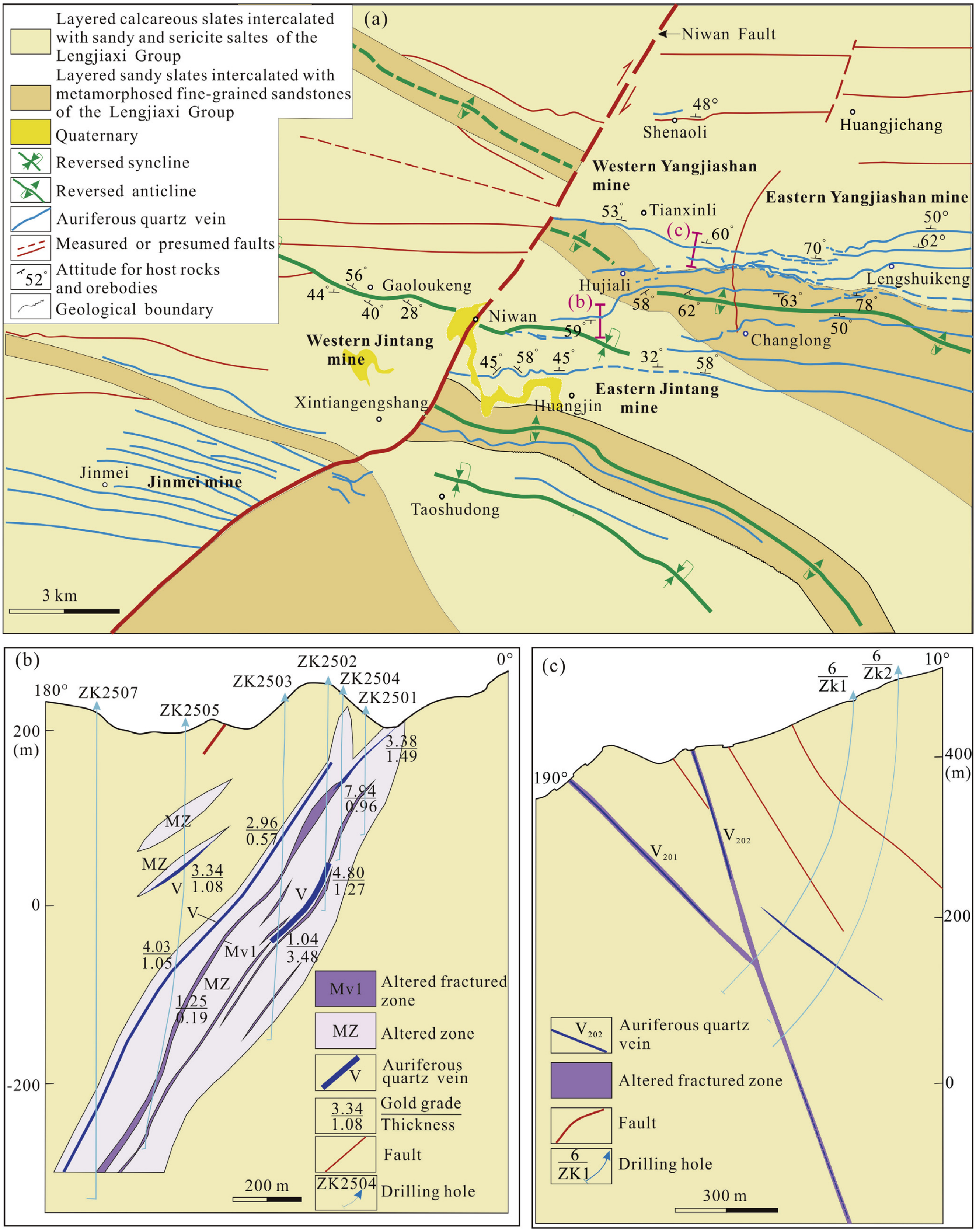

Fig. 7. (a) Schematic map of the Huangjindong gold deposit and (b and c) cross sections showing the occurrences of orebodies, altered zones and host rocks of the deposit (modified after He et al., 2004).

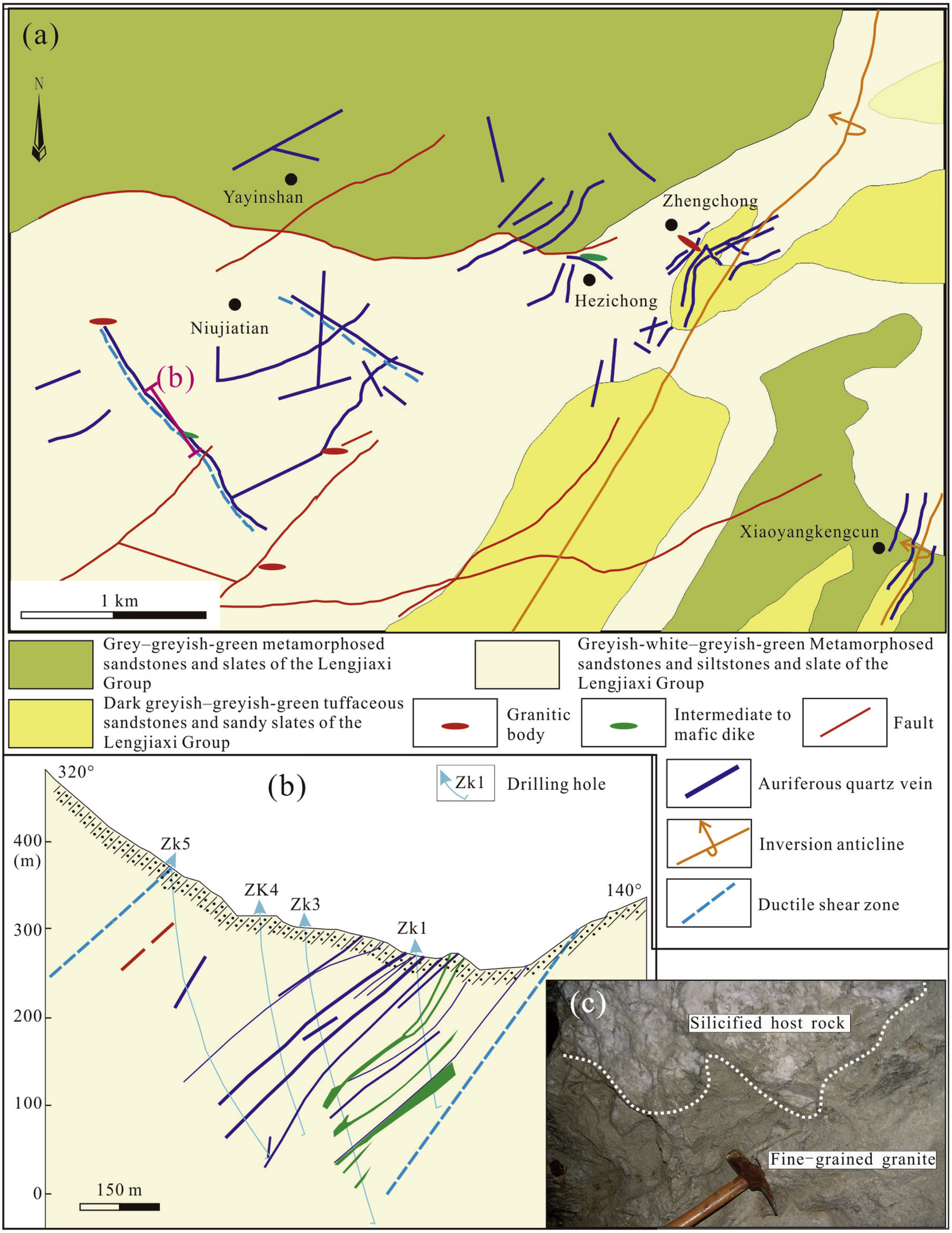

Fig. 8. (a) Geological map of the Yanlinsi gold deposit (modified after Huang et al., 2012); (b) A cross sections showing the occurrence of orebodies (modified after He et al., 2004); (c) Fine-grained granite intruding into the silicified host rocks.

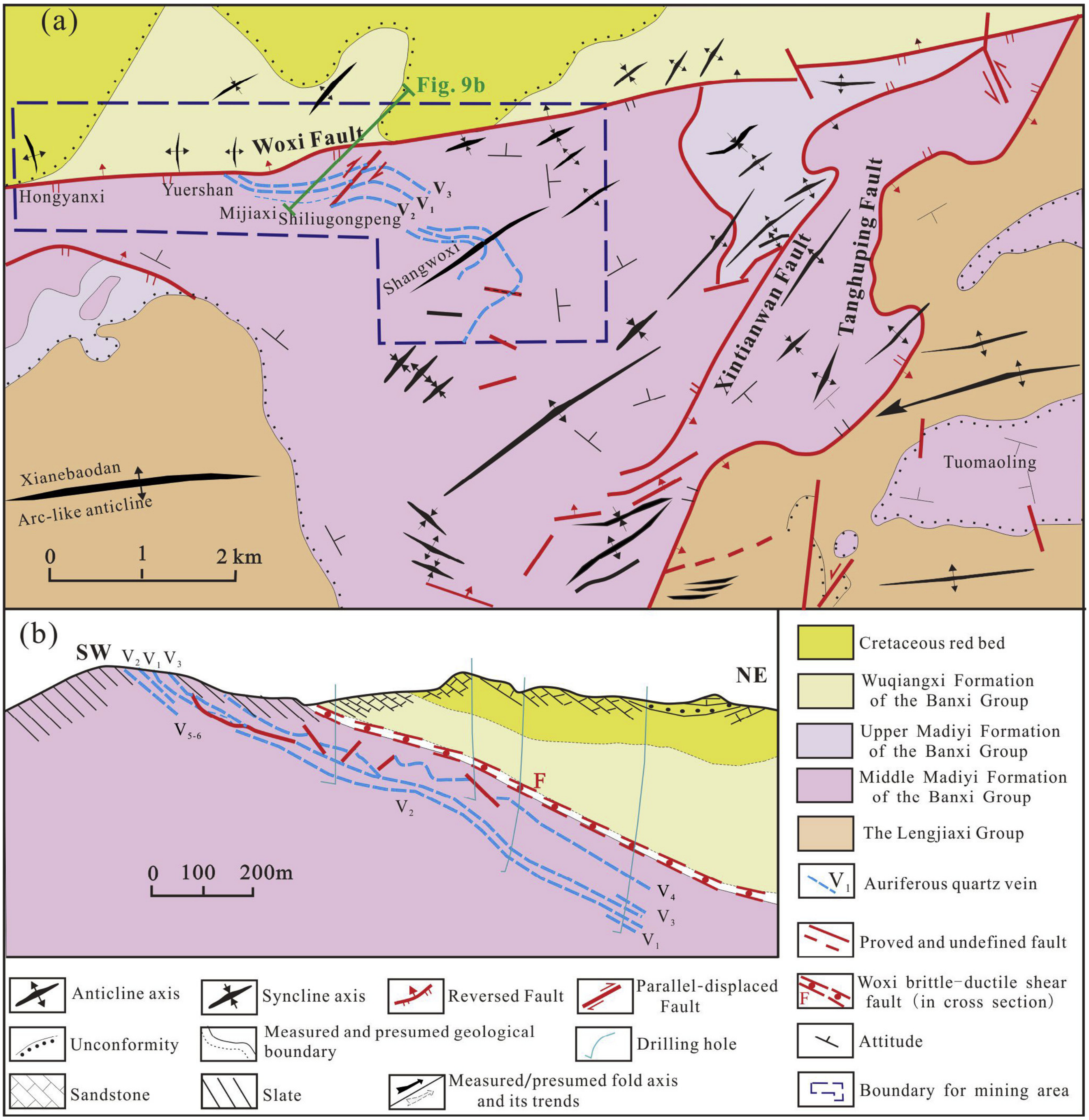

Fig. 9. (a) Sketch map showing geological and structural features of the Woxi Au–Sb–W orefield and its adjacent areas in northwestern Hunan Province; (b) A NE–SW cross section of the Woxi deposit, modified after Luo et al. (1996).

et al., 2003; Peng and Frei, 2004; Liang et al., 2014; Zhu and Peng, 2015), the mineralization process may be divided into three stages (from early to late): 1) quartz + wolframite + scheelite, 2) native gold + sulfide (pyrite, stibnite) + quartz, and 3) quartz + calcite.

3.3.3. Au mineralization in southwestern Hunan Province

Most of the Au–Sb deposits and mineral showings in southwestern Hunan region are hosted by the middle Neoproterozoic Banxi Group, except for a few ore deposits by illite-bearing slate and *meta*-feldspar-quartzose sandstone of the middle to late Neoproterozoic Jiangkou Group (Appendix A1). A swarm of NE- to NNE-trending folds and shear faults, which are crosscut by less-developed, WNW- to NW-trending faults, are the main ore-controlling structures in this region. One of the representative deposits is the Mobin Au–Sb deposit hosted by the Banxi Group (Fig. 10 and Appendix A1). The dominant mineralization style in the deposit is represented by auriferous quartz veins, which are subdivided into veins parallel to the bedding and those oblique to and crosscutting the bedding. The predominant bedding-parallel veins generally occur within inter- or intraformational fracture zones (Fig. 10), which were likely developed due to lithological and rheological contrasts between sedimentary beds during the NE-trending folding, whereas the oblique veins are generally present within the NW- to WNW-trending fracture zones. Quartz is the main gangue minerals, with minor calcite, sericite, chlorite, dolomite, siderite, albite and barite. Ore minerals are dominated

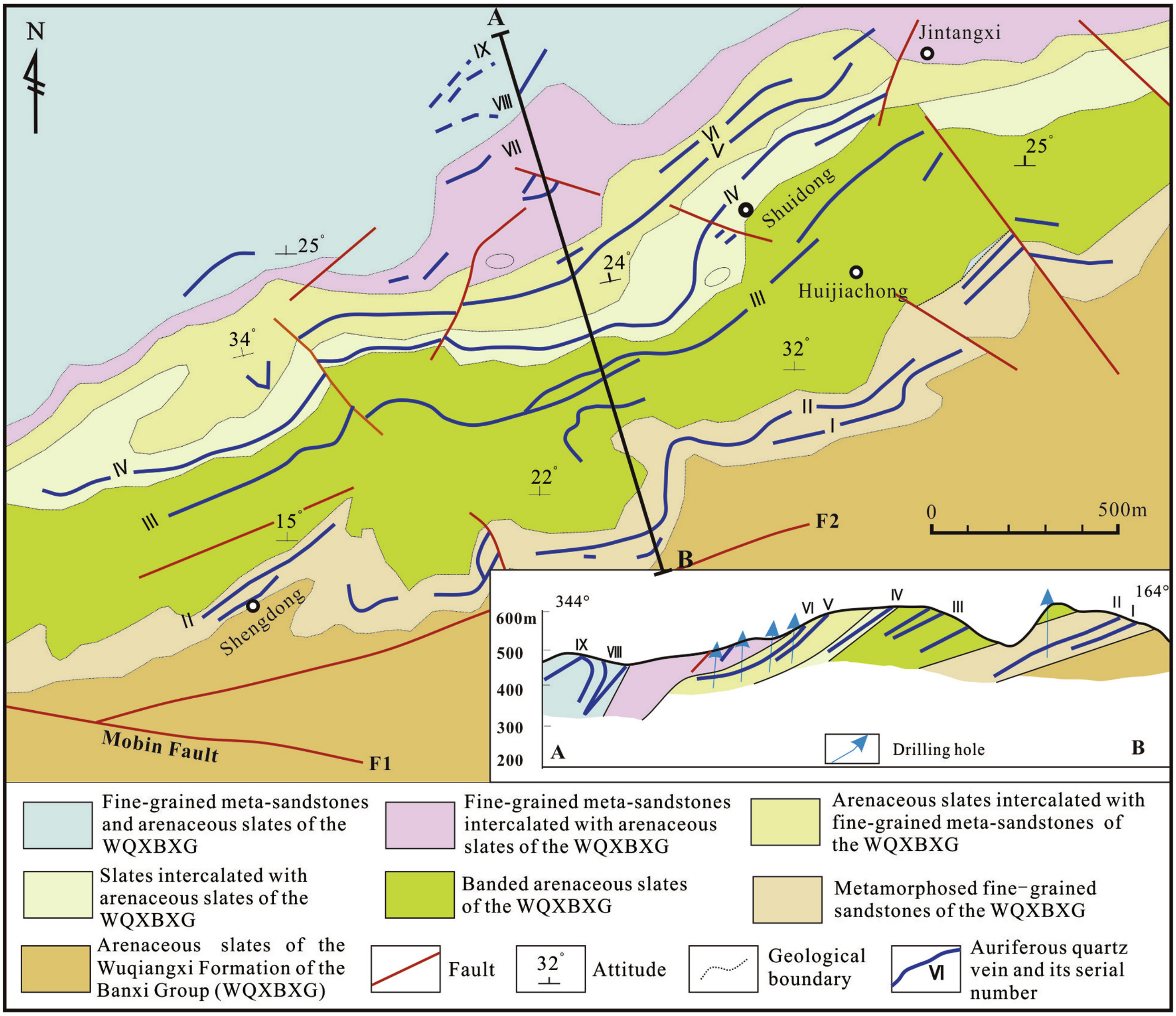

Fig. 10. Sketch map and associated cross section showing the ore geology and orebody distribution of the Mobin Au–Sb ore deposit in southwestern Hunan Province (modified after Zhou et al., 1989).

by pyrite, asenopyrite, native gold (with the fineness between 925 and 960), stibnite, sphalerite, galena and chalcopyrite. Native gold mostly shows irregular morphologies with sizes of 0.015 mm to 1 cm and occurs within fissures, whereas minor invisible gold is disseminated in sulfides. Two stages of mineralization were proposed by Niu and Ma (1991) for the Mobin deposit, including: 1) quartz + pyrite + arsenopyrite at the early stage, and 2) quartz + sulfide + native gold at the late stage. Although mafic/ultramafic rocks, diorites and granites of Neoproterozoic ages (Zhou et al., 1992; Zheng et al., 2001) occur along the NE- to NNE- trending faults in the region, they are absent within the mineral deposits.

3.4. Au mineralization in southeastern Guizhou Province

Recent exploration reveals a significant potential for Au mineralization in the Tianzhu–Jinbing–Liping region, in southeastern Guizhou Province. More than twenty Au deposits and occurrences have been discovered in this region (Figs. 1b and 11), and the representative ones are the Pingqiu, Xianggongtang, Luoli, Gubang, Bake, Jinjing, Longai, Tonggu, Zhongling, Pingdi, Dicha, and Jinchang deposits. The Au mineralization is hosted within the middle Neoproterozoic Xiajiang Group, which is a thick (up to 7 km), turbiditic succession composed of slate, *meta*-sandstone, *meta*-tuff and *meta*-siltstone of greenschist facies. Strong structural deformation in the region is depicted by the NE-trending (trough-like) anticlinoria and associated inter- or intraformational detachment shear faults, NE–NNE- and approximately EW-trending shear faults, and NW-trending faults (Lu et al., 2006; Yang et al., 2012; Zhang et al., 2015). Orebodies are present in both the NE–NNE-trending shear fault zones dipping to NW at an angle of 25°–85° and crosscutting the crests of the NE-trending anticlines, and the intra- or interformational detachment fault zones dipping to NW and SE or SW at an angle of 10°–80°. Au-bearing quartz veins as the dominant style of mineralization mostly occur within the intra- or interformational detachment fault zones and are present parallel to the bedding. Subordinate ores occur as auriferous altered cataclasites within the NE-trending shear fault zones. The Au grades of auriferous quartz veins are highly variable and range from 0.4 g/t to 150 g/t Au. Noticeably, bonanzas are developed in many gold mines of this region, (e.g., an unusual Au grade of up

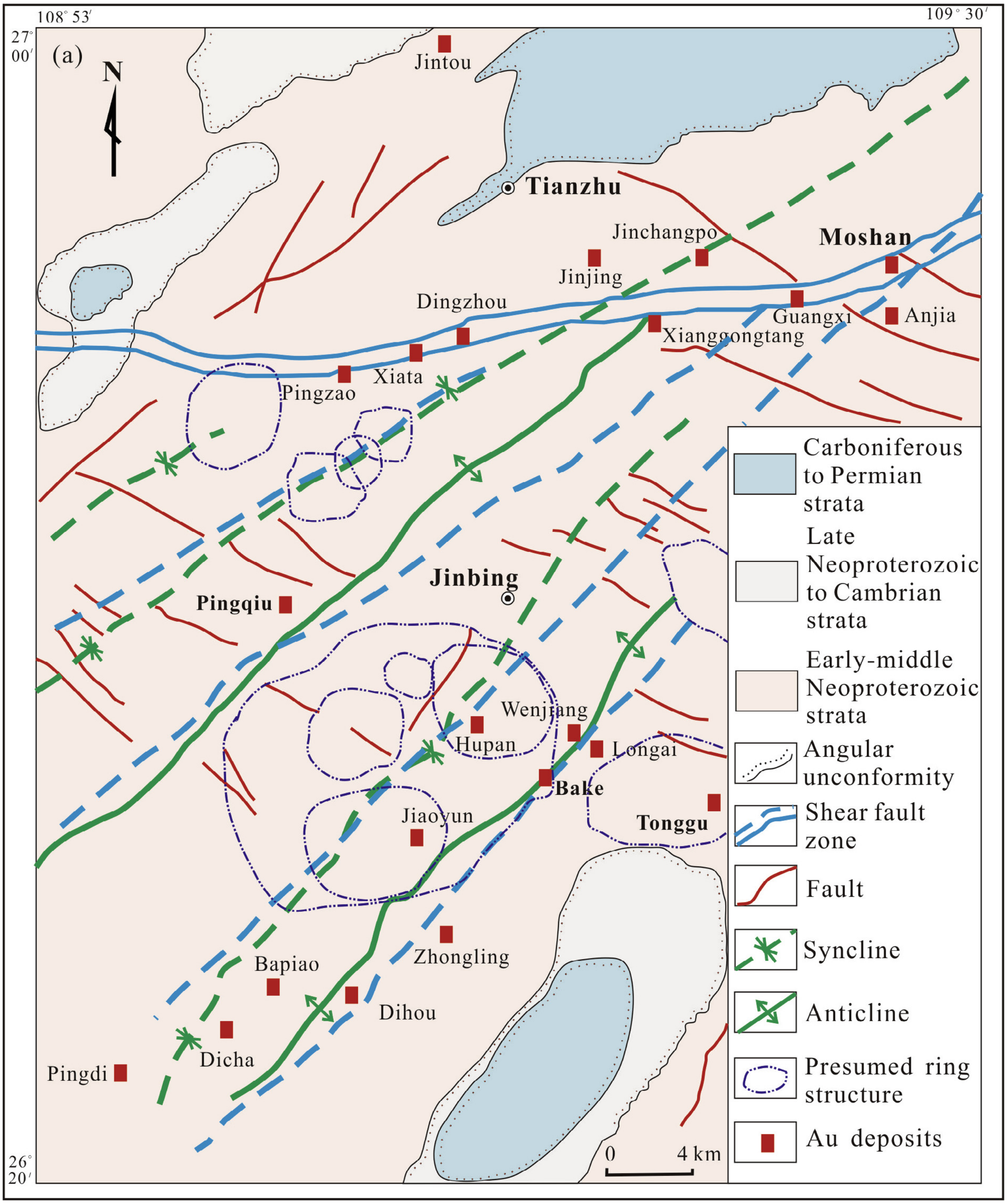

Fig. 11. Geological and structural map of the Jinping–Tianzhu region in the southeastern Guizhou, modified after Lu et al. (2006).

to 5% in the Bake deposit) (Lu et al., 2006). Weak but widespread silicification, pyritic, arsenopyritic, carbonate, and chloritic alterations have been found to be associated with mineralization (Lu et al., 2006). Yang et al. (2013) speculated that there may be hidden mafic–ultramafic and granitic plutons in the region, although no intrusions or dykes have been found in the mining district.

The bedding-parallel Au orebodies often display stratiform, stratiform-like, saddle and lenticular shapes, and are generally characterized by banded and massive structures. The banded structures are highlighted by alternating quartz or sulfide bands with host-rock bands. Brecciated, miarolitic and drusy structures are also abundant in the thick ore veins, suggesting their fillings in extensional fractures. Native gold, pyrite, arsenopyrite, sphalerite and galena are the main Au-bearing minerals, with tetrahedrite, chalcopyrite and/or magnetite or limonite as the minor ore minerals. Gangue minerals are predominantly quartz (more than 95 vol%), with subordinate amounts of ankerite, calcite and chlorite, and minor carbonaceous material, sericite and clay. Native gold occurs as filling in fissures and voids of Au-bearing quartz veins, with the grain sizes ranging from <0.1 mm to 0.8 mm, locally up to 0.5 cm. The fineness of native gold varies from 935 to 980. Minor invisible gold is present as sub-μm to μm-sized inclusions within sulfides (Lu et al., 2006). Four stages of mineralization have been proposed, including: 1) white quartz stage, 2) pyrite + quartz + native gold stage, 3) galena + sphalerite + native gold stage, and 4) calcite + quartz stage, from early to late (Lu et al., 2006).

3.5. Au mineralization in northern Guangxi Province

Gold mineralization in northern Guangxi Province mainly occurs in the middle Neoproterozoic Danzhou Group composed of siltstone, phyllite, sandstone and mafic volcanic rocks (spilites, tuffs) of greenstone-facies metamorphism. Meta-mafic to ultramafic rocks of ca. 980 Ma (zircon U–Pb; Gan et al., 1996) intercalated within the Danzhou Group in this region were regarded as ophiolitic rocks equivalent to those found in southern Anhui and northeastern Jiangxi Province (Chen et al., 1991). Due to the thick Quaternary cover and limited geological investigation, only small-scale auriferous quartz veins and altered cataclasite ores have been discovered and mined so far (e.g., the Fenshuiao deposit and the Baizhushan and Yutang mineral showings; Wu et al., 2012). However, the occurrences of Neoproterozoic host rocks, altered cataclasite zones and Mesozoic granitic intrusions imply a good metallogenetic potential in this region.

The Au deposits and mineral showings in northern Guangxi Province are featured by the metal assemblage of Au–Ag–Sb–As (Zhang, 1991), and mainly occur along the subsidiary NE-trending shear fracture zones closely associated with the regional NE–NNE-trending faults and EW-trending folds (Luo and Chen, 1995). Silicification, sericitic and pyritic alterations are well developed within the mineralized cataclasite zones, and chloritic, pyritic, potassic and sericitic alterations are present around these zones. The average grades of Au and Ag range from 5 to 7 g/t and from 170 to 320 g/t, respectively, indicating low Au/Ag ratios (from 1/1 to 1/67), and the Au fineness ranges from 500 to 600. Compared to those in other provinces, the gold deposits in northern Guangxi appear to have relatively high contents of pyrite (generally >50%), argentite and electrum.

4. Origin and nature of the ore-forming fluids

In order to constrain the origin and nature of ore-forming fluids for the Au (-polymetallic) deposits in the JOB, previously published C, H, O, He–Ar, S and Pb isotopic data as well as fluid inclusion data (Appendices A2–A5), together with the results of new S and Pb isotopic analyses on thirty-seven sulfide separates from lode gold ores of the Wangu, Huangjindong and Yanlinsi deposits in northeastern Hunan Province (Appendices A2–A3), are compiled. The new analytical work was done in the Yichang Institute of Geology and Mineral Resources, Chinese Geological Academy of Sciences, where a Finnigan MAT261 surface ionisation mass spectrometer equipped with 7 Faraday Cup Collectors was used. More details of the analytical method can be found in Ma et al. (1998).

4.1. Sulfur (S) isotopes

The $\delta^{34}S_{VCDT}$ values of sulfide minerals from the Au (-polymetallic) deposits of the JOB are presented in Appendices A2-1–A2-4. Pyrite separates in Au-bearing quartz veins from the Huangshan deposit, northwestern Zhejiang Province, have $\delta^{34}S_{VCDT}$ values ranging from −1.74 to +4.26‰ (Fig. 12), suggesting an origin of sulfur either from their host intrusions (+1.77 to +2.85‰; Ye et al., 1994) or from deep-seated magmas. The Jinshan and Hamashi deposits in northeastern Jiangxi Province have $\delta^{34}S_{VCDT}$ values mostly between +3.1‰ and +7.3‰ (avg. +4.84‰), and between +2.76‰ and +3.40‰ (avg. +3.00‰), respectively (Fig. 12). These $\delta^{34}S_{VCDT}$ values are close to those of the host rocks of the Shuangqiaoshan Group (avg. 4.54‰) but distinct from that for both the Dexing Cu-Mo-Au deposit (including Tongchang, Zhushahong and Fujiawu mines) and associated porphyries (Fig. 12). Therefore, the sulfur of the Au mineralization in the northeastern Jiangxi Province may have been derived from the host rocks rather than from magmatic intrusions.

In the northeastern Hunan Province, the Wangu deposit has depleted $\delta^{34}S_{VCDT}$ values for sulfide minerals (−11.6 to −8.0‰, avg. −9.6‰), approximate to one end-member component of the Lengjiaxi Group (Fig. 12), suggesting a main origin of sulfur from the host rocks. The broad $\delta^{34}S_{VCDT}$ values (−12.9‰ to −3.4‰, Fig. 12) of the Huangjindong deposit suggest extra sulfur sources in addition to that from the Lengjiaxi Group host rocks. In contrast, the Yanlinsi and Jinkengchong deposits have the majority of $\delta^{34}S_{VCDT}$ values ranging from −4.3‰ to −0.2‰ and −0.11‰ to + 0.65‰, respectively. These $\delta^{34}S_{VCDT}$ values are distinct from those of either the Lengjiaxi Group or the Huangjindong and Wangu deposits, but overlapping with those for the intrusion-related Qibaoshan, Aoyushan and Jingchong Cu-polymetallic deposits in the same region (Fig. 12), thus suggesting the Mesozoic intrusions as the dominant source of sulfur. In northwestern Hunan Province, the complex sulfur isotopic compositions for the Au (-polymetallic) deposits are related to different host rocks (Appendix A1). For examples, the Xichong and Woxi deposits have $\delta^{34}S_{VCDT}$ values comparable to those of the Lengjiaxi Group and the Madiyi Formation of the Banxi Group, respectively (Fig. 12), suggesting a major contribution of sulfur from their host rocks. In southwestern Hunan Province, most deposits also have sulfide $\delta^{34}S_{VCDT}$ values similar to their host rocks (e.g., the Mobin, Xiaoniutouzai and Wulipai deposits, Appendices A2-1–A2-4). However, the deviation of $\delta^{34}S_{VCDT}$ values of some deposits from their host rocks (Fig. 12) (e.g., the Yiyangnanjiao and Hexinqiao deposits hosted by the Lengjiaxi Group, the Tongxin, Wangjiacun and Jiangxilong deposits hosted by the Wuqiangxi Formation of the Banxi Group, and the Chanziping and Longshan deposits hosted by the late Neoproterozoic host rocks) suggests contribution of additional sulfur from deep-seated magmatic fluids. Except for several relatively depleted values of −0.96‰ to 5.60‰, most of the $\delta^{34}S_{VCDT}$ values for the Au deposits in southeastern Guizhou Province are +8.3‰ to +13.0‰, with a mean value at +10.61‰ (Fig. 12), also suggesting a main contribution of sulfur from their host rocks.

4.2. Lead (Pb) isotopes

The Pb isotopic compositions of sulfide minerals in the Au (-polymetallic) ore deposits of the JOB are listed in Appendix A3. Most of the Pb isotopic ratios for sulfide minerals from both the Au (-polymetallic) deposits and their Neoproterozoic host rocks in the JOB plot in the field between the upper crust and orogen (Fig. 13). In contrast, both the Mesozoic granitoids and porphyry-related Cu (-polymetallic) deposits in the JOB plot in the mantle- and orogen-derived Pb fields (Fig. 13). The fact that the Au (-polymetallic) deposits have more similarities in Pb isotopic composition to their Neoproterozoic host rocks than to Mesozoic granitoids and associated Cu (-polymetallic) deposits suggests that Pb, and by inference other metals including Au, for Au mineralization in the JOB, were derived from the crust. Involvement of mantle-derived metals into the Au mineralization systems, however, cannot be precluded, as indicated by Fig. 13.

4.3. Carbon (C) and helium (He)–Argon (Ar) isotopes

C and O isotopic data of carbonate minerals (calcite, ankerite and dolomite) from ores and limestones in the host rocks, and C

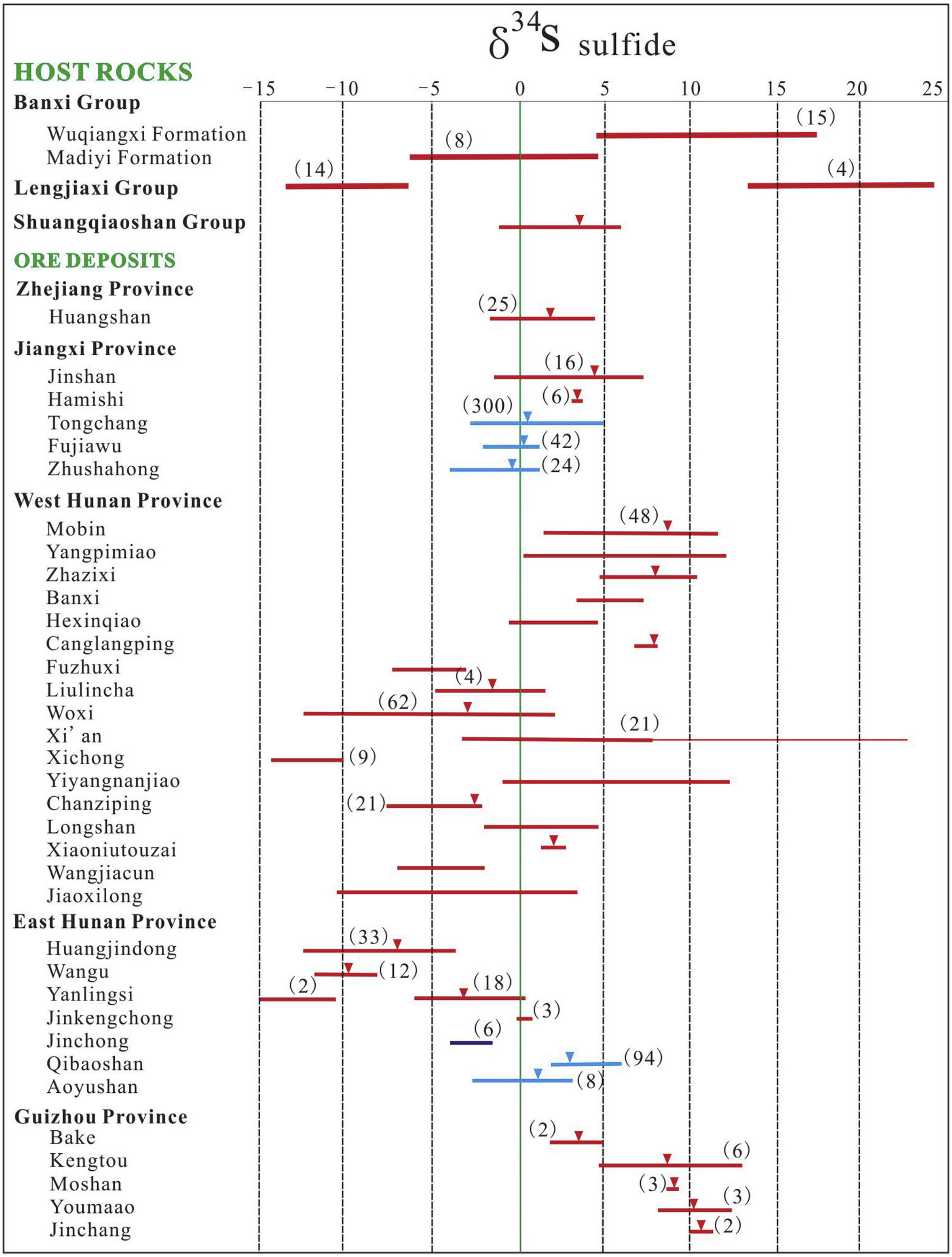

Fig. 12. Comparison of $\delta^{34}S$ values of sulfide separates (pyrite, arsenopyrite, galena, stibnite, sphalerite, chalcopyrite, pyrrhotite, tetrahedrite) from the Au (-polymetallic) deposits, with those in the Neoproterozoic host rocks and intrusion–associated deposits in the JOB. The numbers in bracket represent the analysed sample numbers, and data are from Appendices A2-1–A2-4.

isotopic data of fluid inclusions in quartz of the Au (-polymetallic) deposits of the JOB, are listed in Appendix A4. The carbonate minerals in different types of ores from the Au (-polymetallic) deposits in the JOB have $\delta^{13}C_{VPDB}$ values generally between −6.1‰ and −3.1‰ (Appendix A4), overlapping with both the ranges of mantle (−5 to −7‰) and igneous/magma systems (−3 to −30‰; Hoefs, 2009). This is consistent with the plot of $\delta^{13}C_{VPDB}$ and $\delta^{18}O_{SMOW}$ values within or near the field of granites (Fig. 14), indicating that the CO_3^{2-} or CO_2 in the ore-forming fluids were mainly sourced from magmatic systems. One $\delta^{13}C_{VPDB}$ value of ankerite in the altered host rocks of the Jinshan deposit from northeastern Jiangxi Province is higher than −3.0‰ (Appendix A4 and close to that of

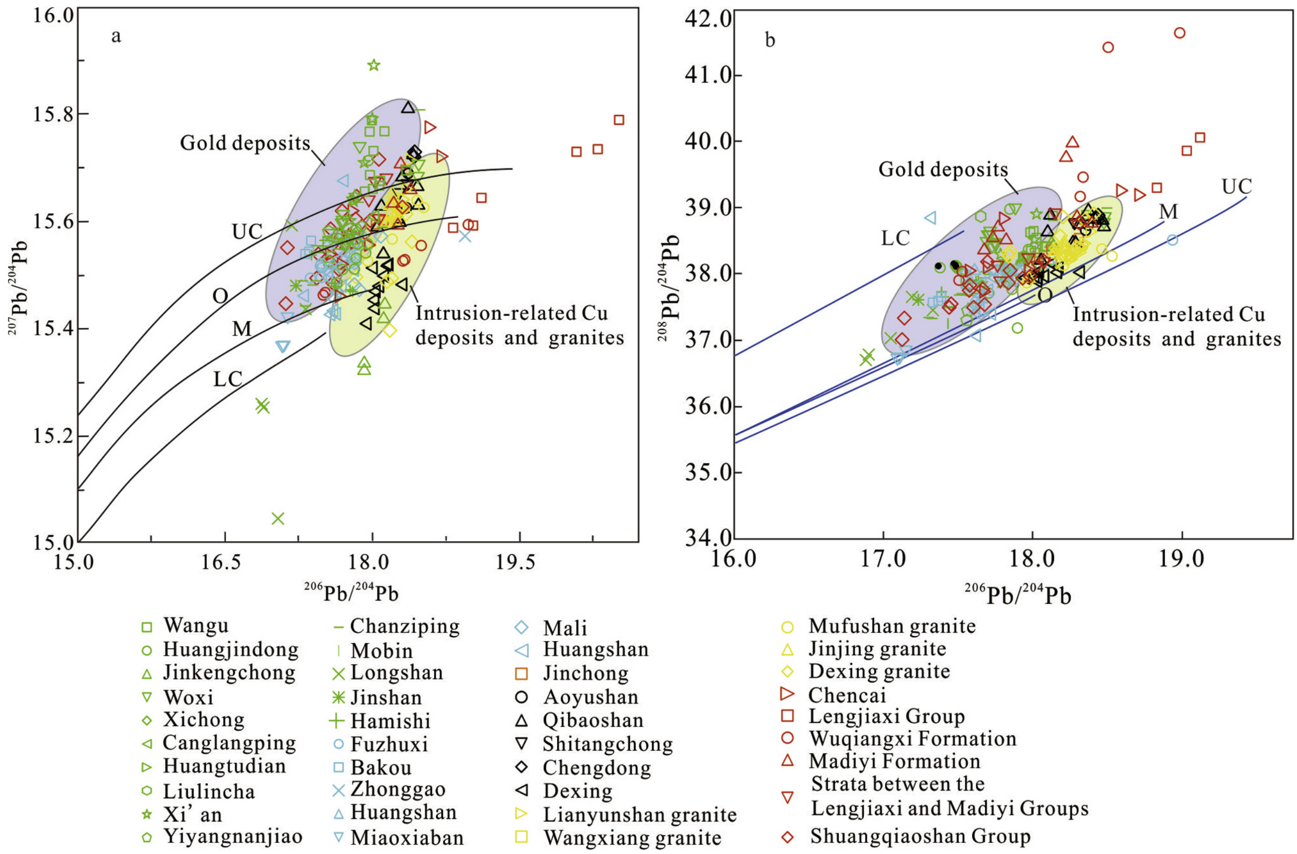

Fig. 13. Plots of lead isotopic compositions in diagrams of (a) $^{207}Pb/^{204}Pb$ vs. $^{206}Pb/^{204}Pb$ and (b) $^{208}Pb/^{204}Pb$ vs. $^{206}Pb/^{204}Pb$ for sulfides, granitoids and wallrocks from the Au (-polymetallic) deposits in the JOB. UC= Upper crust, O= Orogen, M= Mantle, and LC= Lower crust. The average growth lines are from Zartman and Doe (1981). Data are from Appendix A3.

marine carbonates (~0‰; Hoefs, 2009), suggesting a strong low-temperature alteration and/or an origin of CO_3^{2-} or CO_2 in the ore fluids from host rocks (Fig. 14). Similar interpretation can also be made for the Xi'an deposit in Hunan Province, where the limestones in the Neoproterozoic host rocks have $\delta^{13}C_{VPDB}$ and $\delta^{18}O_{VSMOW}$ values of −3.76 to −0.58‰ and +15.80 to +17.56‰, respectively (Appendix A4 and Fig. 14). $\delta^{13}C_{VPDB}$ values of fluid inclusions in quartz are from −0.5 to +2.5‰ for the Jinshan deposit in northeastern Jiangxi Province, and from −7.98 to −2.34‰ for the Tonggu deposit in southeastern Guizhou Province (Appendix A4), suggesting an abiogenic CO_2 (e.g., Luo et al., 2014). The low $\delta^{13}C_{VPDB}$ values of −11.7 to −11.0‰ for fluid inclusions of quartz from the Chanziping deposit in Hunan Province are similar to those of host rocks, indicating a crustal source for CO_2 with possible involvement of organic matter. Thus we suggest that both the dissolution of the marine carbonates and magmatic fluids contributed to the carbon in the ore-forming fluids of Au (-polymetallic) deposits in the JOB.

Fluid inclusions from sulfides (pyrite, stibnite and arsenopyrite) intergrown with quartz in auriferous quartz veins have $^{3}He/^{4}He$ (R/Ra) and $^{40}Ar/^{36}Ar$ values of 0.15 to 0.24 and 575 to 3,060 for the Jinshan deposit in northeastern Jiangxi Province (Li et al., 2010a), 3.5 to 9.8 and 389 to 822 for the Wangu deposit (Mao et al., 2002) and 0.002 to 0.281 and 230 to 2,586 for the Woxi deposit (Zhu and Peng, 2015) in Hunan Province, and 0.035 to 0.078 and 1,046 to 6,929 for the Pingqiu deposit in southeastern Guizhou Province (He et al., 2015), respectively. The He and Ar isotopic values suggest that variable amounts of mantle-derived, crust-derived, and meteoric fluids were involved in the minralizing fluids responsible for Au mineralization in the JOB.

4.4. Hydrogen (H) and oxygen (O) isotopes

The available O and H isotopic data of fluid inclusions in quartz from the Au (-polymetallic) deposits in the JOB are presented in Appendix A5. The $\delta D_{H2O\text{-}VSMOW}$ and $\delta^{18}O_{H2O\text{-}VSMOW}$ values of ore-forming fluids range from −91‰ to −63‰ and from −5.6‰ to −2.8‰ in northwestern Zhejiang Province, and from −90‰ to −30‰ and −0.8‰ to +11.4‰ in northeastern Jiangxi Province, respectively. The $\delta D_{H2O\text{-}VSMOW}$ and $\delta^{18}O_{H2O\text{-}VSMOW}$ values for various types of ores from different mineralizing stages are −73‰ to −38‰ and +1.6‰ to +10.9‰ in northeastern Hunan Province, −118‰ to −45‰ and −0.6‰ to +19.2‰ in northwestern Hunan Province, and −86‰ to −37‰ and −0.4‰ to +9.0‰ in southwestern Hunan Province, respectively (Appendix A5). $\delta D_{H2O\text{-}VSMOW}$ and $\delta^{18}O_{H2O\text{-}VSMOW}$ values for the Au (-polymetallic) deposits vary from −68‰ to −48‰ and from −5.9‰ to −5.5‰ in northern Guangxi Province, and from −93‰ to −33‰ and −3.6‰ to +12.3‰ in southeastern Guizhou Province, respectively. Most of the H and O isotopic data plot within or close to the magmatic- and/or metamorphic water fields (Fig. 15), indicating that either or both of them have contributed to the Au mineralization in the JOB. However, some of the $\delta D_{H2O\text{-}VSMOW}$ values are significantly lower than that of the typical magmatic or metamorphic waters, and some of the H and O isotopic data are plotted in the field between the metamorphic and magmatic waters and the meteoric waters (Fig. 15). This may be attributed to the H isotope fractionation during magmatic degassing (Rye, 1993), input of meteoric waters or basinal brines, and/or contamination by secondary fluid inclusions (Yang et al., 2017).

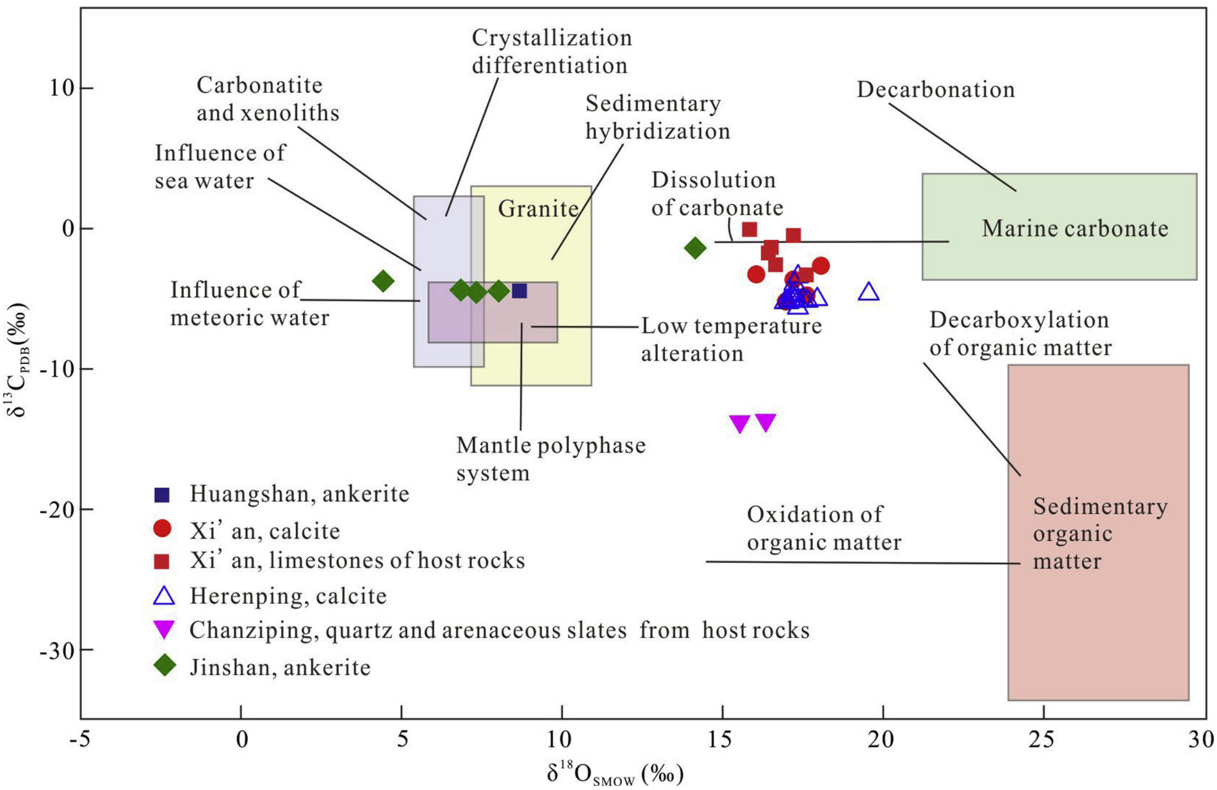

Fig. 14. $\delta^{13}C$–$\delta^{18}O$ diagram of carbonate minerals, limestones and fluid inclusions in quartz (data from Appendix A4) from the Au (-polymetallic) deposits in the JOB, modified after Li et al. (2010a).

4.5. Fluid inclusion data

The major parameters (homogenization temperature, pressure, salinity, oxygen fugacity and pH) of the fluid inclusions in gangue (quartz, ankerite) and ore minerals (scheelite, stibnite, wolframite) from the Au (-polymetallic) deposits in the JOB are compiled and listed in Appendix A5. For most of the Au (-polymetallic) deposits in the JOB, the fluid inclusions in ore and gangue minerals are dominantly biphase (liquid + vapor) inclusons with variable V/L ratios, with subordinate pure aqueous liquid- and CO_2-rich vapor-dominated types, and minor daughter mineral-bearing liquid–vapor type (Liu, 1989; Niu and Ma, 1991; Ji et al., 1994a, 1994b; Yan et al., 1994; Ye et al., 1994; Luo, 1996; Liu et al., 2005b; Ding and Wang, 2009; Li et al., 2011; Yu and Yu, 2011; Zhao et al., 2013a, Ni et al., 2015). Compositionally, the ore fluids for the Au (-polymetallic) deposits in the JOB are generally relatively reductive ($f_{O2} = 10^{-52}–10^{-13}$) and near-neutral (pH = ~6) in nature (Appendix A5), and consist of $H_2O + CO_2 + Na^+ + K^+ + Ca^{2+} \pm Cl^- \pm CO \pm CH_4 \pm HCO_3^- \pm SO_4^{2-} \pm N_2 \pm H_2$, with high but variable contents of CO_2 (1.2 to 509.0 ppm) and Na^+/K^+ (0.5 to 50.0) and CO_2/H_2O (up to 44) ratios (Luo et al., 1984; Zhang, 1985; Liu, 1989; Zhou et al., 1989; Yu, 1990; Ma and Liu, 1991; Niu and Ma, 1991; Fan and Li, 1992; Liu and Wu, 1993; Liu et al., 1994a, b; Yan et al., 1994; Ye et al., 1994; Luo, 1996; Wang and Zhang, 1997; Yu, 1997; Peng and Hu, 1999; Hua et al., 2002; Zeng et al., 2002b; Chen, 2003; Liu et al., 2005b; Wu et al., 2005; Wu, 2009; Li et al., 2011; Tian et al., 2011; Yu and Yu, 2011; Zhao et al., 2013a). The homogenization temperatures of fluid inclusions fall in two main ranges, one from 200 °C to 300 °C, and the other from 150 °C to 180 °C (Fig. 16b). There is a general trend of decreasing homogenization temperatures from early- to late stages of mineralization (Appendix A5 and Fig. 16). The calculated pressures of the ore fluids are mostly between 0.20 kb and 0.99 kb, corresponding to the depths of ~1 to 4 km assuming a lithostatic pressure system (Appendix A5). The dominant salinities of the ore fluids concentrate between 2 and 10 wt.% NaCl $_{equiv}$. (Fig. 16b), although unusually high salinities of 26.5 to 41.9 wt.% NaCl $_{equiv}$. were reported in the Au deposits from northwestern Zhejiang Province, due to the presence of daughter mineral-bearing inclusions (Ye et al., 1994; Ni et al., 2015). Based on the high CO_2 contents, low-medium mineralizing temperatures (< 300 °C), and low salinities (< 10 wt.% NaCl $_{equiv}$.), together with an integration of the C, H, O, He–Ar, S and Pb isotopic data, the ore-forming fluids for Au mineralization in the JOB are inferred to be dominated by metamorphic and/or magmatic waters, with variable input of mantle-derived fluids and meteoric waters.

5. Gold mineralization ages in the JOB

A number of geochronological studies related to Au (-polymetallic) mineralization in the JOB have been carried out, yielding a wide range of mineralization ages from ca. 1.0 Ga to ca. 70 Ma (e.g., Wan, 1986; Luo, 1989; Ye et al., 1993; Chen and Xu, 1996; Mao and Wang, 2000; Li et al., 2003a; Peng et al., 2003; Li et al., 2007a; Dong et al., 2008; Li et al., 2008b; Mao et al., 2013a; Ni et al., 2015). The analytical methods and minerals used include: 1) Ar–Ar dating on quartz separated from ore veins (e.g., Peng et al., 2003; Li et al., 2007a); 2) Sm–Nd dating on scheelite separated from ore veins (e.g., Peng et al., 2003); 3) Rb–Sr dating on whole rocks, ores, illite separated from ores, and fluid inclusions extracted from quartz veins and sulfides (e.g., Chen and Xu, 1996; Mao and Wang, 2000; Li et al., 2008b; Mao et al., 2013a; Ni et al., 2015); 4) K–Ar dating on whole-rock samples of host rocks, and K-feldspar and illite separated from altered host rocks (e.g., Wan, 1986; Li et al., 2003a); 5) Re–Os dating on

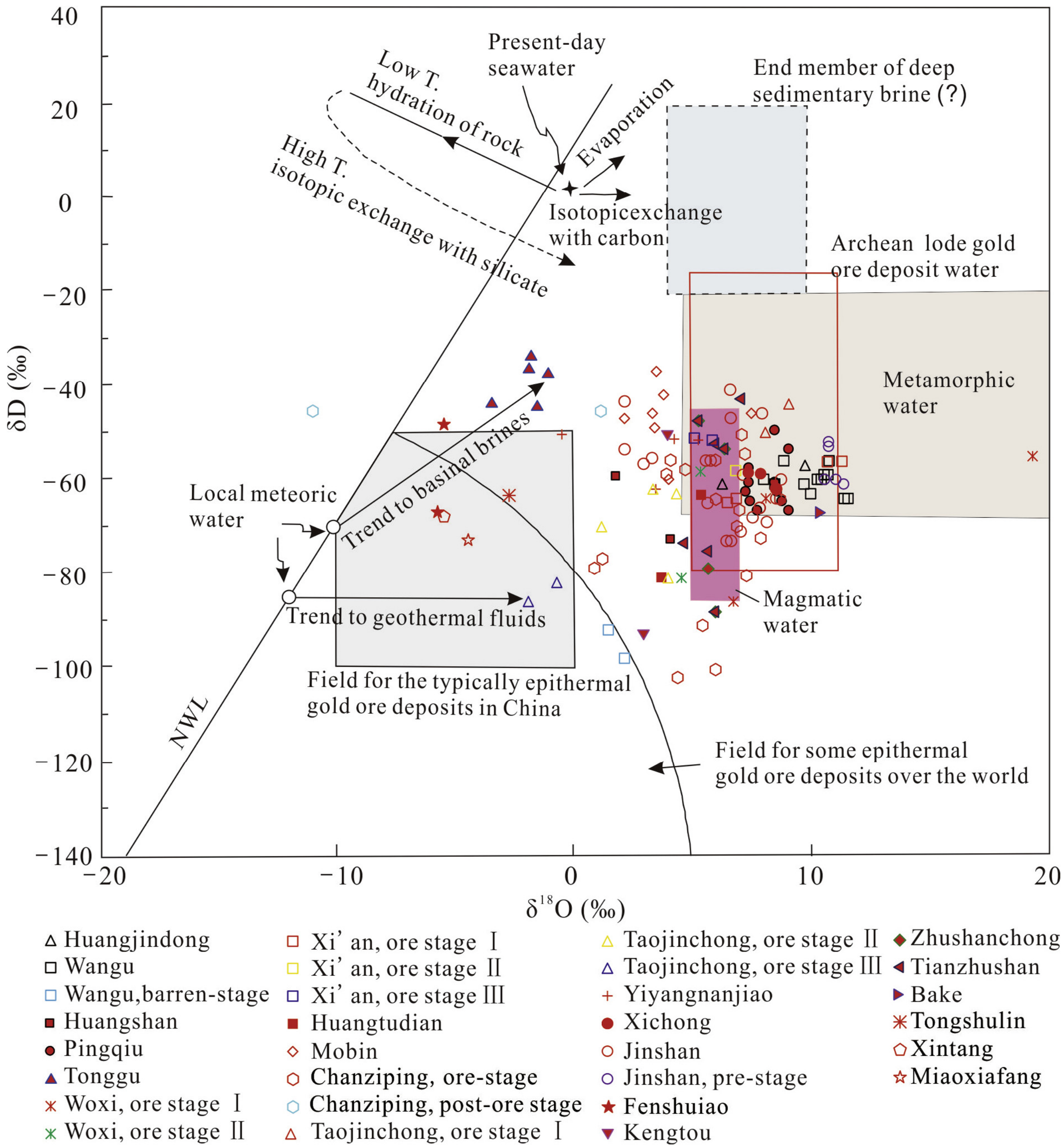

Fig. 15. δD and calculated $\delta^{18}O$ characteristics of ore fluids for the Au (-polymetallic) deposits in the JOB. Data are from Appendix A5. The fields for some epithermal gold deposits and juvenile water are from Ohmoto (1999), the fields for Archean lode Au deposit water and metamorphic waters from McCuaig and Kerrich (1998), and the field for the typically epithermal gold deposits in China from Zhao and Tu (2003), respectively.

arsenopyrite separated from Au-bearing ore veins (Wang et al., 2011a); 6) fission–track dating on quartz separated from ores (Hu et al., 1995); 7) ESR (Electron Spin Resonance) dating on quartz from Au-bearing quartz veins (Huang et al., 2012); and 8) Pb model ages calculated from Pb isotopic components of pyrite and galena separated from ores (e.g., Ye et al., 1993). The ages of (altered) granitoids around or in the Au (-polymetallic) mining districts in the JOB, dated by the zircon SHRIMP and LA-ICPMS U–Pb, and the ages of sericite and muscovite dated by the Ar–Ar method, also provide constraints on the mineralization ages (Appendix A6).

Given the methods and samples used, the reported mineralization ages using different methods need to be evaluated with caution. For example, the Rb–Sr isochron ages generally have relatively large errors (up to ±110 Ma; e.g., Mao et al., 2013b), due to the isotopic resetting corresponding to multistage tectonothermal or tectonomagmatic events in the JOB, or due to involvement of variable proportions of primary and secondary fluid inclusions in the samples analyzed. Given the uncertainty of the Rb–Sr dating method on fluid inclusions in quartz (Pettke and Diamond, 1995) and the Pb model ages (Bielicki and Tischendorf, 1991), most of the ages obtained from these two methods were not considered in this study. Likewise, the Sm–Nd isochron ages obtained from some calcic minerals (e.g., fluorite, calcite, scheelite, tourmalite) and fluid inclusions are likely of large

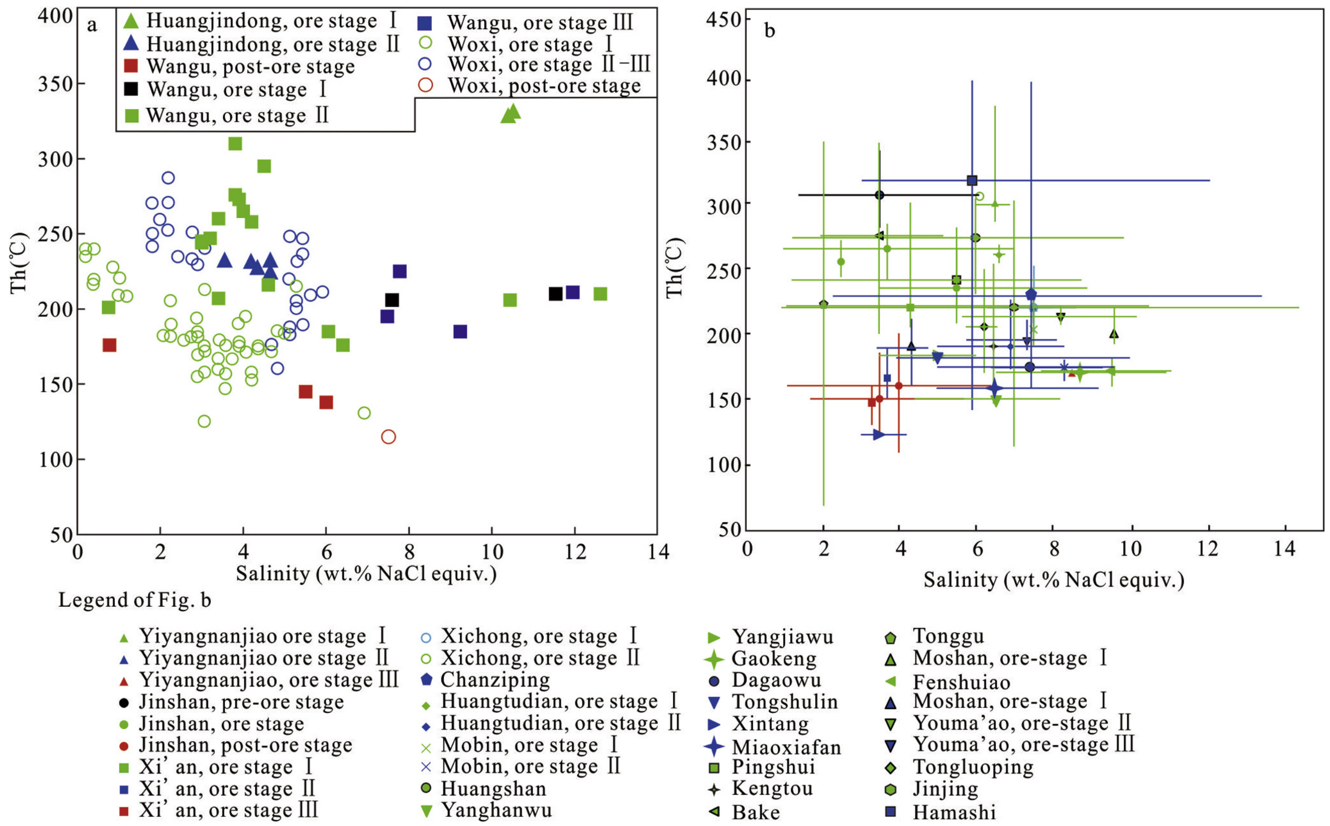

Fig. 16. Characteristics of fluid inclusions in quartz of (a) the Wangu, Huangjindong and Woxi deposits, and (b) other Au (-polymetallic) deposits in the JOB. Data are from Appendix A5.

errors, due to potential initial isotopic heterogeneity and secondary disturbance by overprinting events (Nägler et al., 1995). The age dating methods using fission-track and ESR, and K–Ar and Ar–Ar dating on the K-feldspar and illite also warrant a caution, because they are prone to isotopic resetting by overprinting thermal events. Closure temperatures for argon retention are generally believed to range from 350 °C to 450 °C, 325 °C to 400 °C and 300 °C to 350 °C for muscovite, biotite and sericite, respectively (Harrison et al., 1985; Lee, 2009; Yang et al., 2014), whereas closure temperatures are below 150–100 °C and 260±30 °C for K-feldspar and illite, respectively (Hunziker et al., 1986; Lee, 2009).

Given the limitation of the above-mentioned dating methods, an integrated consideration of the ages with different methods is generally required. For example, Peng et al. (2003) reported two Ar–Ar plateau ages of ca. 423 Ma and 416 Ma together with their isochron age of ca. 422 Ma and 415 Ma for quartz separated from Au-bearing ore veins in the Woxi deposit, northwestern Hunan Province. In combination with the field investigation and microscopy observation, the consistency among the minimum apparent age, plateau age and isochron age within errors, together with the initial $^{40}Ar/^{39}Ar$ ratios coincident with the Nier value (295.5), reveal the reliability of the measured Ar–Ar age data. Furthermore, the minimum apparent Ar–Ar ages are in good agreement with the Sm–Nd age of 402 ± 6 Ma of the disseminated sheelite coeval with native gold. The high Sm contents (relative to Nd) and high and variable Sm/Nd ratios, which are favorable for the Sm–Nd dating, together with the small range of $\varepsilon_{Nd}(t)$ from −30.82 to −30.73 for the disseminated scheelite, suggest that the isochron age should represent the precipitation age of scheelite in the Woxi deposit. In the same region, an Ar–Ar plateau age of ca. 422–397 Ma for quartz from Au-bearing quartz veins in the Banxi deposit was also reported (Peng et al., 2003). These ages are consistent within error with the Re–Os isochron age of 400 ± 24 Ma of arsenopyrite from ore veins in the Pingqiu deposit, southeastern Guizhou Province (Wang et al., 2011a). Therefore, it is believed that there was an early Paleozoic Au metallogenic event in the JOB.

The Jurassic mineralization ages are also common in the JOB. For example, a Re–Os age of 174 ± 15 Ma was obtained from arsenopyrite in Au-bearing quartz veins in the Jinjing deposit of southeastern Guizhou Province (Wang et al., 2011a). This age is consistent within error with the molybednite Re–Os, zircon U–Pb and muscovite Ar–Ar ages of ca. 177–170 Ma for the Dexing–Yinshan porphyry–epithermal Cu–Au–Ag polymetallic mineralizing system in Jiangxi Province (Wang et al., 2004; Li et al., 2007b; Liu et al., 2012; Zhou et al., 2012a; Wang et al., 2015). These ages are interpreted to represent a second metallogenic event in the JOB, corresponding to the subduction of the Paleo-Pacific plate beneath the South China continental margin (Mao et al., 2013a).

Recently, we carried out Ar–Ar dating of muscovite from two muscovite-bearing silicified rock samples present as quartz veins that cut across the Changsha-Pingjiang fault zone which hosts the Dayan Au occurrence in northeastern Hunan Province (Fig. 2; Deng et al., this issue). The obtained Ar-Ar plateau ages are 130.3 ± 1.4 Ma (MSWD = 0.9) and 130.3 ± 1.4 Ma (MSWD = 1.06), and the Ar-Ar isochron ages are 130.6 ± 6.1 Ma (MSWD = 0.093) and 127.9 ± 5.9 Ma (MSWD = 0.036), respectively (Deng et al., this issue and unpublished data). The pre-mineralization Lianyunshan granites, which have an emplacement contact with the Changsha-Pingjiang fault zone, yielded a zircon LA-ICPMS U–Pb age of 144 ± 1.7 Ma (Deng et al., this issue). Considering the common geological characteristics shared by the Dayan gold occurrence and most of the Au deposits (e.g., Wangu and Huangjingdong) in northeastern Hunan Province, the gold mineralization age in this region is constrained at ca. 144–130 Ma. This age interval is in accordance with a widespread early Cretaceous (ca. 150–120 Ma) magmatic event and associated W–Cu polymetallic mineralization (ca. 140–120 Ma) in the JOB (e.g., Chen et al., 2012, 2016; Xiang et al., 2015). Therefore, a third Au metallogenic event in the JOB is inferred to have occurred in the early Cretaceous, in response to the extensional tectonic setting due to slab rollback of the subducted Paleo-Pacific plate (Li and Li, 2007) or an adjustment in the angle of convergence of the Izanagi plate from oblique to parallel to the coastline (Mao et al., 2013a).

In summary, based on the published and our new geochronological data, the JOB may have experienced three epochs of Au mineralization, that is, late Silurian to early Devonian, mid–late Jurassic, and early Cretaceous. The multistage mineralization corresponds to the multiple tectonothermal events characterized by synchronous structural deformation and large-scale granitic magmatism in South China (Li, 1998; Shu et al., 1999, 2014; Zhou et al., 2006; Li and Li, 2007; Sun et al., 2007; Li et al., 2008a; Chen et al., 2011a; Wang et al., 2013a; Mao et al., 2014; Zhu et al., 2014).

6. Types of Au mineralization in the JOB

There has been a debate on the ore genesis of the Au (-polymetallic) deposits in the JOB, including SEDEX-type, orogenic-type, and intrusion-related (Mao and Li, 1997; Gu et al., 2007, 2012; Dong et al., 2007). A key evidence used to support the SEDEX model, as proposed for the Woxi deposit in Hunan Province by Gu et al. (2007, 2012), was the occurrence of stratiform ores immediately overlying stockwork ores. The predominant stratiform ores in the Woxi deposit (>70% ore volumes) consist of rhythmically laminated Au-bearing quartz, sulfides and scheelite, and *meta*-sediments at both macro- and micro-scales (Gu et al., 2007, 2012). The subordinate Au–Sb–W-rich stringer stockworks underlie the stratabound ore layers and are generally subperpendicular to them. In addition, Gu et al. (2007) concluded a pre-metamorphism mineralization based on the folding of the ore layers along with their host rocks. Other lines of evidence in favor of the SEDEX model include: 1) the conformable and sharp contacts between different microbands, which is distinct from a complicated, laterally zoned gangue mineral assemblages generated by a replacement scenario (Gu et al., 2007, 2012); 2) the thicker and more intensive alteration in the footwall than in the hanging wall of the Woxi fault, which is distinct from the alteration pattern of typical epigenetic, hydrothermal replacement or infilling ore deposits (Gu et al., 2012); 3) the pronounced LREE enrichment in fluid inclusions, ores and associated minerals comparable to those of many SEDEX-type deposits, indicating a seawater source for the mineralizing fluids; and 4) the $\delta^{34}S$ values of pyrite from ore veins slightly lower than that of the Madiyi Formation host rocks of the Banxi Group (Fig. 12), indicating a major contribution of sulfur from bacterial reduction of contemporaneous marine sulfates (Gu et al., 2012). However, most of the geological and geochemical features described above cannot be conclusively used to support the SEDEX model. Many epigenetic, fault-controlled deposits, like orogenic and Carlin-type Au deposits, also have ore veins parallel to bedding (Groves et al., 1998; Goldfarb et al., 2001, 2014; Hu et al., 2002; Cline et al., 2005; Chen et al., 2011b). The largely low angle and stratiform Au orebodies of the Carlin-type deposits may have root zones that project toward high-angle feeder faults (Cline et al., 2005). Likewise, epithermal Au deposits have both low-angle stratiform and steep ore veins (Simmons et al., 2005). The folding in the Woxi deposit depicted by Gu et al. (2012) might have occurred simultaneously with or subsequently to the metamorphism and mineralization. Furthermore, the differences in $\delta^{34}S$ values of pyrite between ores and host rocks might just imply a crustal sulfur source for the Woxi deposit. Even if the fluid inclusions have very high La/Yb_N ratios (28–248), both the bulk ores and individual minerals have much lower La/Yb_N ratios (4.56–11.37), which are comparable to those of many granites and (meta)sediments (Taylor and McLennan, 1985; Gu et al., 2002; Li et al., 2005a; Xu et al., 2009). The low-salinity and CO_2-rich nature of the ore fluids (e.g., Zhu and Peng, 2015) is also inconsistent with that of typical SEDEX deposits (Large et al., 2005). Significantly, the ca. 423–416 Ma Ar–Ar ages (Peng et al., 2003) for the Au-bearing ore veins are much younger than the host rocks, and thus argue against the syngenetic mineralization model. Putting all these arguments together, the Woxi deposit, and by extension other Au (-polymetallic) deposits in the JOB, cannot be classified as SEDEX-type.

An intrusion-related model was also proposed for the Au mineralization in the JOB. Various mafic to felsic dikes have been found in some of the mining districts (Appendix A1). Most of the Au deposits and mineral showings in northeastern Hunan Province (Fig. 2) occur surrounding late Mesozoic plutons, despite the lack of granitoids within these mining districts. The presence of positive aeromagnetic and low gravity anomalies in some ore districts and their adjacent areas further suggests that hidden plutons may exist in depth (Yang et al., 2013; Wen et al., 2016). In addition, the Mesozoic mineralization ages yielded from the Ar–Ar, LA–ICPMS and Re–Os dating methods is genetically linked to the Mesozoic intrusions. Mao and Li (1997) interpreted the S, Pb and H–O isotopic data for the Wangu deposit in northeastern Hunan Province as an indicator of ore fluids sourced from both the Neoproterozoic host rocks and the late Mesozoic intrusions. Because of the similarities in ore mineral paragenesis to the neighboring Liaojiaping Au deposit, which has a close association with the Mesozoic granite porphyries (Fig. 3), Peng and Frei (2004) suggested that the Woxi deposit in northwestern Hunan Province is genetically linked to the Mesozoic granitic magmatism. However, most of the Mesozoic granite intrusions near the Au (-polymetallic) deposits in the JOB are ilmenite-series or S type, which are different from those of major intrusion-related Au ore deposits (Groves et al., 2003). Furthermore, the fluid inclusion data from the Au (-polymetallic) deposits in the JOB indicate lower salinities and temperatures than those of the intrusion-related deposits (e.g., Zachariáš et al., 2014). Therefore, the Au (-polymetallic) deposits in the JOB may not be best described as granite intrusion-related type.

Some previous studies also assign the Au mineralization in the JOB (Groves et al., 1998, 2003; Goldfarb et al., 2001; Zhao et al., 2013a; Ni et al., 2015; Zhu et al., 2015) into the orogenic category. The main arguments for this classification scheme include: 1) the Au mineralization is developed within an orogen (JOB); 2) most of the Au (-polymetallic) deposits are hosted by low-grade Neoproterozoic metamorphic rocks; 3) the Au mineralization is primarily controlled by shear fractures; 4) the fluid inclusions of the ore-related minerals are characterized by the $H_2O + CO_2 \pm CO \pm CH_4 \pm H_2$ composition system with low salinities; 5) the O and H isotopic data of ore fluids largely overlap with those found in orogenic gold deposits; and 6) the $\delta^{34}S$ values are generally between −5 and +10 ‰, comparable to those of orogenic-type gold deposits. However, the relatively low homogenization temperatures and mineralization depths inferred from fluid inclusion data for the Au (polymetallic) deposits are not typical of orogenic Au deposits, although they can still be accommodated in the epizonal setting in an orogenic-type scheme (Groves et al., 1998). More importantly, the inference that the main Au mineralization in the JOB took place in an extensional tectonic setting in the late Jurassic to Cretaceous, as further discussed below, is incompatible with the accretionary (Groves et al., 2000) or collisional (Chen, 2013) orogenic environment generally assumed for orogenic-type Au deposits.

On the other hand, the Au (-polymetallic) deposits formed during the Cretaceous in the JOB share similarities with the Carlin-type gold deposits in terms of tectonic setting. The Carlin-type Au deposits in North America were considered to be formed in an extentional regime (Cline et al., 2005; Kesler et al., 2005; Muntean et al., 2011) and southwest China (Hu et al., 2002; Su et al., 2009a, 2012). The typical Basin-and-Range tectonic pattern in South China including the JOB, comparable to that in Nevada of Noith America (Cline et al., 2005; Muntean et al., 2011), has also been interpreted as a result of intracontinental extension of the South China Block during the late Mesozoic (Shu and Wang, 2006; Li and Li, 2007; Shu et al., 2007). Moreover, the structural control on mineralization, spatio-temporal link to the calc-alkaline granitoids, as well as nature of ore-forming fluids (relatively low temperatures and salinities, CO_2-bearing, and δD and δ^{18}O values suggesting involvement of magmatic, metamorphic and meteoric waters) for the Cretaceous Au (-polymetallic) deposits in the JOB, are also comparable to the typical Carlin-type Au deposits (both in Nevada and China). However, many characteristics of the Au (-polymetallic) deposits in the JOB, including the metamorphic host rocks of siliciclastics, the visible native gold-dominated mineralization, the styles of mineralization as auriferous quartz veins and altered cataclasite, as well as the ore metal association of Au–Sb–W–Cu–Pb–Zn and the absence of decarbonation and argillization, are distinct from those of the Carlin-type deposits (e.g., Hu et al., 2002; Peters, 2004; Cline et al., 2005; Kesler et al., 2005; Su et al., 2009a, 2012; de Almeida et al., 2010; Chen et al., 2011b; Muntean et al., 2011; Hickey et al., 2014).

The presence of porphyry Cu deposits in the periphery of some Au deposits in the JOB, such as the Huangjindong and Wangu (Fig. 2), Jinshan (Fig. 4), and Huangshan deposits (Fig. 3), may suggest a genetic classification of these deposits as epithermal Au deposits (Hedenquist et al., 1996). For example, Ye et al. (1994) proposed an epithermal mineralization model for the Huangshan deposit, based on the presences of Ag-bearing and Hg-bearing minerals, and the high Ag contents in some ore veins. However, most of the Au (-polymetallic) deposits in the JOB are hosted in the metamorphic volcaniclastic rocks and have low-angle ore veins generally parallel to the bedding, which is in contrast to most epithermal Au deposits. The latter is hosted by volcanic rocks and characterized by steep veins (Bissig et al., 2002; Simmons et al., 2005; Zhai et al., 2009; Jiang et al., 2013; Simpson et al., 2015). Furthermore, most of the Au (-polymetallic) deposits in the JOB lack alteration mineral assemblages including kaolinite, adularia and alunite indicative of epithermal mineralization, and the low Ag contents and high Au/Ag ratios in sulfides are distinct from those for typical epithermal Au deposits (Simmons et al., 2005).

In summary, although the Au (-polymetallic) deposits in the JOB are comparable with the SEDEX-type, granite intrusion-related, orogenic-type, Carlin-type and epithermal gold deposits to some extent, they cannot be classified into any of them unambiguously. In order to accommodate the various geological and geochemical features, together with the tectonic setting and evolution history, here we propose an umbrella name of "intracontinental reactivation-type" to cover all the Au (-polymetallic) deposits in the JOB. The terms may also be extended either to other regions in South China or to North China Craton where early Cretaceous (ca. 130–120 Ma) Au mineralization has been named "decratonic-type" (Zhu et al., 2015). The South China Block has experienced multiple tectonic events from the Proterozoic to present day, and various structures formed in the earlier tectonic regimes were overprinted and reactivated in the later tectonic events. An important tectonic transformation took place during the Mesozoic, from the ca. 230–210 Ma collisional orogeny, via the ca. 180–160 Ma initial subduction of the Paleo-Pacific plate, to the ca. 150–80 Ma lithospheric thinning and delamination (Zhou et al., 2006; Li and Li; 2007; Mao et al., 2013a). This tectonic transformation, which has previously been termed as the "Yanshanian movement" (Wong, 1927), "Platform reactivation" (Chen, 1956), or "Cratonic destruction" (Zhu et al., 2012), led to the emplacement of voluminous igneous rocks (Zhou and Li, 2000; Li and Li, 2007; Mao et al., 2014), large-scale metallic mineralization (Chen et al., 1998; Zhai et al., 2001; Hua et al., 2003; Mao et al., 2011a, 2013a), and development of a large number of NE- to NNE-trending strike-slip faults, metamorphic core complexes (MCC), and Basin-and-Range like provinces in east China (Ye et al., 1985; Faure el a1., 1996; Li et al., 2004; Shu et al., 2007; Zhang et al., 2007; Lin et al., 2008; Wang et al., 2011b; Zhang et al., 2011; Li et al., 2012, 2013a; Zhang et al., 2012; Li et al., 2013b; Wang et al., 2013b; Shi et al., 2015). Such an extensional tectonic setting, coupled with reactivation of pre-existing structures, provides a favorable environment for Au mineralization, which is the main episode of Au (-polymetallic) mineralization in the JOB.

7. An integrated model for Au mineralization of the JOB

The SCB, as one of three major Precambrian continental blocks (i.e., North China, South China, and Tarim) in China, experienced a multistage tectonothermal evolution since the Proterozoic assembly of the Yangtze and Cathaysia Blocks (Li et al., 2002, 2008a; Wang et al., 2013a; Zhao, 2015; Charvet, 2013). Herein, a multistage model of Au mineralization linked to the tectonic development of the SCB and related tectonomagmatic events is proposed to better described the ore genesis of the Au (-polymetallic) deposits in the JOB.

During the Neoproterozoic, the Lengjiaxi and its overlying Banxi groups, and their equivalents, were deposited in the JOB, with an unconformity between the two groups due to the collision of the Yangtze and Cathaysia Blocks. The Neoproterozoic assembly to form the united SCB and its subsequent breakup generated intensive granitic and mafic magmatic rocks in the JOB. This Neoproterozoic magmatism comprises two epochs, one at ca. 835–800 Ma leading to extensive granitic plutons, and the other at ca. 780–730 Ma yielding bimodal igneous rocks (Li, 1999; Li et al., 2003b; Li et al., 2005a; 2008a). It has been generally accepted that the first epoch was related to the amalgamation of the Yangtze and Cathaysia Blocks, whereas the second epoch took place during the subsequent breakup of the welded SCB (Zhou et al., 2002; Wang et al., 2006, 2012a; Zheng et al., 2007; Zhou et al., 2009; Wang, 2012; Zhao and Cawood, 2012; Zhao et al., 2013b; Yao et al., 2014; Zhao, 2015). Although the exact timing and nature of the assembly between the Yangtze and Cathaysia Blocks have been in debate (Zhou et al., 2002; Li et al., 2008a; Zhou et al., 2009; Wang et al., 2012a; Zhao, 2015), the Neoproterozoic mafic and granitic magmatism may have induced the synchronous Cu–Ni

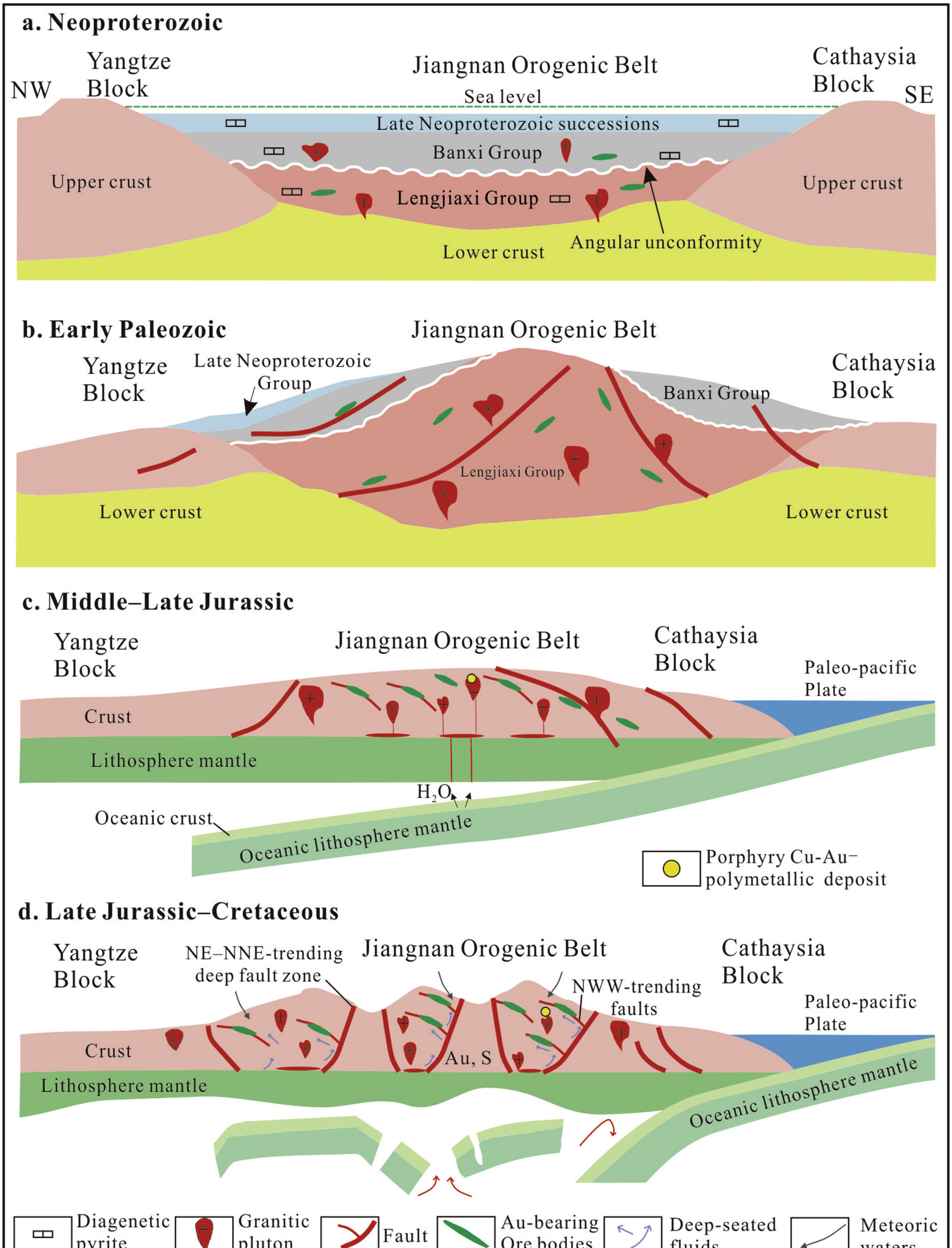

Fig. 17. A conceptual model illustrating the mutistage Au (-polymetallic) mineralization in the JOB. (a) The deposition of the Neoproterozoic Lengjiaxi and Banxi groups, and possible initial Au enrichment from Neopreoterozoic hydrothermal event(s); (b) Early Paleozoic Au mineralizatin and associated metamorphism and magmatism; (c) Large-scale mafic and granitic magmatism and associated Au W, Sn, Bi, and Ag and porphyry Cu–(Mo)–(Au) mineralization in middle–late Jurrassic; and (d) Late Jurrasic–Cretaceous Au mineralization in the extensional Basin-and-Range like province.

sulfide and Sn–Au mineralization in the JOB (Mao and Du, 2001). The hydrothermalism associated with the Neoproterozoic tectono-magmatic and tectonothermal event(s) may have also led to initial Au enrichment most likely sourced from the Neoproterozoic host rocks (Fig. 17a). However, the potential Neoproterozoic Au mineralization events, as suggested by Luo (1988), Liu et al. (1989), Zhu and Fan (1991), and Mao et al. (2008), may have been significantly obscured during subsequent tectonic reworking.

During the early Paleozoic, the SCB went through another tectonothermal event called the Kwangsian event (Wang et al., 2013a). However, there has been a controversy over its tectonic nature and whether it is linked to an intracontinental orogeny or the closure of an oceanic basin. Li (1998), Faure et al. (2009), Li et al. (2010b), Charvet (2013), Wang et al. (2013a) and Shu et al. (2014) argued that the early Paleozoic orogeny, marked by the voluminous Silurian S-type granites and migmatites unconformably overlain by the Devonian succession in the region between the Yangtze and Cathaysia Blocks, occurred within an intraplate environment in nature due to the far-field response to subduction/collision of east Gondwana beyond the southern margin of eastern South China (Chu et al., 2012). This interpretation largely depends on the absence of the early Paleozoic ophiolites and related volcanic rocks, coeval high-pressure blueschists, and mantle-derived juvenile magmatic rocks in South China (Shu et al., 2014). In contrast, other workers (e.g., Hsü et al., 1990; Li, 1993; Yin et al., 1999; Xu et al., 2007; Su et al., 2009b) interpreted the early Paleozoic tectonothermal event(s) as a result of the closure of the late Neoproterozoic to early Paleozoic Huanan Ocean between the Yangtze and Cathaysia Blocks. In any cases, the early Paleozoic tectonothermal event(s) resulted in a swarm of NW- to WNW-trending faults and voluminous granitic intrusions of ca. 445–390 Ma ages in the JOB (Wang et al., 2013a). Slightly earlier at ca. 465–445 Ma (Ni et al., 2015), the Neoproterozoic rocks were subjected to the greenschist to blueschist facies metamorphism. Therefore, the early Paleozoic tectonomagmatic and tectonothermal events likely led to the first epoch of Au (-polymetallic) metallogenesis in the JOB (Fig. 17b) and its adjacent areas (e.g., Peng et al., 2003; Wang et al., 2011a).

Despite of a general consensus that the Mesozoic tectonic development of South China was intracontinental in nature (Li, 1998), various models involving the Mesozoic orogeny or lithospheric thinning had been proposed to elucidate the Mesozoic geodynamics after Hsü et al. (1990). With a magmatic quiescence during the Early Jurassic (205–180 Ma), the Mesozoic granitoids in South China are characterized by two epochs (Zhou et al., 2006), that is, the early Mesozoic (ca. 250–205 Ma) and the late Mesozoic (ca. 180–67 Ma). The genesis of the early Mesozoic granitoids has been in debate. Zhou et al. (2006) and Wang et al. (2013a) argued that the early Mesozoic tectonics of South China was dominated by the Triassic collision of the northern Indochina Block with the SCB along the Song–Ma belt. However, Li and Li (2007) proposed that the flat subduction of Paleo-Pacific plate under the eastern Asian continental margin beginning at the middle Permian controlled the tectonics of the SCB throughout the whole Mesozoic. Zhou and Li (2000) suggested that the westward subduction of the Paleo-Pacific plate was not initiated until around the Mid-Jurassic, because the late Paleozoic to early Mesozoic ophiolites, Permian arc magmatism and foreland basin development have not been unambiguously recognized along the coastal provinces in southeast China so far (Wang et al., 2013a). Nevertheless, Mao et al. (2013a) suggested a contribution of the early Mesozoic tectonothermal event to the Triassic Sn–W–Nb–Ta–Au mineralization in South China. In contrast to the early Mesozoic tectonics, it has been generally accepted that the subduction and subsequent rollback of the Paleo-Pacific plate were responsible for the late Mesozoic tectonomagmatic event(s) in South China (Jahn et al., 1990; Shu and Wang, 2006; Li and Li, 2007; Zhu et al., 2014). Since the middle–late Jurassic, the NW–WNW-ward low-angle or flat subduction of the Paleo-Pacific plate beneath South China continental margin triggered the intensive mafic and granitic magmatism, predominant NE–NNE-trending tectonic pattern and large-scale W, Sn, Bi, Mo, Cu, Ag and Au mineralization of ca. 177–170 Ma ages in South China (Li and Li, 2007; Zhu et al., 2014). This mineralizing event was also recorded by the Cu–Au-polymetallic deposits in the JOB (Fig. 17c). After ca. 160 Ma, the rollback of the subducted Paleo-Pacific plate largely placed the SCB into an extensional tectonic regime. A NE–NNE-trending Basin-and-Range like province together with metamorphic core complex (MCC) formed in the JOB, resembling that in Nevada of North America. Possibly promoted by the late Mesozoic large-scale magmatism, deep-sourced ore fluids ascended and circulated along the NE–NNE-trending strike-slip shear faults in the JOB, leaching ore metals from the Neoproterozoic host rocks or precursor mineralization. Meanwhile, the decompression would cause the subsidiary NW- to WNW-trending faults to dilate, which served as the favorable pathways for the migration and circulation of ore fluids, and/or as the spaces for the deposition of ore metals (Fig. 17d), forming the intracontinental reactivation-type Au (-polymetallic) deposits, as discussed above.

Acknowledgements

This research was financially co-supported by the DREAM project of MOST, China (No. 2016YFC0600401), the National Natural Science Foundation of China (Nos. 41472171, 41672077) and Chinese Ministry of Land and Resources (200646092). We are grateful to Prof. Jingwen Mao for his innovative idea on the manuscript. Discussion with Prof. Chen Yanjing has helped the improvement of the paper. A particular thank is given to Prof. Liqiang Yang and an anonymous reviewer for their thorough and constructive reviews, and the Editor-in-Chief Franco Pirajno and guest editor Yanhua Zhang for their editorial handling of the paper.

Appendix A.

See Appendices A1–A6.

Appendix A1

Summary of the fundamental characteristics of the representative Au (-polymetallic) ore deposits in the JOB, South China.

Locality	Deposit	Gold reserve (t)/grade (g/t)	Host rock	Associated intrusion and/or dike	Ore mode, ore-controlling structure and occurrence of orebody	Ore metal association, mineral paragenesis, major alteration, ore- and gangue minerals
Northwestern Zhejiang Province	Huangshan	About 4.5/9	Hosted by the ca. 844–808 Ma intrusive complex consisting of pyroxene diorite, quartz diorite and diorite	A possible genetic link to minor diabasic, felsite porphyric and lamprophric dikes	Controlled by NE-trending ductile shear zone as northeastern part of the regionally Jiangshao deep fault; auriferous quartz veins and altered cataclasites occurring within subsidiary NE- and NW-trending phyllonite sub-zones; Au quartz veins characterized by lenticular ribbon structure	Au–Ag; ore minerals including predominant pyrite and minor chalcopyrite, galena and sphalerite; Au minerals dominated by native gold (fineness at 950), with minor calaverite, petzite and Au-bearing coloradoite; gangue minerals including predominant quartz, with subordinate sericite, calcite, ankerite, aphrizite and chlorite; three stages of metallogenesis including quartz-sulfide-native gold, quartz-invisible native gold and native silver-sulfide-electrum, and quartz-calcite, from early to late
Northeastern Jiangxi Province	Jinshan	~300/4 to n × 100 g/t	Hosted by the early Neoproterozoic Shuangqiaoshan Group	Minor intrusive rocks including diabase- and pyroxene diorite dikes occurring in the mining district	Ore bodies present as stratiform, stratiform-like and lenticular shapes mainly occurring in (ultra) mylonites related to a NEE-trending ductile shear zone with dipping 5°–35° to NW and/or to NE. This shear zone is limited by both the Bashiyuan–Tongchang strike-slip shear fault to the west and the Jiangguang–Fujiawu strike-slip shear fault to the east and occupies the eastern limb of the Sizhoumiao synclinorium. Altered mylonites and gold-bearing quartz veins are main ore-types	Au–Cu–Pb–Zn, with a fineness of 954 to 970 in native gold; pyrite-quartz (pre-ore stage), native gold-quartz-sulfide-sericite-chlorite-calcite (ore-stage), chlorite-calcite-quartz (post-ore stage), and quartz-pyrite (latest ore-stage), from early to late stages of mineralization; native gold, pyrite, magnetite, hematite, sphalerite, galena and chalcopyrite as main ore minerals, whereas quartz–dominated, quartz, sericite, albite, ankerite and chlorite as main gangue minerals; silicification, pyritic, sericitic, carbonate and chloritic alterations
NEHP	Wangu	>85/3–73 (average 6.8)	Hosted by the early Neoproterozoic Lengjiaxi Group	Showing spatial relationship to the late Mesozoic Jinjing pluton, with minor lamprophric dikes present in mining district	Sited in the Mufushan–Ziyunshan uplift; Au-bearing quartz veins and auriferous altered fractured rocks mainly occurring in subsidiary NWW-trending intraformational shear fracture zones, with individual lode gold ranging from 350 to 2800 m in length along strike, from 0.41 to 6.83 m in width and from 300 to 400 m in a down-dip extension; orebodies generally dipping to NE to NEE at an angle of 25–82°	Au–As–Sb–(W) or Au–As–(Cu) –(Co); quartz–calcite (pre-ore stage), quartz–pyrite–arsenopyrite (ore stage 1), sulfide–native gold–quartz (ore stage 2) and quartz–calcite (post-ore stage); silicification, sericitic, chloritic, carbonate and pyritic alterations; pyrite and arsenopyrite with minor galena, sphalerite, chalcopyrite and zinkenite; quartz, sericite and chlorite
	Huangjindong	>80/4–10 (average 4)	Hosted by the early Neoproterozoic Lengjiaxi Group	Showing spatial relationship to the late Mesozoic Lianyunshan pluton	Sited in the Lianyunshan–Hengyang uplift; Au-bearing quartz veins and auriferous altered fractured rocks mainly occurring in a group of subsidiary NWW-trending inter- or intrafromational shear fracture zones intimately associated with NWW- to EW trending reversed anticlinorium; A main lode gold is up to 2645 m long and 2 m wide, with a down-dip extension of >600 m, dipping to N at an angle of 40–75°	Au, Au–Ag–Te, Au–As and Au–Sb–(W); quartz–pyrite– calcite (pre-ore stage), Au-bearing scheelite–pyrite–quartz (ore stage 1), sulfide (pyrite–arsenopyrite)–native gold (with fineness between 963 and 998)–quartz (ore stage 2) and quartz–calcite (post-ore stage); silicification, sericitic, chloritic, epidotic and pyritic alterations; pyrite and arsenopyrite with minor galena, chalcopyrite and sphalerite; quartz and sericite with minor chlorite and calcite
	Yanlinsi	~50/0.6–24.7	Hosted by the early Neoproterozoic Lengjiaxi Group	Dioritic, granodioritic, lamprophyric and gabbroic/diabasic dikes widely present in the mining district	Regionally controlled by NNE-trending reversed anticlinorium; both the NE-trending cleavage (brittle-ductile) zone with dipping to NW at an angle of 25–60° and the NW-trending ductile shear zone commonly hosting Au quartz veins of variable width (8 cm to >80 cm) and length (100 m to >1.5 km)	Au, Au–Cu, Au–W and Au–Ag; the first stage of mineralization forming ore minerals within the NE-trending cleavage (brittle-ductile) zones, whereas the second stage of mineralization forming ore minerals within the NW-trending ductile shear zones; silicification, pyritic, chloritic, carbonate alterations; native gold, pyrite, arsenopyrite and limonite; quartz, sericite, chlorite, muscovite and calcite

(*continued on next page*)

Appendix A1 (*continued*)

Locality	Deposit	Gold reserve (t)/grade (g/t)	Host rock	Associated intrusion and/or dike	Ore mode, ore-controlling structure and occurrence of orebody	Ore metal association, mineral paragenesis, major alteration, ore- and gangue minerals
NWHP	Woxi	>40/12.98	Hosted by the Madiyi Formation of the middle Neoproterozoic Banxi Group	No consistent spatial or genetic relationship to any intrusion and/or dike	Sited in the Xufengshan uplift and hosted by a series of interbedded shear fracture zones developed together with a number of anticlines and synclines; regionally controlled by the approximately EW-trending Woxi brittle-ductile shear fault dipping to N at an angle of 20°. This fault is >20 km long with a width between 0 and 2000 m. Manto (stratiform)- and stockwork mineralization occurs in the footwall of the fault and accounts for the total ore reserve of >70%. EW-striking shear zone-hosted tabular and lenticular orebodies are parallel to the main fault plane. Main Au quartz veins are up to 350 m long and 1.5 m wide, with a down-dip extension of >3500 m, dipping N to NW at an angle of 20–30°	W–Sb–Au, Au and Au–Sb; quartz–calcite (pre-ore stage), scheelite–wolframite–quartz (ore stage 1), pyrite–gold–quartz (ore stage 2), sulfide (sphalerite, stibnite) –native gold–quartz (ore stage 3) and calcite–quartz (post-ore stage); alteration including silicification, pyritic, sericitic, carbonate, chloritic and tourmalitic alterations, with Au, Sb and W mineralization intimately associated with silicification, pyritic and sericitic alterations; ore minerals depicted mainly by scheelite, wolframite, stibnite, native gold (with fineness between 976 and 997) and pyrite, and minor by arsenopyrite, sphalerite, galena, chalcopyrite, and cinnabar, with quartz, calcite, sericite and chlorite as gangue minerals
	Fuzhuxi	More than 10/ 0.6 to 13.8 with Sb grade of 0.02–22.82 wt.%	Hosted by the Madiyi Formation of the middle Neoproterozoic Banxi Group	Showing genetic link to diabase dikes and granite porphyre dikes	Commonly controlled by the regionally EW-trending tight folds and thrust faults; orebodies present as auriferous quartz veins and auriferous altered cataclasites hosted within the subsidiary NNW-, NW- and NEE-trending fracture zones	Au–Sb; ore minerals dominated by native gold (fineness at 998), stibnite and pyrite, with subordinate arsenopyrite, chalcopyrite and scheelite; with predominant quartz and subordinate dolomite, calcite, feldspar, sericite and chlorite as gangue minerals; Au hosted mainly by pyrite and subordinately by stibnite; three stages of Au–Sb mineralization including quartz-pyrite, quartz-sulfide-native gold, and quartz-calcite, from early to late
	Shenjiaya	33/3.81–43.51	Hosted by the Madiyi Formation of the middle Neoproterozoic Banxi Group	No consistent spatial or genetic relationship to any intrusion and/or dike	Commonly controlled by the NEE-trending (strike-slip) deep faults and anticlinorium; Auriferous quartz veins and altered cataclasites mainly occurring within interformational fracture zones; orebodies dipping to N or S with a length between 200 m and 5400 m along trend; with increasing depth, the thickness and Au grades of orebodies increasing	Au; ore minerals dominated by native gold (with 904 of fineness) + pyrite + arsenopyrite, with minor galena, sphalerite, chalcopyrite, bornite and limonite; Gangue minerals predominant in quartz, and sericite, and subordinate in chlorite, calcite and feldspar; from orebodies to host rocks, zoned alteration from pyritic alteration, via silicification to sericitic, carbonate and chloritic alterations
	Banxi	40.925 t/20% (Sb)	Hosted by the Wuqiangxi Formation of the middle Neoproterozoic Banxi Group	Granite-porphyry dykes occurring in the mining district	Controlled by EW- and NNE-trending structures, and positioned in their intersections. This deposit includes 21 ore veins and altered zones, and the ore modes are stibnite-bearing quartz veins, stibnite-bearing stockwork veins and Sb- and Au-bearing ore veins	Sb and Au–Sb; quartz (pre-ore stage), sulfide–quartz (ore stage 1), stibnite–sulfide (ore stage 2) and calcite–quartz (post-ore stage); stibnite and arsenopyrite with minor pyrite and chalcopyrite; quartz is the main gangue minerals, calcite and dolomite are second with rare barite; silicification, pyritic, sericitic, carbonate and chloritic alterations
	Xi'an		Hosted by the Madiyi Formation of the Banxi Group and the underlying Lengjiaxi Group	No consistent spatial or genetic relationship to any intrusion and/or dike	Quartz veins planar to bedding between the early Neoproterozoic Lengjiaxi Group and the middle Neoproterozoic Banxi Group, or as oblique veins crosscutting the host rocks	W–Sb–Au; scheelite–quartz–calcite (ore stage 1), sulfide (chalcopyrite, pyrite, scheelite)–native gold–quartz (ore stage 2) and calcite–quartz (post-ore stage); silicification, pyritic, sericitic, carbonate and chloritic alterations with Au, Sb and W mineralization spatially related to silicification, pyritic and sericitic alterations; ore minerals depicted mainly by scheelite, native gold, pyrite, and minor by galena and chalcopyrite, with quartz, calcite, sericite and chlorite as gangue minerals
	Yiyangnanjiao		Hosted by the early Neoproterozoic Lengjiaxi Group	Granodioritic dikes occurring in the mining district		Au, Au–Ag–Te, Au–As and Au–Sb–(W); pyrite–arsenopyrite–quartz (ore stage 1), sulfide (sphalerite, galena)–native gold (with a fineness of about 900) – quartz (ore stage 2) and calcite–quartz (post-ore stage)

Appendix A1 (*continued*)

Locality	Deposit	Gold reserve (t)/grade (g/t)	Host rock	Associated intrusion and/or dike	Ore mode, ore-controlling structure and occurrence of orebody	Ore metal association, mineral paragenesis, major alteration, ore- and gangue minerals
	Xicong		Hosted by the Early Neoproterozoic Lengjiaxi Group	No consistent spatial or genetic relationship to any intrusion and/or dike		Au, Au–Ag–Te, Au–As and Au–Sb–(W); quartz–scheelite (ore stage 1), quartz–sulfide–native gold (ore stage 2) and quartz–calcite (post-ore stage); native gold with a fineness between 963 and 998
	Daping	More than 30 t/4.8 to 28.58	Hosted by the middle Neoproterozoic Furong Group	Showing spatial relationship to the Indosinian plutons	Controlled by NNE-trending shear fault zones; auriferous quartz veins and altered cataclasites hosted within both the NW- and the NE-trending altered fracture zones	Au; ore minerals dominated by native gold, pyrite and arsenopyrite, with quartz and sericite as predominant gangue minerals; strong silicification, pyritic, sericitic and arsenopyritic alterations
SWHP	Mobin		Hosted by the Wuqiangxi Formation of the middle Neoproterozoic Banxi Group	No consistent spatial or genetic relationship to any intrusion and/or dike	Au quartz veins planar to bedding of the Banxi Group and/or crosscutting the host rocks, and parallel to the NW- to NNW- striking faults, with individual lodes ranging discontinuously from 1600 to 3000 m in striking length, from 0.11 to 2 m in width and from 50 to 458 m in a down-dip extension, respectively; dipping to NEE or NNW at an angle of 20–30°	Au and Au–Sb; pyrite–arsenopyrite–quartz (ore stage 1), sulfide (sphalerite, galena)–native gold–quartz (ore stage 2) and calcite–quartz–pyrite (post-ore stage); silicification-dominated, sericitic, chloritic, pyritic and carbonate alterations; native gold (with fineness between 925 and 960), pyrite, arsenopyrite and zinckenite with minor sphalerite; quartz, plagioclase, sericite, muscovite and chlorite
	Taojinchong		Hosted by the Wuqiangxi Formation of the middle Neoproterozoic Banxi Group	Rare occurrence of diabase dikes in the mining district	Commonly controlled by regionally NE-trending anticlinorium, synclinorium and faults; auriferous quartz veins and/or altered fractured rocks hosted within subsidiary NNW- to NWW-striking fracture zones	Au, Sb–Au and Au–Sb–As; pyrite–arsenopyrite–quartz (ore stage 1), sulfide (pyrite, sphalerite, galena, chalcopyrite) –native gold (fineness at 952)–quartz (ore stage 2) and calcite–quartz–pyrite (post-ore stage); silicification, chloritic, pyritic, carbonate alterations; pyrite, arsenopyrite and zinckenite with minor sphalerite; quartz and calcite
	Chanziping	More than 21 t/3.35 to 31.23	Hosted by the middle to late Neoproterozoic Jiangkou Group	Showing spatial relationship to the Indosinian Baimashan and Zhonghuashan plutons	Controlled by NNE-trending overthrusted shear fault; with an average thickness of 0.1–1.9 m and crosscutting the regionally foliations, orebodies hosted within the subsidiary NW-trending inter- or intraformational fracture zones in the footwall of the regionally NS-trending fault	Au; ore minerals including native gold (with fineness up to 993), pyrite, arsenopyrite, galena, chalcopyrite, bismuthine, and stibnite, with quartz, sericite, chlorite and tourmalite as gangue minerals; three stages of mineralization including quartz-pyrite-arsenopyrite, quartz-sulfide-native gold, and quartz-calcite, from early to late; dominated by silicification, pyritic, sericitic, and arsenopyritic alterations
	Pingcha	More than 10 t/3.11 to 121.68	Hosted by the middle to late Neoproterozoic Jiangkou Group		Auriferous quartz veins hosted within subsidiary fissures or fracture zones crosscutting the bedding	Au; two stages of mineralization including quartz-native gold and native gold-sulfide-quartz, from early to late; ore minerals dominated by visible native gold, pyrite, arsenopyrite, stibinite and bournonite, with predominant quartz and subordinate sericite and chlorite as gangue minerals; weak chloritic, pyritic, and arsenopyritic alterations
Southeastern Guizhou Province	More than twenty Au deposits and mineral showings		Hosted by the middle Neoproterozoic Xiajiang Group	No consistent spatial or genetic relationship to any intrusion and/or dike	Controlled by NE-trending anticlinorium and associated inter- or intraformational decollement faults, and NE–NNE- and approximately EW-trending shear faults; stratiform, stratiform-like, saddle-backed and lenticular orebodies present as auriferous quartz veins and altered cataclasites occurring within both the NE–NNE-trending shear fault zones crosscutting the crests of the NE-trending anticlines and the intra- or interformational decollement fault zones	Au; ore minerals dominated by Au-bearing minerals, pyrite, arsenopyrite, sphalerite and galena, with minor tetrahedrite, chalcopyrite and/or magnetite or limonite; gangue minerals predominant in quartz, subordinate in ankerite, calcite and chlorite, and minor in carbonaceous material, sericite and clay; Au-bearing minerals dominated by native gold with a fineness at 935–980; four stages of metallogenesis including: white quartz, pyrite-quartz-native gold, galena-sphalerite-native gold, and calcite-quartz, from early to late

Note: NEHP, NWHP and SWHP represent the northeastern-, northwestern- and southwestern Hunan Province of the JOB, respectively.

Appendix A2-1
Sulfur isotope compositions of sulfides from the Au ore deposits in northwestern Zhejiang Province of the JOB, South China.

Mineral	Sample description	Host rock	Location	$^{34}S/‰$	References
Py	Gold-bearing quartz veins	Chencai Group	Huangshan Au deposit	+1.91 to +4.26 (avg. +2.66)	Ye et al. (1994)
Py				−1.74 to +1.14 (avg. −0.9)	Li (1990)

Appendix A2-2
Sulfur isotope compositions of sulfides from the Au ore deposits and Dexing Cu-Mo-Au deposit in northeastern Jiangxi Province of the JOB, South China.

Sample No.	Mineral	Sample description	Host rock	Location	$\delta^{34}S/‰$	References
JS159–2	Py	Disseminated ores	Shuangqiaoshan Group	Jinshan Au deposit	+3.7	Zhao et al. (2013a)
JS205	Py	Disseminated ores			+4.5	
JS208–3	Py	Disseminated ores			+3.9	
JS099	Arsp	Quartz vein ores			+4.4	
JS218–2	Py	Quartz vein ores			+4.2	
JS075	Arsp	Quartz vein ores			+3.6	
JS077	Arsp	Quartz vein ores			+3.4	
JS080	Arsp	Quartz vein ores			+4.0	
JS080	Py	Quartz vein ores			+4.3	
JS083	Py	Quartz vein ores			+4.6	
JS094	Py	Quartz vein ores			+4.3	
JS346	Py	Quartz vein ores			+3.3	
JS346	Py	Quartz vein ores			+4.1	
JS344	Py	Quartz vein ores			+3.7	
JS044	Py	Quartz vein ores			+3.9	
JS056	Py	Quartz vein ores			+4.6	
JS330	Py	Quartz vein ores			+3.6	
JS111	Arsp	Phyllites	Shuangqiaoshan Group		+4.1	
JS245–6	Arsp				+4.3	
JS088	Arsp				+4.2	
JS256	Arsp				+3.3	
	Py				−1.4 to +6.0 (avg. +5.47)	Zeng et al. (2002a)
	Py	Gold-bearing quartz veins	Shuangqiaoshan Group		+3.5 to +4.5 (avg. +4.1)	
	Py	Auriferous altered rocks			−1.5 to +5.1 (avg. +4.18)	
	Py	Mafic volcanics	Shuangqiaoshan Group		+3.1	Huang and Yang (1990)
	Py	Gold-bearing quartz veins	Shuangqiaoshan Group		+3.5 to +4.3 (avg. +4.1)	
	Py	Mineralized volcanic tuffs			+2.08 to +5.05 (avg. +3.71)	Zhu and Fan (1991)
	Py	Gold-bearing quartz veins			+2.94 to +5.90 (avg. +4.42)	
	Py	Phyllites	Shuangqiaoshan Group		+6.41	
91	Py	Gold-bearing quartz veins	Shuangqiaoshan Group		−0.4	Li (2009)
96–1	Py	Auriferous mylonites			+4.9	
96–3	Py	Auriferous mylonites			+5.9	
95–4	Py	Gold-bearing quartz veins			+7.3	
325–4	Py	Gold-bearing quartz veins			+5.0	
325–1	Py	Gold-bearing quartz veins			+5.7	
325–3	Py	Gold-bearing quartz veins			+3.2	
325–2	Py	Gold-bearing quartz veins			+5.6	
H–090–3	Py	Gold-bearing quartz veins			+5.0	
	Py	Host rocks	Shuangqiaoshan Group		+2.57to +5.60 (avg. +3.80)	Wei (1995)
	Py	Host rocks			+1.80 to +5.80 (avg. +3.94)	
	Py	Auriferous altered mylonites	Shuangqiaoshan Group		+3.1to +6.0 (avg. +4.71)	
D1	Py	Gold-bearing quartz veins	Shuangqiaoshan Group	Hamashi Au deposit	+2.90	Mao (1998)
DaI–S3–1	Py	Gold-bearing quartz veins			+2.85	
DaI–S3–2	Py	Gold-bearing quartz veins			+2.76	
DaI–S3–3	Py	Gold-bearing quartz veins			+3.40	
K(I)–S2–1	Py	Gold-bearing quartz veins			+3.00	
K(I)–S2–2	Py	Gold-bearing quartz veins			+3.07	
	Py	Granodiorites		Dexing Cu-Mo-Au deposit	−2.80 to +3.10 (avg. +0.15)	Zhu et al. (1983)
	Py	Granodiorites			−0.60 to +1.00 (avg. +0.48)	
	Py	Sulfide–bearing quartz veins		Tongchang mine of the Dexing Cu-Mo-Au deposit	− 1.3 to +3.1 (avg. +0.2)	Huang and Yang (1990)
	Py				−1.2 to +1.6 (avg. +0.21)	
	Py				−0.7 to +2.8 (avg. +0.44)	

Appendix A2-2 (*continued*)

Sample No.	Mineral	Sample description	Host rock	Location	δ^{34}S/‰	References
	Py	Sulfide–bearing quartz veins			−2.5 to +3.1 (avg. +0.36)	Zhao et al. (2013a)
	Py				−0.1 to +3.0 (avg. +1.25)	
	Ccp				−2.8 to +1.4 (avg. −1.07)	
	Ccp				+4.0 to +5.0 (avg. +4.67)	
	Py+Ccp				−2.3 to +3.1 (avg. +0.15)	
	Py			Fujiawu mine of the Dexing Cu-Mo-Au deposit	−0.6 to +1.0 (avg. +0.45)	
	Ccp				−0.1 to +1.0 (avg. +0.54)	
	Py+Ccp				−0.6 to +1.0 (avg. +0.48)	
	Py				−0.8 to +1.1 (avg. +0.05)	
	Ccp				−2.1 to +0.3 (avg. −0.83)	
	Sph			Zhushahong mine of the Dexing Cu-Mo-Au deposit	−4.01	
	Gn				−2.41	
	Py+Ccp+Sph +Gn				−4.0 to +1.1 (avg. −0.48)	

Appendix A2-3
Sulfur isotopic compositions of sulfides from the Au (-polymetallic) and Cu-polymetallic ore deposits in Hunan Province of the JOB, South China.

Region	Sample No.	Mineral	Sample description	Host rock	Location	δ^{34}S/‰	References
NEHP		Py	Host rocks	Lengjiaxi Group		+12.90 to +23.50 (avg. +18.5)	Luo (1990)
		Py				−13.10 to −6.26	Luo (1988), Zhang and Luo (1989), Liu et al. (1994a) and Liu et al. (1999)
	HD01−8	Py	Auriferous quartz veins	Lengjiaxi Group	Huangjindong Au deposit	-12.92	This study
	HD01−9	Py	Auriferous quartz veins			-10.02	This study
	HD01−12	Py	Auriferous quartz veins			-12.56	This study
	HD01−10	Py	Auriferous quartz veins			-5.93	This study
	HD01−11	Py	Auriferous quartz veins			-6.84	This study
	HD01−13	Py	Auriferous quartz veins			-8.62	This study
	HD01−4	Arsp	Auriferous quartz veins			-6.7	This study
	HD01−5	Arsp	Auriferous quartz veins			-5.8	This study
	HD01−10	Arsp	Auriferous quartz veins			-4.83	This study
	HD01−11	Arsp	Auriferous quartz veins			-5.69	This study
	1	Py	Auriferous quartz veins			-7.22	Luo (1988)
	2	Arsp	Auriferous quartz veins			-6.06	
	3	Arsp	Auriferous quartz veins			-6.97	
	4	Py	Auriferous quartz veins			−8.3 to −5.6 (avg. −6.69)	Zhang (1985)
	5	Py	Auriferous quartz veins			−8.3 to −6.6 (avg. −7.22)	Liu et al. (1999)
	6	Py	Auriferous quartz veins			−12.0 to −5.6 (avg. −8.16)	Ye et al. (1988)
	7	Py	Auriferous quartz veins			−12.2 to −4.4 (avg. −7.80)	
	8	Arsp	Auriferous quartz veins			−6.1 to −3.4 (avg. −4.45)	
	9	Py	Auriferous altered host rocks			−8.5 to −4.2 (avg. −6.83)	
		Py	Auriferous quartz veins	Lengjiaxi Group	Yanlinsi Au deposit	−5.73 to −4.57 (avg. −5.65)	Liu et al. (1999)
	YLS01−1	Py	Auriferous quartz veins			−2.6	This study
	YLS01−2	Py	Auriferous quartz veins			−1.08	This study
	YLS01−4	Py	Auriferous quartz veins			−6.04	This study
	YLS01−5	Py	Auriferous quartz veins			−1.3	This study
	YLS01−6	Py	Auriferous quartz veins			−4.33	This study
	YLS01−7	Py	Auriferous quartz veins			−10.34	This study
	YLS01−8	Py	Auriferous quartz veins			−1.48	This study
	YLS01−9	Py	Auriferous quartz veins			−0.58	This study
	YLS01−10	Py	Auriferous quartz veins			−14.76	This study
	YLS01−1	Py	Auriferous quartz veins			−1.62	This study
	YLS01−2	Py	Auriferous quartz veins			−1.34	This study
	YLS01−4	Arsp	Auriferous quartz veins			−0.54	This study
	YLS01−5	Arsp	Auriferous quartz veins			−1.35	This study
	YLS01−6	Arsp	Auriferous quartz veins			−0.91	This study

(*continued on next page*)

Appendix A2-3 (*continued*)

Region	Sample No.	Mineral	Sample description	Host rock	Location	$\delta^{34}S$/‰	References
	YLS01−7	Arsp	Auriferous quartz veins			−1.16	This study
	YLS01−8	Arsp	Auriferous quartz veins			−1.46	This study
	YLS01−9	Arsp	Auriferous quartz veins			−0.24	This study
	YLS01−10	Arsp	Auriferous quartz veins			−1.67	This study
	DD02−1	Py	Auriferous quartz veins	Lengjiaxi Group	Wangu Au deposit	−8.64	This study
	DD02−3	Py	Auriferous quartz veins			−9.30	This study
	DD02−5	Py	Auriferous quartz veins			−7.97	This study
	DD02−2	Arsp	Auriferous quartz veins			−9.67	This study
	DD02−3	Arsp	Auriferous quartz veins			−10.20	This study
	DD02−4	Arsp	Auriferous quartz veins			−9.54	This study
	DD02−5	Arsp	Auriferous quartz veins			−9.23	This study
	DD02−1	Arsp	Auriferous quartz veins			−9.35	This study
	SPY–01	Py	Auriferous quartz veins			−10.10	Liu et al. (1994a)
	SPY–02	Py	Auriferous quartz veins			−10.40	
	SAS–01	Arsp	Auriferous quartz veins			−8.90	
	SBB–01	Sti	Auriferous quartz veins			−11.60	
		Py	Auriferous quartz veins		Jinkengchong Au deposit	−0.11 to +0.65	Luo (1990)
	1	Py	Orebodies		Qibaoshan porphyry–associated Cu–polymetallic deposit	+1.8 to +5.4 (avg. +3.72)	Liu et al. (2001)
	2	Ccp				+2.73 to +4.24 (avg. +3.48)	
	3	Po				+3.37	
	4	Sph				+2.2 to +4.89 (avg. +3.47)	
	5	Gn				+0.58 to +2.5 (avg. +1.36)	
	1	Py	Orebodies		Aoyushan porphyry–associated Cu–polymetallic deposit	−2.9 to +3.3 (avg. +0.73)	
	2	Sph				+0.2 to +2.9 (avg. +1.78)	
	3	Gn				+2.20	
		Py	Orebodies		Jingchong Cu–polymetallic deposit	−3.39 to 1.88 (avg. −2.54)	
		Ccp				−3.89 to 1.66 (avg. −2.70)	
NWHP		Py	Host rocks	Wuqiangxi Formation of the Banxi Group		+4.50 to +12.02	Luo, 1990
		Py				+6.30 to +17.20	
		Py	Host rocks	Madiyi Formation of the Banxi Group		−1.8 to +1.9	Zhang and Luo (1989), Luo (1990)
		Py				−5.5	
		Ccp				−6.3	
		Py	Auriferous quartz veins	Madiyi Formation of the Banxi Group	Woxi Au–Sb–W deposit	−4.0 to +2.2 (avg. −2.2)	Zhang (1985)
		Py	Auriferous quartz veins			+0.9 to +1.9	Zhang and Luo (1989)
	1	Sti	Auriferous quartz veins			−1.6	Gu et al. (2012)
	2	Sti	Auriferous quartz veins			−2.5	
	3	Sti	Auriferous quartz veins			−2.4	
	4	Sti	Auriferous quartz veins			−2.1	
	5	Sti	Auriferous quartz veins			−2.4	
	6	Sti	Auriferous quartz veins			−2.4	
	7	Sti	Auriferous quartz veins			−2.3	
	8	Sti	Auriferous quartz veins			−2.2	
	9	Sti	Auriferous quartz veins			−2.6	
	10	Sti	Auriferous quartz veins			−1.2	
	11	Sti	Auriferous quartz veins			−1.5	
	12	Sti	Auriferous quartz veins			−1.8	
	13	Sti	Auriferous quartz veins			−1.7	
	14	Sti	Auriferous quartz veins			−2.1	
	15	Sti	Auriferous quartz veins			−2.3	
	16	Sti	Auriferous quartz veins			−2.8	
	17	Sti	Auriferous quartz veins			−2.2	
	18	Sti	Auriferous quartz veins			−2.6	
	19	Py	Auriferous quartz veins			−1.7	
	20	Py	Auriferous quartz veins			−6.7	
	21	Py	Auriferous quartz veins			−6.2	
	22	Py	Auriferous quartz veins			−7.4	
	23	Ga	Auriferous quartz veins			−12.3	
	24	Sph	Auriferous quartz veins			−8.3	
	25	Sph	Auriferous quartz veins			−5.0	

Appendix A2-3 (*continued*)

Region	Sample No.	Mineral	Sample description	Host rock	Location	$\delta^{34}S$/‰	References
	WXB088	Py	Altered host rocks			−4.05	Chen (2013)
	WXB051	Py	Qtz–Sti ore veins			−1.99	
	WXB045	Py	Qtz–Sch–Sti ore veins			+0.07	
	WXB002	Py	Sch ore veins			+1.66	
	WXB015	Py	Qtz–Sti ore veins			−3.21	
	WXB021	Py	Sch–Sti ore veins			+0.42	
	WXB034	Py	Qtz–Sti ore veins			−0.56	
	WXB030	Py	Qtz–Cal ore veins			−0.74	
	WXB057	Py	Qtz–Sch–Sti ore veins			−2.15	
	WXB090	Sti	Sti ore veins			−2.71	
	WXB092	Sti	Sti ore veins			−3.28	
	WXB046	Sti	Qtz–Sch–Sti ore veins			−2.88	
	WXB006	Sti	Qtz–Sti ore veins			−2.96	
	WXB001	Sti	Qtz–Sti ore veins			−1.74	
	WXB017	Sti	Qtz–Sti ore veins			−2.89	
	WXB015	Sti	Qtz–Sti ore veins			−4.99	
	WXB021	Sti	Sch–Sti ore veins			−1.52	
	WXB053	Sti	Qtz–Sti ore veins			−2.83	
		Py	Bedding ores			−1.3 to 2.2 (avg. −1.7)	Luo et al. (1984)
		Sti	Bedding ores			−3.1 to +2.1 (avg. −1.59)	
		Sph	Bedding ores			−3.8	Luo (1990)
		Gn	Bedding ores			−5.1	
		Ccp	Bedding ores			+1.1	
		Py	Altered host rocks			−4.1 to 0.3 (−2.5)	
		Py	Auriferous quartz veins		Huangtudian Au deposit	+4.9	Luo (1990)
		Py+Ccp+ Gn+Tet	Auriferous quartz veins	Between the Lengjiaxi Group and the Madiyi Formation of the Banxi Group	Xi'an W–Sb–Au deposit	−3.5 to +22.3	Luo (1990)
		Sti	Auriferous quartz veins	Late Neoproterozoic host rocks	Xiaoniutouzai Sb–Au deposit	+1.27 to +2.72 (avg. 1.92)	Luo (1994c)
		Arsp		Late Neoproterozoic host rocks	Longshan Sb–Au deposit	−2.1 to +1.2 (avg. −0.43)	
		Py				+0.6 to +4.6 (avg. 2.47)	
		Arsp				−1.6 to +3.2 (avg. 0.28)	
		Tet				+1.9	
		Sti		Late Neoproterozoic host rocks	Wulipai Sb–Au deposit	+6.3	
		Sti	Auriferous quartz veins	Wuqiangxi Formation			
	Wangjiacun Sb–Au deposit	−2.11 to 4.16 (avg. −3.05)					
		Arsp				−4.26 to 6.92 (avg. −5.69)	
		Sti			Yangpimao Sb–Au–W deposit	+0.6 to +5.2 (avg. +2.43)	
		Py				+9.20	
		Arsp				+3.4 to +12.3 (avg. 5.8)	
		Sti			Jiangxilong Sb–Au deposit	−10.3 to +3.4 (avg. −6.68)	
		Arsp				−9.6	
		Sti			Tongxin Sb–Au deposit	+1.4	
		Sti			Zhazixi Sb–Au–W deposit	+4.7 to +10.4 (avg. +8.0)	
		Sti			Banxi Sb–Au–W deposit	+3.3 to +6.6 (avg. +4.8)	
		Py				+6.1 to +6.5 (avg. +6.3)	
		Arsp				+5.0 to +7.3 (avg. 6.0)	
		Sti	Auriferous quartz veins	Lengjiaxi Group	Xichong Au–Sb–Ag–Te–As–(W) deposit	−14.3 to 12.1 (avg. −13.3)	
		Py				−13.6 to 9.8 (avg. −11.7)	
		Py	Auriferous quartz veins		Yiyangnanjiao Au–Sb–Ag–Te–As–(W) deposit	−1.2 to +1.0	

(*continued on next page*)

Appendix A2-3 (*continued*)

Region	Sample No.	Mineral	Sample description	Host rock	Location	$\delta^{34}S$/‰	References
		Sti	Auriferous quartz veins		Hexinqiao Sb–Au–W deposit	−0.7 to +1.5 (avg. +0.4)	
		Py	Auriferous quartz veins			+2.0 to +4.6 (avg. +3.3)	
		Py	Auriferous quartz veins			−0.7 to +4.6	Zhang (1985)
		Sti	Sb–Au-bearing quartz veins	Madiyi Formation of the Banxi Group	Fuzhuxi Sb–Au deposit	−3.6 to 7.3 (avg. −5.7)	Luo (1994c)
		Py				−4.4 to +2.0 (avg. −2.3)	
	1	Sti	Sb–Au-bearing quartz veins			−3.6	Yao and Zhu (1993)
	2	Sti	Sb–Au-bearing quartz veins			−5.0	
	3	Py	Sb–Au-bearing quartz veins			−3.0	
	4	Py	Sb–Au-bearing quartz veins			+2.0	
	5	Sti	Sb–Au-bearing quartz veins			−6.9	Luo (1991)
	6	Sti	Sb–Au-bearing quartz veins			−7.3	
	7	Py	Sb–Au-bearing quartz veins			−4.4	
	8	Py	Sb–Au-bearing quartz veins			−3.7	
		Py	Auriferous quartz veins			−7.3 to 3.1 (avg. −5.3)	Zhang (1985)
		Py	Auriferous quartz veins		Liulincha Sb–Au–W deposit	−4.8 to +1.5 (avg. −0.9)	
		Py	Auriferous quartz veins	Wuqiangxi Formation of the Banxi Group			
	Yangpimao Sb–Au–W deposit	+0.6 to +12.30 (avg. +3.9)					
		Py	Auriferous quartz veins		Banxi Sb–Au–W deposit	+3.3 to +7.3 (avg. +4.0)	
		Py	Auriferous quartz veins		Canglangping Sb–Au–W deposit	+6.8 to +7.2 (avg. +7.0)	
		Py	Auriferous quartz veins		Zhazixi Sb–Au–W deposit	+5.4 to +10.3 (avg. +8.0)	
SWHP	22	Py	Host rocks	Late Neoproterozoic host rocks		+6.77	Wei (1993), Luo (1996)
	23	Py				+7.96	
	24	Py				+6.77	
	25	Py				+5.01	
		Py				+2.0 to +4.6	Luo (1990)
	1	Py	Auriferous quartz veins	Late Neoproterozoic host rocks	Chanziping Au deposit	−1.2	Wei (1993), Luo (1996)
	2	Py	Auriferous quartz veins			+0.32	
	3	Py	Auriferous quartz veins			−2.14	
	4	Py	Auriferous quartz veins			−1.24	
	5	Py	Auriferous quartz veins			−1.81	
	6	Py	Auriferous quartz veins			−0.2.09	
	7	Py	Auriferous quartz veins			−2.72	
	8	Py	Auriferous quartz veins			−5.38	
	9	Py	Auriferous quartz veins			−1.10	
	10	Py	Auriferous quartz veins			−2.96	
	11	Py	Auriferous quartz veins			−1.13	
	12	Py	Auriferous quartz veins			−2.89	
	13	Py	Auriferous quartz veins			−1.20	
	14	Py	Auriferous quartz veins			−2.95	
	15	Py	Auriferous quartz veins			−3.11	
	16	Py	Auriferous quartz veins			−4.18	
	17	Py	Auriferous quartz veins			−0.70	
	18	Py	Auriferous quartz veins			−0.03	
	19	Py	Auriferous quartz veins			0.01	
	20	Arsp	Auriferous quartz veins			−6.01	
	21	Gn	Auriferous quartz veins			−7.58	
	Sm02	Py	Auriferous quartz veins	Wuqiangxi Formation of the Banxi Group			
	Mobin Au-Sb deposit	+8.31	Zhou et al. (1989)				
	Sm03	Py	Auriferous quartz veins			+7.87	
	Sm04	Py	Auriferous quartz veins			+7.86	

Appendix A2-3 (*continued*)

Region	Sample No.	Mineral	Sample description	Host rock	Location	$\delta^{34}S$/‰	References
	Sm05–1	Py	Auriferous quartz veins			+7.95	
	Sm05–2	Py	Auriferous quartz veins			+8.82	
	Sm06	Arsp	Auriferous quartz veins			+8.25	
	Sm08	Py	Auriferous quartz veins			+6.13	
	Sm09	Py	Auriferous quartz veins			+2.53	
	Sm12	Py	Auriferous quartz veins			+6.85	
	Sm13	Py	Auriferous quartz veins			+8.86	
	Sm14	Ccp	Auriferous quartz veins			+8.55	
	Sm15	Sph	Auriferous quartz veins			+6.25	
	Sm16	Gn	Auriferous quartz veins			+5.89	
	Sm17	Py	Auriferous quartz veins			+6.95	
	Sm18	Py	Auriferous quartz veins			+1.36	
	Sm19	Py	Auriferous quartz veins			+8.63	
	Sm20	Py	Auriferous quartz veins			+10.69	
	Sm22–1	Py	Auriferous quartz veins			+5.47	
	Sm22–2	Arsp	Auriferous quartz veins			+8.00	
	Sm23	Py	Auriferous quartz veins			+9.46	
	MBy070	Arsp	Auriferous quartz veins			+7.57	
	MBy065	Py	Auriferous quartz veins			+8.52	
	MBy069	Py	Auriferous quartz veins			+7.17	
	MBy070	Arsp	Auriferous quartz veins			+7.57	
	Sb01	Py	Auriferous quartz veins			+9.34	
	Sm24	Py	Auriferous quartz veins			+4.85	
	Sm01	Py	Auriferous quartz veins			+9.10	
	1	Py	Auriferous quartz veins			+2.12	
	2	Py	Auriferous quartz veins			+4.50	
	3	Py	Auriferous quartz veins			+11.40	
	4	Py	Auriferous quartz veins			+9.20	
	5	Py	Auriferous quartz veins			+10.90	
	6	Py	Auriferous quartz veins			+10.90	
	7	Arsp	Auriferous quartz veins			+9.60	
	8	Py	Auriferous quartz veins			+9.80	
	9	Py	Auriferous quartz veins			+8.20	
	10	Py	Auriferous quartz veins			+10.85	
	11	Py	Auriferous quartz veins			+11.40	
	12	Gn	Auriferous quartz veins			+8.20	
		Py	Auriferous quartz veins			+6.0 to +9.2 (avg. +7.9)	Zhang (1985)

Appendix A2-4
Sulfur isotope compositions of sulfides from the Au ore deposits in southeastern Guizhou Province of the JOB, South China.

Sample No.	Mineral	Sample description	Host rock	Location	$\delta^{34}S$/‰	References
1	Arsp	Gold-bearing quartz veins	Middle Neoproterozoic Xiajiang Group	Bake Au deposit	+5.0	Yu (1997)
2	Arsp	Gold-bearing quartz veins			+1.6	
3	Arsp	Gold-bearing quartz veins		Moshan Au deposit	+9.64	Zhang et al. (1998)
4	Py	Gold-bearing quartz veins			+9.34	
5	Py	Gold-bearing quartz veins			+8.90	
6	Arsp	Gold-bearing quartz veins		Youma'ao Au deposit	+8.30	
8	Py	Gold-bearing quartz veins			+12.54	
7	Py	Gold-bearing quartz veins			+10.03	
9	Py	Gold-bearing quartz veins		Jinchangpo Au deposit	+11.42	
10	Arsp	Gold-bearing quartz veins			+10.03	
11	Py	Gold-bearing quartz veins		Tongluoping Au deposit	−0.96	
PD258–1	Py	Gold-bearing quartz veins		Kengtou Au deposit	+12.99	Tian et al. (2011)
PD258–3	Py	Gold-bearing quartz veins			+4.83	
PD258–3	Arsp	Gold-bearing quartz veins			+5.60	
PD568–2	Py	Gold-bearing quartz veins			+11.63	
PD568–4	Py	Gold-bearing quartz veins			+12.04	
PD568–4	Arsp	Gold-bearing quartz veins			+4.76	

Note: NEHP = northeastern Hunan Province, NWHP = northwestern Hunan Province, and SWHP = southwestern Hunan Province; Qtz = quartz, Cal = Calcite, Py = pyrite, Arsp = arsenopyrite, Gn = galena, Sch = Scheelite, Sti = stibnite, Sph = sphalerite, Ccp = chalcopyrite, Po = pyrrhotite, Tet = tetrahedrite.

Appendix A3
Pb isotopic data of the major Au (-polymetallic) and Cu-polymetallic deposits, host rocks and associated intrusions in the JOB.

Region	Deposit/host rock/pluton	Mineral or lithology	Ore or rock	$^{208}Pb/^{204}Pb$	$^{207}Pb/^{204}Pb$	$^{206}Pb/^{204}Pb$	References
Northwestern Zhejiang Province	Zhongao Au deposit	Py	Auriferous quartz vein	37.569	15.514	17.621	Lin (1988)
		Py		38.508	15.575	18.938	
	Huangshan Au deposit	Py	Auriferous quartz vein	38.045	15.551	17.907	Ye et al. (1993)
		Py		38.056	15.569	17.925	
		Py		38.043	15.516	17.610	
		Py		37.613	15.469	17.659	
	Miaoxiaban Au deposit	Py	Auriferous quartz vein	36.742	15.367	17.108	
		Gn		36.722	15.366	17.093	
		Gn		36.85	15.42	17.15	
	Mali Au deposit	Py	Auriferous quartz vein	38.06	15.53	17.82	
		Py		37.91	15.47	17.88	
		Py		37.88	15.48	17.83	
		Py		38.17	15.57	18.10	
		Gn		37.99	15.55	17.55	
				38.05	15.52	17.83	
	Huangshan Au deposit	Ore	Auriferous quartz vein	38.041	15.536	17.801	Chen and Xu (1996)
		Ore		37.791	15.493	17.566	
		Ore		38.006	15.558	17.844	
		Ore		37.848	15.503	17.573	
		Ore		37.898	15.507	17.831	
		Ore		38.037	15.556	17.731	
		Ore		37.391	15.674	17.726	
		Ore		38.048	15.538	17.743	
		Ore		37.855	15.525	17.660	
		Ore		37.064	15.570	17.624	
		Ore		38.845	15.459	17.323	
		Qtz		37.517	15.453	17.619	
		Qtz		37.746	15.477	17.707	
		Qtz		37.486	15.424	17.594	
		Qtz		37.935	15.518	17.743	
		Qtz		37.444	15.425	17.648	
		Qtz		37.417	15.431	17.621	
		Qtz		37.661	15.466	17.655	
	Chencai Group	Py	Biotite–plagioclase gneisses	38.833	15.618	17.803	Yuan (1992)
		Py		39.190	15.720	18.710	
		Py		38.051	15.554	17.970	
		Gn		39.258	15.774	18.588	
		Host rocks	Quartz diorites hosting the Huangshan deposit	38.097	15.518	17.694	Chen and Xu (1996)
				38.045	15.536	17.573	
				37.727	15.458	17.670	
Northeastern Jiangxi Province	Jinshan Au deposit	Py	Auriferous quartz vein	37.767	15.522	17.573	Huang and Yang (1990)
		Py	Mineralized altered host rocks	37.860	15.583	17.575	
		Py	Mineralized phyllites	37.490	15.487	17.432	
		Py	Auriferous quartz vein	37.338	15.487	17.300	Zhu and Fan (1991)
		Py		37.321	15.440	17.325	
		Py		37.939	15.547	17.675	
		Py		38.995	15.807	18.495	Zeng et al. (2002a)
		Py	Auriferous (ultra)mylonites	38.140	15.587	18.112	
		Py		37.500	15.540	17.450	
		Py		37.650	15.479	17.402	
		Py		37.551	15.482	17.595	
		Py		37.756	15.508	17.667	
		Py	Mineralized phyllites	38.071	15.634	17.870	
		Py	Auriferous altered rocks	38.140	15.587	18.112	
		Py	Auriferous quartz vein	37.495	15.541	17.446	
		Py	Disseminated–type ores	37.678	15.563	17.548	Zhao et al. (2013a)
		Py		38.031	15.566	17.683	
		Py		37.901	15.567	17.601	
		Py	Auriferous quartz vein	37.497	15.553	17.438	
		Py		37.699	15.563	17.524	
		Py		37.705	15.561	17.624	

Appendix A3 (*continued*)

Region	Deposit/host rock/pluton	Mineral or lithology	Ore or rock	$^{208}Pb/^{204}Pb$	$^{207}Pb/^{204}Pb$	$^{206}Pb/^{204}Pb$	References
		Py		37.853	15.558	17.657	
		Py		37.671	15.541	17.581	
		Py		37.677	15.552	17.507	
		Py		37.808	15.586	17.652	
		Py		37.989	15.581	17.704	
	Hamashi Au deposit	Py	Auriferous quartz vein	37.246	15.558	17.431	Mao (1998)
		Gn		37.876	15.750	17.662	
	Dexing porphyry Cu–Mo-Au deposit	Py	Disseminated–type ores	38.018	15.515	18.167	Zhou et al. (2013)
		Py		37.959	15.477	18.082	
		Py		38.035	15.467	18.046	
		Py		38.019	15.48	18.320	
		Py		38.098	15.517	18.178	
		Py		37.888	15.451	18.033	
		Py		37.933	15.435	18.037	
		Py		37.935	15.407	17.954	
		Py		38.153	15.496	18.133	
		Py		37.951	15.511	18.016	
		Porphyries	Earliest late Mesozoic intrusions	38.813	15.612	18.348	Zhou et al. (2012a)
				38.569	15.394	18.185	
				38.859	15.492	18.203	
				38.265	15.494	17.838	
				38.337	15.541	17.849	
				38.307	15.539	17.832	
				38.385	15.485	18.155	
				38.905	15.560	18.410	
	Shuangqiaoshan Group	Slate	Host rocks	38.77	15.625	18.311	Zeng et al. (2002a)
		Graywacke		38.196	15.714	18.073	
		Slate		37.96	15.600	17.982	Zhao et al. (2013a)
		Slate		37.002	15.444	17.124	
		Slate		37.329	15.549	17.138	
		Slate		37.486	15.492	17.439	
		Slate		37.543	15.537	17.453	
		Slate		37.747	15.522	17.573	
		Slate		37.766	15.508	17.664	
		Slate		37.486	15.483	17.603	
		Slate		37.531	15.544	17.676	
		Slate		37.827	15.584	17.578	
		Slate		37.934	15.577	17.932	
		Slate		37.858	15.603	17.837	
		Slate		38.049	15.645	17.847	
		Slate		38.182	15.618	17.697	
Hunan Province	Lengjiaxi Group	Slates and phyllites	Host rocks	39.294	15.586	18.832	Liu and Zhu (1994)
				39.858	15.590	19.034	
				41.786	15.728	20.089	
				43.388	15.733	20.308	
				41.792	15.788	20.525	
				40.057	15.642	19.122	
				46.917	15.937	22.038	
	Wuqiangxi Formation of the Banxi Group	Tuffaceous slates	Host rocks	38.028	15.465	17.528	
				37.897	15.460	17.507	
				39.163	15.524	18.318	
				41.421	15.553	18.506	
				39.455	15.526	18.338	
				41.640	15.592	18.986	
	Madiyi Formation of the Banxi Group	Slates	Host rocks	38.854	15.705	18.297	
				38.354	15.572	17.674	
				38.759	15.657	18.396	
				38.509	15.555	17.821	
				39.971	15.591	18.266	
				38.542	15.553	17.733	
				39.753	15.632	18.223	
				38.701	15.572	17.768	
Northeastern Hunan Province	Wangu Au deposit	Arsp	Auriferous altered cataclasites and associated Au quartz veins	38.539	15.73	18.024	Deng et al. (2013)
		Arsp		38.403	15.665	18.082	

(*continued on next page*)

Appendix A3 (*continued*)

Region	Deposit/host rock/pluton	Mineral or lithology	Ore or rock	$^{208}Pb/^{204}Pb$	$^{207}Pb/^{204}Pb$	$^{206}Pb/^{204}Pb$	References
		Arsp		38.623	15.766	17.983	
		Arsp		38.872	15.767	18.135	
		Arsp		38.886	15.693	18.358	
		Arsp		38.318	15.659	18.015	
		Arsp		38.344	15.685	17.988	
		Arsp		38.247	15.654	17.934	
		Arsp		38.645	15.787	18.005	
		Arsp		38.412	15.674	18.091	
	Huangjindong Au deposit	Py	Lengjiaxi Group	38.365	15.712	17.970	Luo (1989)
		Py		38.069	15.584	17.848	
		Py	Auriferous quartz vein	37.178	15.589	17.897	
		Py		38.974	15.564	17.845	
		Py		38.223	15.556	17.963	
		Py		37.762	15.556	17.860	
		Py		38.262	15.539	17.943	
		Py		38.020	15.529	17.846	
		Py		38.088	15.509	17.830	
		Py		37.702	15.508	17.706	
	Jinkengchong Au deposit	Gn	Auriferous quartz vein	38.188	15.319	17.928	Luo (1989)
		Gn		38.210	15.333	17.928	
		Gn	Quartz vein within granites	38.416	15.443	18.139	
		Gn		38.453	15.416	18.124	
	Aoyushan porphyry-associated Cu-polymetallic deposit	Gn	Ore vein	38.73	15.688	18.372	Liu et al. (2001)
		Sph		38.655	15.623	18.356	
	Qibaoshan porphyry-associated Cu-polymetallic deposit	Gn	Ore vein	38.464	15.596	18.287	
		Py		38.201	15.587	18.055	
		Gn		38.746	15.681	18.313	
		Gn		38.882	15.537	18.118	
		Gn		38.708	15.628	18.478	
		Gn		38.806	15.663	18.467	
		Gn		38.818	15.723	18.420	
		Gn		38.468	15.602	18.268	
		Gn		38.628	15.626	18.100	
		Gn		38.948	15.809	18.372	
		Gn		38.464	15.596	18.287	
	Jingchong Cu-polymetallic deposit	Py	Ore quartz vein	38.237	15.592	18.042	
		Ccp		38.362	15.600	18.124	
		Py		38.814	15.695	18.345	
		Ccp		38.536	15.621	18.310	
	Shitangchong Cu-polymetallic deposit	Gn	Ore quartz vein	38.829	15.669	18.369	
		Sph		38.775	15.652	18.280	
	Chengchong Cu-polymetallic deposit	Gn	Ore quartz vein	38.839	15.719	18.430	
		Sph		38.883	15.728	18.438	
	Lianyunshan pluton	Granite	Late Mesozoic Intrusions	38.385	15.623	18.312	This study
		Granite		38.456	15.659	18.341	
		Granite		38.631	15.713	18.382	
		Granite		38.351	15.62	18.297	
		Granite		38.219	15.607	18.251	
		Granite		38.323	15.619	18.311	
		Granite		38.164	15.593	18.181	
		Granite		38.315	15.623	18.281	
		Granite		38.414	15.639	18.311	
		Granite		38.354	15.624	18.294	
		Granite		38.355	15.63	18.258	
		Granite		38.283	15.612	18.251	
		Granite		38.328	15.615	18.275	
	Wangxiang pluton	Granite		38.247	15.592	18.252	
		Granite		38.256	15.599	18.243	
	Mufushan pluton	Granite		38.124	15.565	18.209	
		Granite		38.286	15.606	18.231	
		Granite		37.859	15.524	17.96	
		Granite		38.264	15.612	18.202	
		Granite		38.528	15.696	28.449	
		Granite		38.263	15.624	18.532	
		Granite		38.368	15.637	18.464	
		Granite		38.413	15.623	18.335	
	Jinjing pluton	Granite		37.92	15.559	17.976	
		Granite		38.287	15.595	18.145	
		Granite		38.333	15.593	18.148	
		Granite		38.469	15.65	18.21	
		Granite		38.368	15.627	18.185	
		Granite		38.359	15.627	18.208	
		Granite		38.402	15.639	18.21	

Appendix A3 (*continued*)

Region	Deposit/host rock/pluton	Mineral or lithology	Ore or rock	$^{208}Pb/^{204}Pb$	$^{207}Pb/^{204}Pb$	$^{206}Pb/^{204}Pb$	References
Northwestern Hunan Province	Woxi Au–Sb–W deposit	Gn	Ore vein	38.999	15.739	17.882	Luo (1989)
		Py		38.781	15.683	18.477	
		Py		38.865	15.706	18.484	
		Sph		38.593	15.601	17.708	Peng and Frei (2004)
		Sph		38.646	15.612	17.713	
		Sph		38.585	15.596	17.707	
		Sph		38.491	15.569	17.689	
		Sph		38.593	15.596	17.699	
		Sti		38.477	15.555	17.744	
		Sti		38.463	15.568	17.753	
		Sti		38.445	15.561	17.751	
		Sti		38.417	15.555	17.727	
	Xichong Au deposit	Gn	Auriferous quartz vein	37.927	15.577	17.855	Luo (1989)
	Canglangping Au deposit	Py	Auriferous quartz vein	38.136	15.607	18.037	Luo (1989)
	Huangtudian Au deposit	Py	Auriferous quartz vein	37.908	15.558	17.543	Luo (1989)
	Liulincha Au deposit	Py	Auriferous quartz vein	38.869	15.483	17.650	Luo (1989)
	Xi'an Au deposit	Gn	Auriferous quartz vein	38.903	15.890	18.025	Wan (1986), Luo (1989)
		Gn		38.290	15.600	17.783	
		Gn		38.510	15.790	18.010	
		Gn		38.180	15.640	17.810	
		Gn		37.864	15.577	17.790	
		Gn		38.062	15.647	17.834	
		Gn		38.033	15.636	17.820	
		Gn		38.168	15.708	17.929	
	Yiyangnanjiao Au deposit	Py	Auriferous quartz vein	37.439	15.579	17.565	Luo (1989)
		Py		37.293	15.524	17.559	
	Between the Lengjiaxi Group and the Madiyi Formation of the Banxi Group from the Xi'an deposit	Limestones	Host rocks	38.246	15.639	17.970	Wan (1986)
		Limestones		37.895	15.573	17.783	
		Limestones		38.183	15.604	18.076	
		Limestones		38.920	15.680	18.151	
		Slates		38.128	15.673	18.032	
		Slates		38.133	15.567	17.763	
	Fuzhuxi Sb–Au deposit	Py	Ore quartz vein	38.089	15.492	17.378	Yao and Zhu (1993)
		Py		38.104	15.493	17.490	
		Py		38.077	15.511	17.497	
		Py		38.121	15.515	17.482	
		Py		38.106	15.519	17.492	
Southwestern Hunan Province	Chanziping Au deposit	Py	Auriferous altered cataclasite	37.900	15.482	17.633	Wei (1993)
		Py		37.888	15.477	17.619	
		Py		38.133	15.467	17.810	
		Py		38.119	15.470	17.782	
		Gn		37.726	15.535	17.388	
	Mobin Au–Sb deposit	Gn	Auriferous quartz vein	37.026	15.042	17.047	Luo (1989)
		Gn		37.450	15.434	17.329	
		Gn		37.650	15.591	17.189	
		Gn		36.696	15.257	16.880	
		Gn		36.779	15.250	16.899	
	Longshan Au–Sb deposit	Gn	Auriferous quartz vein	37.603	15.478	17.232	Luo (1989)
Southeastern Guizhou Province	Bake Au deposit	Gn	Auriferous quartz vein	37.588	15.541	17.368	Yu (1997)
		Gn		37.646	15.562	17.388	
		Gn		37.562	15.537	17.331	

Note: Py = pyrite, Gn = galena, Arsp = arsenopyrite, Sph = sphalerite, Sti = Stibnite, Orp = Orpiment, Rlr = Realgar, Qtz = quartz.

Appendix A4
Summary of the C and O isotopic data of the representative Au (-polymetallic) deposits in the JOB.

Region	Sample No.	Mineral/ Objective	Mineralizing stage	Ore type	Deposit	$\delta^{13}C_{V-PDB}$/‰	$\delta^{18}O_{V-SMOW}$/‰	$\delta^{18}O_{V-PDB}$/‰	References
Northwestern Zhejiang Province		Ankerite	Ore-stage	Auriferous ankerite veins	Huangshan Au deposit	−4.9	+8.65	−21.52	Ye et al. (1994)

(*continued on next page*)

Appendix A4 (*continued*)

Region	Sample No.	Mineral/ Objective	Mineralizing stage	Ore type	Deposit	$\delta^{13}C_{V-PDB}$/‰	$\delta^{18}O_{V-SMOW}$/‰	$\delta^{18}O_{V-PDB}$/‰	References
Northeastern Jiangxi Province	J08	Ankerite	Ore-stage	Quartz-albite-ankerite-pyrite-bearing altered host rocks	Jinshan Au deposit	−5.0	+7.3	−22.9	Li et al. (2010a)
	J11	Ankerite	Ore-stage	Quartz-albite-ankerite-pyrite-bearing altered host rocks Auriferous quartz veins		−4.2	+4.4	−25.7	Li et al. (2010a), Fan and Li (1992)
	J18	Ankerite	Ore-stage			−4.9	+8.0	−22.2	
	G503	Ankerite	Ore-stage			−1.89	+14.11	−15.33	
	G028	Ankerite	Ore-stage			−4.84	+6.82	−22.41	Fan and Li (1992), Ji et al. (1994a)
	J-11	Fluid inclusions in quartz	Ore-stage			−0.5 (CO_2)	+17.1	−13.33	
	J-12	Fluid inclusions in quartz	Ore-stage	Auriferous quartz veins		+2.5 (CO_2)	+18.0	−12.46	Ji et al. (1994a)
Hunan Province	G-1–3	Calcite	Ore-stage	Auriferous quartz veins	Xi'an Au deposit	−5.67	+16.93	−13.50	Wan (1986)
	G-17	Calcite	Ore-stage	Auriferous quartz veins		−3.74	+16.01	−14.39	
	G-18–2	Calcite	Ore-stage	Auriferous quartz veins		−5.22	+17.57	−12.88	
	G35-2	Calcite	Ore-stage	Auriferous quartz veins		−3.15	+18.02	−12.44	
	K-56	Calcite	Ore-stage	Auriferous quartz veins		−4.12	+17.17	−13.26	
	G-29	Limestones	Host rocks	Between the Lengjiaxi Group and the Madiyi Formation of the Banxi Group		−2.24	+16.39	−14.02	
	G-30	Limestones	Host rocks			−3.06	+16.61	−13.81	
	G-34	Limestones	Host rocks			−1.84	+16.47	−13.94	
	G-37	Limestones	Host rocks			−0.58	+15.80	−14.59	
	K-66	Limestones	Host rocks			−1.01	+17.17	−13.26	
	F-105	Limestones	Host rocks			−3.76	+17.56	−12.89	
	HRP-2	Calcite	Ore-stage	Auriferous quartz veins	Herenping Au deposit	−5.1	+17.2	−13.3	Hu and Peng (2015)
	HRP-15	Calcite	Ore-stage	Auriferous quartz veins		−5.6	+17.3	−13.2	Hu and Peng (2015), Cao et al. (2015b)
	HRP-18	Calcite	Ore-stage	Auriferous quartz veins		−5.2	+17.1	−13.4	
	HRP-22	Calcite	Ore-stage	Auriferous quartz veins		−5.5	+17.2	−13.3	
	HRP-24	Calcite	Ore-stage	Auriferous quartz veins		−6.1	+17.3	−13.2	
	HRP-28	Calcite	Ore-stage	Auriferous quartz veins		−5.6	+17.1	−13.4	
	CLG-1	Calcite	Ore-stage	Auriferous quartz veins		−5.7	+17.0	−13.5	
	CLG-3	Calcite	Ore-stage	Auriferous quartz veins		−5.6	+17.2	−13.3	
	CLG-12	Calcite	Ore-stage	Auriferous quartz veins		−5.7	+16.9	−13.6	
	CLG-21	Calcite	Ore-stage	Auriferous quartz veins		−5.6	+17.6	−13.0	
	CLG-22	Calcite	Ore-stage	Auriferous quartz veins		−5.6	+17.5	−13.0	
	CLG-35–1	Calcite	Ore-stage	Auriferous quartz veins		−4.4	+17.2	−13.3	
	QZC-13–1	Calcite	Ore-stage	Auriferous quartz veins		−5.1	+19.5	−11.1	
	QZC-15	Calcite	Ore-stage	Auriferous quartz veins		−5.5	+17.9	−12.6	
	TSM-6	Calcite	Ore-stage	Auriferous quartz veins		−3.9	+17.3	−13.2	
	CZP-B4	Fluid inclusions in quartz	Ore-stage	Auriferous quartz veins	Chanziping Au deposit	−11.1 (CO_2)	+14.7	−15.7	
	CZP-B5		Ore-stage	Auriferous quartz veins		−11.0 (CO_2)	+14.4	−16.0	Cao et al. (2015b)
	CZP-B6		Ore-stage	Auriferous quartz veins		−11.4 (CO_2)	+15.7	−14.7	
	CZP-B9		Ore-stage	Auriferous quartz veins		−11.7 (CO_2)	+15.4	−15.0	
	CZP-B7	Host rocks	Barren	Arenaceous slates		−14.0	+16.3	−14.1	
	CZP-B8		Barren	Arenaceous slates		−14.1	+15.5	−15.0	
Southeastern Guizhou Province	JJ03	Fluid inclusions in quartz	Ore-stage	Auriferous altered cataclasite ores	Tonggu Au deposit	−2.94 (CO_2)			Wu et al. (2005)
	TG9801		Ore-stage	Auriferous altered cataclasite ores		−7.98 (CO_2)	–		
	TG9802		Ore-stage	Interbedded auriferous veins		−3.99 (CO_2)			
	TG9803		Ore-stage	Auriferous altered cataclasite ores		−6.18 (CO_2)			
	TG9804		Ore-stage	Auriferous stockworks		−2.34 (CO_2)			

Note: $\delta^{18}O_{V-PDB} = 0.9706*\delta^{18}O_{V-SMOW} - 29.92$.

Appendix A5
H and O isotope data and fluid inclusion characteristics of the representative Au (-polymetallic) deposits in the JOB, South China.

Region	Deposit	Description	Mineral	$O_{mineral}$	D_{H2O} (‰)	O_{H2O} (‰)	Th (°C)	Pressure (kba)	Salinity (wt.% NaCl $_{equiv.}$)	f_{O2}(n×10^{-n})	pH	References
Northwestern Zhejiang Province	Yanghanwu	Ore-stage	Quartz				151	0.40	4.4–8.2 (avg. 6.45)			Ye et al. (1994)
	Yangjiawu	Ore-stage	Quartz				185	0.48	3.4–6.6 (avg. 5.0)			
	Gaokeng	Ore-stage	Quartz				171	0.45	6.5–10.5 (avg. 8.7)		6.60	
	Dagaowu	Ore-stage	Quartz				176	0.46	4.9–9.6 (avg. 7.4)			
	Tongshulin	Ore-stage	Quartz	+10.05	−63.5	−2.81	183	0.48	3.9–9.9 (avg. 4.90)		6.80	
	Xintang	Ore-stage	Quartz	+12.39	−68	−5.55	125	0.32	2.9–4.2 (avg. 3.40)		6.70	
	Miaoxiafan	Ore-stage	Quartz	+10.27	−73	−4.53	158	0.41	4.1–9.2 (avg. 6.53)		6.80	
	Huangshan	Ore-stage	Quartz	+12.02	−72.1	−2.95	156	0.42	2.6–24.0 (avg. 9.9)		6.76	
		Ore-stage	Quartz	+9.48	−58.7	−5.49	156					
		Ore-stage	Ankerite			−4.3	135					
		Ore-stage	Quartz				350	0.59	4.2	35	4–6	Ma and Liu (1991)
		Ore-stage	Quartz	+10.75–+12.21 (avg. +11.35)	−64.04 to −91.07 (avg. −79.75)		206–318					Li (1990)
		H_2O-CO_2 inclusions	Quartz				253–304		1.2–6.4			Ni et al. (2015)
		Aqueous inclusions	Quartz				236–295		3.2–9.8			
	Pingshui	H_2O-CO_2 inclusions	Quartz				225–282		1.2–6.0			
		Aqueous inclusions	Quartz				214–271		2.7–8.7			
Northeastern Jiangxi Province	Jinshan	Ore-stage	Quartz		−63.67	+7.67						Huang and Yang (1990)
			Quartz		−58.06	+10.41						
			Quartz		−59.91	+8.74						
		Ore-stage	Quartz		−63.4	+2.23						Wei (1995)
			Quartz		−63.9	+11.35						
			Quartz		−52.9	+4.15						
			Quartz		−60.5	+10.49						
			Quartz		−43.9	+10.24						
		Auriferous mylonites	Quartz				220–260	0.95		46	4.60	Hua et al. (2002)
		Au quartz veins	Quartz					0.16		47	5.17	
		Ore-stage	Quartz	+15.27		+6.30						
			Quartz	+15.53	−41	+6.46						
			Quartz	+14.10	−56	+5.43						
			Quartz	+15.40		+6.43						
			Quartz	+14.60		+5.63						
			Quartz	+14.60	−56	+5.63						
			Quartz	+12.30		+3.33						
			Quartz	+15.45	−47	+6.48						
			Quartz	+15.20		+6.25						
		Post-ore stage	Quartz	+8.17		−0.8						
		Ore-stage	Quartz	+10.06	−55.46	+3.16	300	0.35–0.77	12.3–14.5	40.5–45.2		Fan and Li (1992)
			Quartz	+10.06	−56.68	+2.80	290					
			Quartz	+10.06	−43.47	+2.00	270					
			Quartz	+10.06	−53.62	+2.00	270					

(continued on next page)

Appendix A5 (*continued*)

Region	Deposit	Description	Mineral	$O_{mineral}$	D_{H2O} (‰)	O_{H2O} (‰)	Th (°C)	Pressure (kba)	Salinity (wt.% NaCl $_{equiv.}$)	f_{O2}($n\times10^{-n}$)	pH	References
		Ore-stage I	Quartz				275–310				7.34	
			Quartz								6.76	
		Ore-stage II	Quartz				250–285				6.68	
			Quartz								6.64	
		Ore-stage III	Calcite				220–250				7.69	
			Calcite								7.25	
		Barren quartz from the host rocks	Quartz		−30.71		140–300				7.35	
			Quartz								4.88	
		Ore-stage	Quartz	+17.1	−88.6		140–220		11.9			Ji et al. (1994a)
			Quartz	+18.0	−59.2							
			Quartz	+15.0	−66.3							
			Quartz	+15.0	−45.8							
			Quartz	+15.3	−89.8							
		Barren quartz from the host rocks	Quartz	+17.1	−70.1		240–280		6.3			
			Quartz	+17.6	−58.5							
			Quartz	+15.5	−58.5							
		Pre-ore stage	Quartz	+16.8	−60	+10.4	315					Zhao et al. (2013a)
			Quartz	+17.1	−60	+10.9	320					
			Quartz	+16.8	−52	+10.6	320					
			Quartz	+17.6	−61	+11.2	315					
			Quartz	+17.3	−53	+10.6	305					
		Ore-stage	Quartz	+16.3	−71	+6.9	240					
			Quartz	+17.4	−64	+8.4	250					
			Quartz	+16.2	−59	+7.0	245					
			Quartz	+16.2	−66	+7.7	260					
			Quartz	+16.3	−46	+7.8	260					
			Quartz	+17.1	−60	+8.6	260					
		Pre-ore stage	Quartz				285–340		1.4–6.1			
		Ore-stage	Quartz				241–292		1.0–7.0			
			Quartz				243–272		0.6–3.6			
			Quartz				208–266		3.5–8.9			
		Post-ore stage	Quartz				109–201		1.1–6.4			
			Calcite				124–186		1.7–5.7			
		Ore-stage	Quartz				260–295	0.50–0.79	15.3–16.5	34–36	6.1–7.4	Ma and Liu (1991)
			Quartz				200–280		15–16	42	6.48–7.7	Zeng et al. (2002a-b)
			Quartz				230–370	0.48–0.58	12.5–15.8	39–42	5.3–6.9	
		Ore-stage	Quartz	+15.3	−62	+8.4						Li et al. (2010a)
			Quartz	+13.2	−73	+6.3						
			Quartz	+12.4	−65	+5.5						
			Quartz	+14.6	−66	+7.7						
			Quartz	+13.4	−73	+6.5						
			Quartz	+14.9	−69	+8.0						
			Quartz	+14.3	−68	+7.4						
		Ore-stage	Quartz				271–372	0.71–	1.9–10.0 (avg. 4.2)			Li (2009)

Appendix A5 (*continued*)

Region	Deposit	Description	Mineral	$O_{mineral}$	D_{H2O} (‰)	O_{H2O} (‰)	Th (°C)	Pressure (kba)	Salinity (wt.% NaCl $_{equiv.}$)	f_{O2}($n \times 10^{-n}$)	pH	References
							(avg. 330)	0.73				
			Quartz				207–312 (avg. 273)		1.4–3.2 (avg. 2.1)			
			Quartz				188–319 (avg. 251)		5.3–7.6 (avg. 6.6)			
			Quartz				230–307 (avg. 272)		0.6–10.0 (avg. 3.4)			
			Quartz				200–296 (avg. 261)		2.2–10.0 (avg. 6.4)			
			Quartz				152–295 (avg. 189)		1.9–11.3 (avg. 5.4)			
			Quartz				229–275 (avg. 247)		0.6–6.9 (avg. 4.2)			
	Hamashi	Ore-stage	Quartz				145–421 (avg. 318)		2.9–13.1 (avg. 5.9)			
			Quartz	+12.66	−72.8						6.8	Mao (1998)
			Quartz	+14.64							6.5	
			Quartz								7.4	
			Quartz	+13.89							6.3	
			Quartz	+14.26							6.05	
			Quartz	+9.98							6.63	
		Barren quartz from the host rocks	Quartz	+16.63			340				6.56	
			Quartz	+17.32			320				6.75	
		Ore-stage	Quartz	+14.59	−57.64		215–301 (avg. 235–280)					Hu (1995)
			Quartz	+14.04	−58.60							
			Quartz	+13.61								
			Quartz	+11.81								
			Quartz	+14.34	−58.23							
			Quartz	+13.45								
			Quartz	+12.54								
	Shiwu	Ore-stage	Quartz	+11.5 to +15.45	−70.5 to −46.7		180 to 260	0.29 to 0.39		13.2 to 43.5	4.46 to 8.43	Li and Chen (2005)
	Dexing Cu-polymetallic deposit	Ore-bearing prophyries	Quartz			+8.17 to +9.99						Huang and Yang (1990)
		Ore-bearing quartz veins with porphyries	Quartz			+4.65 to +9.18						
NEHP	Yanlinsi	NE-trending veins (Ore-stage I)	Quartz	+13.82	−72.6	+4.18 to +7.87	250–350		3.59		5.92	Liu and Wu (1993)
		NW-trending veins (Ore-stage II)	Quartz	+12.92	−60.6	+5.3 to +8.23	300–400		2.16		6.54	
	Huangjindong	Main ore-stage	Quartz		−61	+9.6						Mao and Li (1997)

(*continued on next page*)

Appendix A5 (*continued*)

Region	Deposit	Description	Mineral	$O_{mineral}$	D_{H2O} (‰)	O_{H2O} (‰)	Th (°C)	Pressure (kba)	Salinity (wt.% NaCl $_{equiv.}$)	f_{O2}(n×10^{-n})	pH	References
			Quartz		−57	+6.1						
		Stage I (barren)	Quartz	+16.14		+9.42	305					Luo (1988)
		Ore-stage II (low grade)	Quartz	+16.59		+8.51	270					
			Scheelite	+4.94 to +5.22(avg. +5.08)		+5.92 to +6.29(avg. +6.11)	260–265					
		Ore-stage III (high grade)	Quartz	+17.12		+8.16	250					
		Stage IV (barren)	Quartz	+16.79		+7.59	245					
		Main ore-stage	Quartz	+18.67		+3.62 to +5.59	155–180				5.13–6.90	Liu (1989)
			Quartz	+12.46	−38.4	+1.67 to +3.02	215–240					
			Quartz	+15.70	−47.1	+4.91 to +5.83	215–230					
			Quartz	+16.50		+5.71 to +6.51	215–230					
		Main ore-stage II?	Quartz				233		3.55			Li et al. (2011)
			Quartz				225		4.65			
			Quartz				232		4.18			
			Quartz				228		4.34			
			Quartz				233		4.65			
		Main ore-stage I?	Quartz				339		10.86			
			Quartz				336		10.73			
		Ore-stage	Quartz				397–280	0.99	5.8–9.5	31–35	6.6–7.4	Ma and Liu (1991)
	Wangu	Ore-forming stage	Quartz	+15.45	−64.2	+3.09	201		0.75	5.27 (41)	5.68	Liu et al. (1994a)
			Quartz	+17.91	−55.0	+3.81	176		6.40	1.40 (43)	6.24	
		Barren stage	Quartz	+17.50	−60.5	+3.40	198		0.77	3.50 (41)	5.87	
		Ore-stage	Quartz	+19.6	−61	+7.8	207		3.4			Mao et al. (2002)
			Quartz	+19.5	−59	+9.9	247		3.2			
			Quartz	+18.5	−64	+10.9	295		4.5			
			Quartz	+18.7	−60	+9.6	258		4.2			
			Quartz	+17.8	−64	+10.8	310		3.8			
			Quartz	+18.1	−60	+9.8	276		3.8			
			Quartz	+17.9	−56	+8.2	245		3.0			
			Quartz	+18.6	−60	+7.4	216		4.6			
			Quartz	+18.1	−63	+9.3	265		4.0			
			Quartz	+18.5	−59	+10.1	273		3.9			
			Quartz	+19.1	−56	+10.1	260		3.4			
			Quartz	+18.8	−61	+9.1	244		3.0			
		Barren stage	Quartz	+17.7	−92	+1.3	145		5.5			
			Quartz	+22.0	−86	+2.0	138		6.0			
		Ore-stage I	Quartz				206		7.59			Deng et al. (2013)
			Quartz				210		11.53			
		Ore-stage II	Quartz				185		6.05			
			Quartz				206		10.43			

Appendix A5 (*continued*)

Region	Deposit	Description	Mineral	$O_{mineral}$	D_{H2O} (‰)	O_{H2O} (‰)	Th (°C)	Pressure (kba)	Salinity (wt.% NaCl $_{equiv.}$)	f_{O2}(n×10^{-n})	pH	References
			Quartz				210		12.61			
		Ore-stage Ⅲ	Quartz				195		7.47			
			Quartz				185		9.23			
			Quartz				225		7.77			
			Quartz				211		11.94			
NWHP	Woxi	Ore-stage	Quartz	+16.5	−64							Zhang (1985)
			Scheelite	+3.60								
			Quartz	+18.3								
			Quartz	+18.2	−64							
			Quartz	+16.8								
			Quartz	+16.9								
			Quartz	+18.3								
			Quartz	+16.9								
			Quartz	+16.7								
			Wolframite	+3.60								
			Quartz	+17.8	−118							
			Quartz	+17.3								
			Quartz	+16.9								
			Quartz	+17.3								
			Quartz	+15.7	−69							
			Quartz	+15.3								
			Quartz	+17.4	−81							
			Quartz	+18.1								
			Quartz	+17.8								
		Banxi Group host rocks	Slates	+17.1								
				+17.1								
				+15.4								
		Ore-stage Ⅰ	Quartz	+26.1	−54.99	+19.2	300					Ma and Liu (1991)
		Ore-stage Ⅱ	Quartz	+16.9	−58.35	+5.2	200					
			Quartz	+18.3	−85.96	+6.6	200					
			Quartz				200–280	0.47	7.5		7.2–6.4	
		Ore stage Ⅰ	Quartz	+17.8		+13.6	396	0.35	1.7			Luo et al. (1984)
			Quartz	+16.5 to +16.7 (avg. +16.6)	−64	+8.0 to +8.2 (avg. +8.1)	259	0.14	2.5–3.8 (avg. 2.9)			
			Wolframite	+3.6		+9.8	259					
			Scheelite	3.6		+9.8	259					
		Ore-stage Ⅱ	Quartz				209	0.16	2.2–11.6 (avg. 5.2)			
			Quartz				212	0.11	2.8–12.5 (avg. 6.6)			
			Quartz	+15.3 to +18.2 (avg. +17.1)	−81	+4.3 to +7.2 (avg. +6.1)	213					
		Ore stage Ⅲ	Quartz	+18.1		+2.0	143	0.25	10			
		Ore-stage Ⅰ	Quartz				163–342		2.41–5.56			Zhu and Peng (2015)
			Quartz				259–357					
			Quartz				354					

(*continued on next page*)

Appendix A5 (*continued*)

Region	Deposit	Description	Mineral	$O_{mineral}$	D_{H2O} (‰)	O_{H2O} (‰)	Th (°C)	Pressure (kba)	Salinity (wt.% NaCl $_{equiv.}$)	$f_{O2}(n\times10^{-n})$	pH	References
			Scheelite				151–337		4.65–5.86			
			Scheelite				258–263					
			Scheelite				217–287		1.18–2.77			
		Ore-stage Ⅱ-Ⅲ	Quartz				131–254		0.88–6.88			
			Quartz				190–246		0.02–1.22			
			Stibnite				109–274		2.24–5.11			
		Ore-stage Ⅰ	Quartz				264	0.27	5.7	36	8.11	Liu et al. (1994b)
		Ore-stage Ⅱ	Quartz				200	0.19	4.3–8.2 (avg. 7.0)	42	6.42	
		Ore stage Ⅲ	Quartz				115	0.19	7.5	48	6.01	
	Xi'an	Ore-stage Ⅰ	Quartz	+21.72	−56.1	+11.2	219	0.66	4.3		5.7	Wan (1986)
			Quartz	+20.61	−56.2	+10.5	228					
			Quartz	+17.41	−64.83	+6.3	210					
			Scheelite		−49.92							
			Scheelite		−48.74							
			Quartz	+17.46		+6.4						
			Scheelite		−55.5							
		Ore-stage Ⅱ	Quartz	+20.04	−58.1	+6.7	176		3.7		5.9	
			Pyrite		−80.9							
			Quartz	+19.2		+6.1	180					
			Quartz	+19.78	−64.0							
		Ore-stage Ⅲ	Quartz	+20.69	−51.2	+4.9	147		3.3		6.3	
			Quartz	+20.92	−51.65	+5.7	153					
			Calcite	+16.92		+4.8	151					
	Yiyangnanjiao	Ore-stage Ⅱ	Quartz		−51.4	+4.09						Liu et al. (1994b)
			Quartz		−50.4	−0.64						
			Quartz		−62.0	+3.32						
			Quartz		−51.6	+5.10						
		Ore-stage Ⅰ	Quartz				300	0.29	6.5	34	8.30	
		Ore-stage Ⅱ	Quartz				220	0.19	7.5	41	6.42	
		Ore stage Ⅲ	Quartz				170	0.19	8.5	45	6.40	
		Ore-stage	Quartz				325–280	0.43	7.8	35	7.8–8.8	Ma and Liu (1991)
	Xichong	Ore-stage Ⅱ	Quartz		−58.8	+7.48						Liu et al. (1994b)
			Quartz		−61.9	+8.04						
			Quartz		−58.5	+6.96						
		Ore-stage Ⅰ	Quartz				304		6.1	36	8.41	
		Ore-stage Ⅱ	Quartz				220		7.5	41	7.06	
		Ore stage Ⅲ	Quartz				150			47	6.49	
		Ore-stage	Quartz				200–300	0.48	7.2	34–43	6.7–8.3	Ma and Liu (1991)
	Huangtudian	Ore-stage Ⅱ	Quartz		−63.2	+5.2						Liu et al. (1994b)
			Quartz		−80.9	+3.6						
		Ore-stage Ⅰ	Quartz				260	0.48	6.6	36	7.06	
		Ore-stage Ⅱ	Quartz				190	0.39	6.9	44	6.50	
	Canglangping	Ore-stage	Quartz	+19.5								Zhang (1985)
			Quartz	+18.3								
	Fuzhuxi	Ore-stage	Quartz	+15.56	−55.2							Yao and Zhu (1993)
			Quartz	+18.78	−56.7							

Appendix A5 (*continued*)

Region	Deposit	Description	Mineral	$O_{mineral}$	D_{H2O} (‰)	O_{H2O} (‰)	Th (°C)	Pressure (kba)	Salinity (wt.% NaCl $_{equiv.}$)	f_{O2}($n\times10^{-n}$)	pH	References
			Quartz	+18.28	−56.1							
			Quartz	+17.24								
SWHP	Chanziping	Ore-stage	Quartz	+16.25	−70.1	+6.80	240					Wei (1993)
			Quartz	+16.35	−64.3	+8.62	278					
			Quartz	+16.58	−54.7	+7.14	240					
		Post-ore stage	Calcite	+17.60	−45.6	+1.06	240					
		Ore-stage	Quartz	+14.7	−102.3	+4.3	157–224 (avg. 220)	0.40–0.51	8.95–13.72			Cao et al. (2015a-b)
			Quartz	+14.4	−100.6	+5.9	180–318 (avg. 259)	0.48–0.64	7.73–13.72			
			Quartz	+15.7	−80.6	+7.2	163–402 (avg. 259)	0.38–0.61	7.17–9.73			
			Quartz	+16.3	−72.6	+7.8	259					
			Quartz	+15.5	−50.6	+7.0	259					
			Quartz	+15.4	−66.6	+6.9	259					
			Quartz				177–329	0.47–0.71	6.88–9.34			
			Quartz				285–365	0.75–0.94	6.10–12.28			
			Quartz				226–385	0.78–0.96	2.24–7.02			
		Ore-stage	Quartz	+16.35	−64.3	5.91	240					Luo (1996)
			Quartz	+15.80	−91.2	5.35	219					
			Quartz	+15.07	−58	4.62	219					
			Quartz	+11.58	−77	1.13	219					
			Quartz	+14.45	−56	4.00	219					
			Quartz	+16.34	−56	5.89	219					
			Quartz	+11.24	−79	0.79	219					
			Quartz	+14.28	−59	3.83	219					
		Post-ore stage	Calcite	+1.06	−45.6	−11.08	150					
	Mobin	Ore-stage	Quartz	+15.85	−42	+2.64	174		2.12–4.17		6.7–6.9	Zhou et al. (1989)
			Quartz	+14.50	−47	+1.99	184					
			Quartz	+17.72	−60	+3.85	164					
			Quartz	+16.80	−49	+3.27	169					
			Quartz	+16.61	−46	+7.33	245					
			Quartz	+16.61	−46	+3.16	170					
			Quartz	+16.65	−37	+3.35	172					
			Quartz	+14.72	−51	−0.44	148					
		Ore-stageⅠ	Quartz				203	0.24	6.3–9.2 (avg. 7.5)		6.56	Niu and Ma (1991)
		Ore-stage Ⅱ	Quartz				174	0.21	6.4–9.3 (avg. 8.3)		6.40	
		Ore-stage	Quartz				160–180	0.69–0.79	8.5	46	6.1–6.4	Ma and Liu (1991)
	Taojinchong	Ore-stage Ⅰ	Quartz	+20.65	−44	+8.92	224	0.58–0.77	3–9 with most between 6 and 8		0.68–1.75	Yan et al. (1994)
			Quartz	+20.03	−50	+7.94	218					
		Ore-stage Ⅱ	Quartz	+18.98	−81	+3.83	174					
			Quartz	+19.42	−63	+4.19	173					
			Quartz	+19.52	−62	+3.20	160					
			Quartz	+18.16	−70	+1.03	151					
		Ore stage Ⅲ	Quartz	+16.87	−82	−0.84	145					
			Quartz	+16.47	−86	−2.04	137					
Southeastern Guizhou Province	Pingqiu Au deposit	Ore-stage	Quartz	+17.4	−64	+8.7						Long et al. (2015)

(*continued on next page*)

Appendix A5 (*continued*)

Region	Deposit	Description	Mineral	$O_{mineral}$	D_{H2O} (‰)	O_{H2O} (‰)	Th (°C)	Pressure (kba)	Salinity (wt.% NaCl $_{equiv.}$)	f_{O2}(n×10^{-n})	pH	References
		Ore-stage	Quartz	+17.7	−66	+9.0						
		Ore-stage	Quartz	+17.2	−62	+8.5						
		Ore-stage	Quartz	+16.2	−60	+7.3	250–350	0.37	0.53–20.07			Wu (2009)
		Ore-stage	Quartz	+17.3	−49	+8.4						
		Ore-stage	Quartz	+16.2	−57	+7.3						
		Ore-stage	Quartz	+17.3	−60	+8.4						
		Ore-stage	Quartz	+17.9	−53	+9.0						
		Ore-stage	Quartz				293–352	0.35	1.02–4.98			
		Ore-stage	Quartz				216–320		1.81–2.39			
		Ore-stage	Quartz				307–312	0.50	1.42–2.00			
		Ore-stage	Quartz				284–318		1.02–3.25			
		Ore-stage	Quartz				282–294	0.48	1.42–3.89			
		Ore-stage	Quartz				292–293		1.62–2.20			
		Ore-stage	Quartz				265–304	0.41	1.62–3.15			
		Ore-stage	Quartz				297–324		2.00–3.15			
		Ore-stage	Quartz				160–323	0.48	1.40–16.71			
		Ore-stage	Quartz				192–207		0.53–12.28			
		Ore-stage	Quartz				215–272		5.26–20.07			
		Ore-stage	Quartz				107–330		1.06–7.31			
		Ore-stage	Quartz				287		0.63–3.15			
		Ore-stage	Quartz	+17.4	−64	+7.37						He et al. (2015)
		Ore-stage	Quartz	+17.7	−66	+7.67						
		Ore-stage	Quartz	+17.2	−62	+7.17						
	Bake Au deposit	Ore-stage	Quartz				277–301		1.42–2.58			Wu (2009)
		Ore-stage	Quartz				278–283		1.81–2.20			
		Ore-stage	Quartz				154		0.35–2.24			
		Ore-stage	Quartz				139–198	0.80	1.91–6.45			
		Ore-stage	Quartz				132–183	0.59	5.11–6.16			
		Ore-stage	Quartz	+17.46	−66.5	+10.26	300	0.46	0.35–6.45			Yu (1997), Wu (2009)
	Tonggu Au deposit	Ore-stage	Quartz				97–145		1.23–9.21			Wu (2009)
		Ore-stage	Quartz				136–225		1.06–5.41			
		Ore-stage	Quartz				155–249		2.24–10.36			
		Ore-stage	Quartz		−43.5	−3.52	200–300		3.76		6.60	Wu et al. (2005), Wu (2009)
		Ore-stage	Quartz		−44.1	−1.61			3.31		6.70	
		Ore-stage	Quartz		−33.4	−1.87			3.11		6.85	
		Ore-stage	Quartz		−37.1	−1.14			2.13		6.75	
		Ore-stage	Quartz		−36.1	−1.96			0.78		6.60	
	Gubang	Ore-stage	Quartz		−33.4 to −44.3	−1.14 to −3.52	250–350					Sun (2011)
	Tianzhushan (Youma'ao, Moshan, Tongluoping, Jinchang)	Ore-stage	Quartz	+16.75	−87.6	+5.9	214					Zhang et al. (1997)
		Ore-stage	Quartz	+16.16	−74.8	+5.6	220					
		Ore-stage	Quartz	+17.32	−47.0	+5.2	193					
		Ore-stage	Quartz	+17.06		+4.7	190					
		Ore-stage	Quartz	+18.04	−53.0	+6.3	220					
		Ore-stage	Quartz	+16.41	−72.9	+4.6	199					
		Ore-stage	Quartz	+17.25	−51.9	+5.9	205					
		Ore-stage	Quartz	+15.46	−42.4	+7.0	265					
		Ore-stage	Quartz	+15.95								

Appendix A5 (*continued*)

Region	Deposit	Description	Mineral	$O_{mineral}$	D_{H2O} (‰)	O_{H2O} (‰)	Th (°C)	Pressure (kba)	Salinity (wt.% NaCl $_{equiv.}$)	f_{O2}($n\times10^{-n}$)	pH	References
		Tuffaceous slates of the Xiajiang Group	Quartz	+12.97								
	Kengtou	Ore-stage	Quartz	+18.55	−92.1	+2.88	148	0.39	6.36	52	8.5	Tian et al. (2011)
		Ore-stage	Quartz	+17.41	−49.8	+3.89	174				8.6	
		Ore-stage	Quartz	+15.37		+6.60	254				8.5	
		Ore-stage	Quartz	+18.27		+6.30	196				8.7	
Northern Guangxi Province	Fenshuiao	Ore-stage	Quartz	+9.52	−67.2	−5.86	160	0.22–0.68	7.7–10.0 (avg. 9.1)			Wang and Zhang (1997)
			Quartz	+8.04	−48.6	−5.55	183		8.9–11.0 (avg. 10.2)			
			Quartz				178		9.1–10.7 (avg. 10.1)			

Note: NEHP, NWHP and SWHP represent the northeastern-, northwestern- and southwestern Hunan Province of the JOB, respectively.

Appendix A6
Summary of the reliable geochronological data of the major Au (-polymetallic) deposits and associated intrusions in the JOB.

Region	Deposit/pluton	Age (Ma)	Method	References
Northwestern Zhejiang Province	Tongshulin–Huangshan ductile shear zone	343 Ma	K–Ar dating on phengite from Au quartz veins	Ye et al. (1993)
		373 Ma	K–Ar dating on Au-bearing mylonites	
		325 Ma	K–Ar dating on muscovite from Au quartz veins	
		329.9 Ma	K–Ar dating on sericite from Au-bearing mylonites	
		353 Ma	Ar–Ar dating on muscovite from Au-bearing mylonites	
		345 Ma		
	Mali Au deposit	145.82 ± 3 Ma	K–Ar dating on felsite porphyric dykes	
	Pingshui Cu–Au–Pb–Zn deposit	450 ± 21 Ma (MSWD = 10.5)	Rb–Sr dating on fluid inclusions in quartz	Ni et al. (2015)
	Tongcun Cu–Mo deposit	168.7 ± 2.3 Ma (MSWD = 1.2)	SHRIMP U–Pb dating on zircon from granite porphyries	Zhu et al. (2014)
		165.7 ± 2.1 Ma (MSWD = 1.8)	SHRIMP U–Pb dating on zircon from granodiorites	
		162 ± 3 Ma (MSWD = 2.7)		
		165.8 ± 2.4 Ma (MSWD = 1.2)		
		160.3 ± 2.6 Ma (MSWD = 15)		
		162 ± 2.1 Ma (MSWD = 3.0)		
		162 ± 3 Ma (MSWD = 1.12)		
Southern Anhui Province	Jinde pluton	141 ± 1 Ma (MSWD = 0.57)	LA-ICP-MS U–Pb dating on zircon from granodiorites	Zhou et al. (2014)
	Dongyuan pluton	146.7 ± 1.5 Ma (MSWD = 0.85)	LA-ICP-MS U–Pb dating on zircon from granodioritic porphyries	Zhou et al. (2015)
Northeastern Jiangxi Province	Jinshan Au deposit	ca. 660–560 Ma	Ar–Ar dating on sericite	Li et al. (2007a)
	Yinshan Ag–Cu-polymetallic deposit	Plateau age 178.2 ± 1.4 Ma; Isochron age 179.6 ± 2.9 Ma (MSWD = 0.64)	Ar–Ar dating on muscovite from dacite porphyries	Li et al. (2007d)
		Plateau age 175.3 ± 1.1 Ma; Isochron age 176.6 ± 3.3 Ma (MSWD = 0.19)	Ar–Ar dating on muscovite from quartz porphyries	
		Plateau age 175.4 ± 1.2 Ma; Isochron age 176.2 ± 5.1 Ma (MSWD = 0.32)	Ar–Ar dating on muscovite from altered quartz porphyries	
		183 ± 3 Ma (MSWD = 1.5)	SHRIMP U–Pb dating on zircon from dacite porphyries	
	Fujiawu porphyry	170.2 ± 0.88 Ma (MSWD = 0.61)	LA-ICP-MS U–Pb dating on zircon	Zhou et al. (2012a)
		170 ± 1 Ma (MSWD = 0.37)	LA-ICP-MS U–Pb dating on zircon	Wang et al. (2015)
		171 ± 3 Ma (MSWD = 0.4)	SHRIMP U–Pb dating on zircon	Wang et al. (2004)
	Tongchang porphyry	173.8 ± 1.3 Ma (MSWD = 2.6)	SIMS U–Pb dating on zircon	Liu et al. (2012)
		171.9 ± 1.0 Ma (MSWD = 1.3)		
		173.2 ± 0.8 Ma (MSWD = 1.1)		
		173.0 ± 0.9 Ma (MSWD = 1.6)		
		171.4 ± 1.0 Ma (MSWD = 2.0)		
		171.0 ± 0.84 Ma (MSWD = 0.86)	LA-ICP-MS U–Pb dating on zircon	Zhou et al. (2012a)
		171.0 ± 2 Ma (MSWD = 1.5)	LA-ICP-MS U–Pb dating on zircon	Wang et al. (2015)
		153.5 ± 2.4 Ma (MSWD = 2.5)	SHRIMP U–Pb dating on zircon	Zhou et al. (2012b)
		171 ± 3 Ma (MSWD = 0.47)	SHRIMP U–Pb dating on zircon	Wang et al. (2004)
	Zhushahong porphyry	170.7 ± 0.84 Ma (MSWD = 0.60)	LA-ICP-MS U–Pb dating on zircon	Zhou et al. (2012a)
		170 ± 1 Ma (MSWD = 1.7)	LA-ICP-MS U–Pb dating on zircon	Wang et al. (2015)
Northeastern Hunan Province	Dayan altered breccia–type Au occurrence	Ar–Ar plateau age 130 ± 1.4 Ma (MSWD = 0.9)Ar–Ar isochronic age 130.6 ± 6.1 Ma (MSWD = 0.093)	Ar–Ar dating on muscovite	This study
		Ar–Ar plateau age 130 ± 1.4 Ma (MSWD = 1.06)Ar–Ar isochronic age 127.9 ± 5.9 Ma (MSWD = 0.036)	Ar–Ar dating on muscovite	
	Meixian Mo deposit	138 ± 5.7 Ma (MSWD = 5.8)	Re–Os dating on molybdenite	
	Lianyushan granitoids	145 ± 1 Ma (MSWD = 1.9)	LA-ICP-MS U–Pb dating on zircon	
Northwestern Hunan Province	Woxi Au–Sb–W deposit	402 ± 6 Ma (MSWD = 0.3)	Sm–Nd dating on scheelite	Peng et al. (2003)
		Plateau age 423.2 ± 1.2 Ma; Isochron age 421.6 ± 4.5 Ma (MSWD = 1.93)	Ar–Ar dating on quartz	
		Plateau age 416.2 ± 0.8 Ma; Isochron age 415.1 ± 3.1 Ma (MSWD = 1.08)		

Appendix A6 (*continued*)

Region	Deposit/pluton	Age (Ma)	Method	References
	Huangmaoyuan pluton	222.3 ± 1.7 Ma (MSWD = 4.28)	SHRIMP U–Pb dating on zircon from biotite granites	Li et al. (2008b)
	Banxi Sb–Au deposit	397.4 ± 0.4 Ma	Ar–Ar plateau ages dating on quartz	Peng et al. (2003)
		422.2 ± 0.2 Ma	Ar–Ar plateau ages dating on quartz	Peng et al. (2003)
	Darongxi W deposit	223.3 ± 3.9 Ma (MSWD = 0.63)	Re–Os dating on molybdenite	Zhang et al. (2014)
Southwestern Hunan Province	Mobin Au–Sb deposit	404.2 Ma	K–Ar dating on K-feldspar	Wang et al. (1999)
	Yangwatuan Au–Sb deposit	381.7 ± 0.4 Ma	Ar–Ar plateau ages dating on quartz	Peng et al. (2003)
Southeastern Guizhou Province	Pingqiu Au deposit	400 ± 24 Ma (MSWD = 0.96)	Re–Os dating on arsenopyrite	Wang et al. (2011a)
	Jinjing Au deposit	174 ± 15 Ma (MSWD = 1.07)	Re–Os dating on arsenopyrite	Wang et al. (2011a)
Northern Guangxi Province	Fenshuiao Au deposit	166.4 ± 25.7 Ma	Rb–Sr dating on auriferous quartz veins	Wang and Zhang (1997)

References

Bielicki, K.H., Tischendorf, G., 1991. Lead isotope and Pb- Pb model age determinations of ores from Central Europe and their metallogenetic interpretation. Contrib. Miner. Petrol. 106, 440–461.

Bissig, T., Clark, A.H., Lee, J.K., Hodgson, C.J., 2002. Miocene landscape evolution and geomorphologic controls on epithermal processes in the El Indio-Pascua Au-Ag-Cu belt, Chile and Argentina. Econ. Geol. 97, 971–996.

Cao, L., Duan, Q.F., Peng, S.G., Zhou, Y., 2015a. Characteristics of fluid inclusions in the Chanziping gold deposit in western Hunan Province and their geological implications. Geol. Explor. 51 (2), 212–224 (in Chinese with English abstract).

Cao, L., Duan, Q.F., Peng, S.G., Zhou, Y., 2015b. Characteristics and geological significance of stable isotopes in the Chanziping gold deposit of Xuefeng Mountains. Geol. Mineral Resour. South China 31 (2), 157–175 (in Chinese with English abstract).

Charvet, J., 2013. The Neoproterozoic-Early Paleozoic tectonic evolution of the South China Block: an overview. J. Asian Earth Sci. 74, 198–209.

Chen, G.D., 1956. Examples of "activated region" in Chinese Plateform with special reference to the "Cathaysia" problem. Acta Geol. Sinica 36, 239–272 (in Chinese with English abstract).

Chen, M.X., 2003. Characteristics of quartz inclusion gold evolution in Xiangxi gold deposits and its periphery. Mineral Resour. Geol. 17 (4), 519–522 (in Chinese with English abstract).

Chen, Y.J., 2013. The development of continental collision metallogeny and its application. Acta Petrol. Sin. 29 (1), 1–17 (in Chinese with English abstract).

Chen, J.F., Jahn, B.M., 1998. Crustal evolution of southeastern China: Nd and Sr isotopic evidence. Tectonophysics 284, 101–133.

Chen, H.S., Xu, B.T., 1996. Isotope geochemical study on the Huangshan gold deposit, Zhejiang. Geol. Zhejiang 12 (1), 74–82 (in Chinese with English abstract).

Chen, J.F., Foland, K.A., Xing, F.M., Xu, J., Zhou, T.X., 1991. Magmatism along the southeast margin of the Yangtze block: Precambrian collision of the Yangtze and Cathaysia blocks of China. Geology 19, 815–818.

Chen, Y.J., Guo, G.J., Li, X., 1998. Metallogenic geodynamic background of Mesozoic gold deposits in granite-greenstone terrains of North China Craton. Sci. China (Series D) 41 (2), 113–120.

Chen, F.W., Dai, P.Y., Mei, Y.P., Li, H.Q., Wang, D.H., Cai, H., 2008. Metallogenetic and isotopic chronological study on the Shenjiaya gold deposit in Xuefeng Mountains, Hunan Province. Acta Geol. Sin. 82 (7), 906–911 (in Chinese with English abstract).

Chen, C.H., Hsieh, P.S., Lee, C.Y., Zhou, H.W., 2011a. Two episodes of the Indosinian thermal event on the South China Block: constraints from LA-ICPMS U-Pb zircon and electron microprobe monazite ages of the Darongshan S-type granitic suite. Gondwana Res. 19, 1008–1023.

Chen, M.H., Mao, J.W., Bierlein, F.P., Norman, T., Uttley, P.J., 2011b. Structural features and metallogenesis of the Carlin-type Lannigou gold deposit, Guizhou Province, China. Ore Geol. Rev. 43 (1), 217–234.

Chen, G.H., Wan, H.Z., Shu, L.S., Zhang, C., Kang, C., 2012. An analysis on ore-controlling conditions and geological features of the Cu-W polymetallic ore deposit in the Zhuxi area of Jingdezhen, Jiangxi Province. Acta Petrol. Sin. 28, 3901–3914 (in Chinese with English abstract).

Chen, G.H., Shu, L.S., Shu, L.M., Zhang, C., Ouyang, Y.P., 2016. Geological characteristics and mineralization setting of the Zhuxi tungsten (copper) polymetallic deposit in the Eastern Jiangnan Orogen. Sci. China Earth Sci. 59 (4), 803–823.

Chu, Y., Lin, W., Faure, M., Wang, Q.C., Ji, W.B., 2012. Phanerozoic tectonothermal events of the Xuefengshan Belt, central South China: implications from U-Pb age and Lu-Hf determinations of granites. Lithos 150, 243–255.

Cline, J.S., Hofstra, A.H., Muntean, J.L., Tosdal, R.M., Hickey, K.A., 2005. Carlin-type gold deposits in Nevada: critical geologic characteristics and viable models. In: Economic Geology 100th Anniversary Volume 100, pp. 451–484.

de Almeida, C.M., Olivo, G.R., Chouinard, A., Weakly, C., Poirier, G., 2010. Mineral paragenesis, alteration, and geochemistry of the two types of gold ore and the host rocks from the Carlin-type deposits in the southern part of the Goldstrike property, northern Nevada: implications for sources of ore-forming elements, ore genesis, and mineral exploration. Econ. Geol. 105 (5), 971–1004.

Deng, J., Wang, Q.F., 2016. Gold mineralization in China: Metallogenic provinces, deposit types and tectonic framework. Gondwana Res. 36, 219–274.

Deng, H.J., Xia, H.D., Xi, C.Z., Cui, Y.L., 2013. Geochemical characteristics of ore-forming fluids for Tongyuan-Heshangpo gold deposit, Pingjiang County, Hunan Province. Acta Mieral. Sin. 33 (4), 691–697 (in Chinese with English abstract).

Ding, Q.F., Wang, G., 2009. Study on fluid inclusions and genesis of Mobin gold deposit in Hunan Province. Global Geol. 28 (4), 467–475 (in Chinese with English abstract).

Dong, S.W., Zhang, Y.Q., Long, C.X., Yang, Z.Y., Ji, Q., Wang, T., Hu, J.M., Chen, X.H., 2007. Jurassic tectonic revolution in China and new interpretation of the Yanshanian movement. Acta Geol. Sinica 81 (11), 1449–1461 (in Chinese with English abstract).

Dong, G.J., Xu, D.R., Wang, L., Chen, G.H., He, Z.L., Fu, G.G., Wu, J., Wang, Z.L., 2008. Determination of mineralizing ages on gold ore deposits in the eastern Hunan Province, south China and isotopic tracking on ore-forming fluids –re-discussing gold ore deposit type. Geotectonica et Metallogenia 32 (4), 484–493 (in Chinese with English abstract).

Fan, H.R., Li, Z.L., 1992. Geological characteristics, physicochemical conditions and source materials for mineralization of the Jinshan gold deposit. Sci. Geol. Sin. (suppl.), 147–160 (in Chinese with English abstract).

Faure, M., Sun, Y., Shu, L., Monié, P., Charvet, J., 1996. Extensional tectonics within a subductiontype orogen: the case study of the Wugongshan dome (Jiangxi Province, southeastern China). Tectonophysics 263, 77–106.

Faure, M., Shu, L.S., Wang, B., Charvet, J., Choulet, F., Monié, P., 2009. Intracontinental subduction: a possible mechanism for the Early Paleozoic Orogen of SE China. Terra Nova 21 (5), 360–368.

Fu, Z.R., Li, Z.J., Zheng, D.Y., 1999. Structural pattern and tectonic evolution of NNE trending strike slip orogenic belt in the border region of Hunan and Jiangxi provinces. Earth Sci. Front. 6 (4), 263–272 (in Chinese with English Abstract).

Fu, H.H., Tang, W.G., Tang, Y.P., 2011. Re-understanding of Chanziping gold deposit ore-controlling factors and prospects analysis of deep side prospecting. Mineral Resour. Geol. 25 (2), 91–97 (in Chinese with English Abstract).

Gan, X.C., Li, X.H., Zhao, F.Q., Huang, H.B., 1996. Zircon U-Pb and Sm-Nd isochron ages of spilites from Danzhou Group, Guangxi Autonomous Region. Geochimica 25 (3), 270–276 (in Chinese with English abstract).

Gao, L.Z., Dai, C.G., Liu, Y.X., Wang, M., Wang, X.H., Chen, J.S., Ding, X.Z., Zhang, C.H., Cao, Q., Liu, J.H., 2010. Zircon SHRIMP U-Pb dating of tuff bed of the Sibao Group in southeastern Guizhou-northern Guangxi area, China and its stratigraphic implication. Geol. Bull. China 29 (9), 1259–1267 (in Chinese with English abstract).

Gao, L.Z., Liu, Y.X., Ding, X.Z., Zhang, C.H., Wang, Z.Q., Chen, J., Liu, Y.R., 2012. SHRIMP dating of Cangshuipu Group in the middle part of the Jiangnan Orogen and its implications for tectonic evolutions. Geol. China 39 (1), 12–20 (in Chinese with English abstract).

Gao, L.Z., Chen, J.S., Dai, C.G., Ding, X.Z., Wang, X.H., Liu, Y.X., Wang, M., Zhang, H., 2014. SHRIMP zircon U-Pb dating of tuff in Fanjingshan Group and Xiajiang Group from Guizhou and Hunan Provinces and its stratigraphic implications. Geol. Bull. China 33 (7), 949–959 (in Chinese with English abstract).

Goldfarb, R.J., Groves, D.I., Gardoll, S., 2001. Orogenic gold and geologic time: a global synthesis. Ore Geol. Rev. 18, 1–75.

Goldfarb, R.J., Taylor, R.D., Collins, G.S., Goryachev, N.A., Orlandini, O.F., 2014. Phanerozoic continental growth and gold metallogeny of Asia. Gondwana Res. 25, 48–102.

Greentree, M.R., Li, Z.X., Li, X.H., Wu, H.C., 2006. Late Mesoproterozoic to earliest Neoproterozoic basin record of the Sibao orogenesis in west South China and relationship to the assembly of Rodinia. Precambr. Res. 151, 79–100.

Groves, D.I., Goldfarb, R.J., Gebre-Mariam, M., Hagemann, S.G., Robert, F., 1998. Orogenic gold deposits: a proposed classification in the context of their crustal distribution and relationship to other gold deposit types. Ore Geol. Rev. 13, 7–27.

Groves, D.I., Goldfarb, R.J., Knox-Robinson, C.M., Ojala, J., Gardoll, S., Yun, G., Holyland, P., 2000. Late-kinematic timing of orogenic gold deposits and significance for computer-based exploration techniques with emphasis on the Yilgarn block, Western Australia. Ore Geol. Rev. 17, 1–38.

Groves, D.I., Goldfarb, R.J., Robert, F., Hart, C.J.R., 2003. Gold deposits in metamorphic belts: overview of current understanding, outstanding problems, future research, and exploration significance. Econ. Geol. 98, 1–29.

Gu, X.X., Liu, J.M., Zheng, M.H., Tang, J.X., Qi, L., 2002. Provenance and tectonic setting of the Proterozoic turbidites in Hunan, south China: geochemical evidence. J. Sedeimentary Res. 72, 393–407.

Gu, X.X., Schulz, O., Vavtar, F., Liu, J.M., Zheng, M.H., Fu, S.H., 2007. Rare earth element geochemistry of the Woxi W-Sb-Au deposit, Hunan Province, South China. Ore Geol. Rev. 31 (1), 319–336.

Gu, X., Zhang, Y., Schulz, O., Vavtar, F., Liu, J., Zheng, M., Zheng, L., 2012. The Woxi W-Sb-Au deposit in Hunan, South China: an example of Late Proterozoic sedimentary exhalative (SEDEX) mineralization. J. Asian Earth Sci. 57, 54–75.

Harrison, T.M., Duncan, I., McDougall, L., 1985. Diffusion of ^{40}Ar in biotite: temperature, pressure and compositional effects. Geochim. Cosmochim. Acta 49, 2261–2468.

He, Z.L., Xu, D.R., Chen, G.H., Xia, B., Li, P.C., Fu, G.G., 2004. Gold poly-metallic ore-forming geochemistry of the Yanshanian intra-continental collision orogen, northeastern Hunan Province. Mineral Deposits 23 (1), 39–51 (in Chinese with English abstract).

He, M.Q., Long, C.X., Wang, G.L., 2015. Origin of ore-forming fluids of Pingqiu Au ore deposit in Jinping County, southeast Guizhou Province, China. Acta Mineral. Sin. 35 (4), 497–501 (in Chinese with English abstract).

Hedenquist, J.W., Izawa, E., Arribas, A., White, N.C., 1996. Epithermal gold deposits: styles, characteristics, and exploration. Resour. Geol. Spec. Publ., 1–15

Hickey, K.A., Barker, S.L., Dipple, G.M., Arehart, G.B., Donelick, R.A., 2014. The brevity of hydrothermal fluid flow revealed by thermal halos around giant gold deposits: implications for Carlin-type gold systems. Econ. Geol. 109 (5), 1461–1487.

Hoefs, J., 2009. Stable Isotope Geochemistry. Springer-Verlag, Berlin Heidelberg, pp. 48–54.

HRGI (Hunan Regional Geological Institute),, 1995. Granites in Hunan province and their relation to mineralization. Hunan Geol. (Spec. Publ.) 8, 1–59 (in Chinese).

Hsü, K.J., Li, J.L., Chen, H.H., Wang, Q.C., Sun, S., Sengor, A.M.C., 1990. Tectonics of South China: key to understanding West Pacific geology. Tectonophysics 183, 9–39.

Hu, T.L., 1995. Characteristics of the quartz vein in the Hamoshi gold deposit and its auriferous index, Jiangxi. Geol. Jiangxi 9 (2), 113–123 (in Chinese with English abstract).

Hu, S.Q., Peng, J.T., 2015. Carbon and oxygen isotope of calcite in the Herenping gold deposit, western Hunan. Nonferrous Min. Metall. 31 (3), 4–8 (in Chinese with English abstract).

Hu, R.Y., Chen, J.P., Guo, S.L., Hao, X.H., 1995. Application of fission track technique to study of gold deposits. Geochimica 24 (2), 188–192 (in Chinese with English abstract).

Hu, R.Z., Su, W.C., Bi, X.W., Tu, G.Z., Hofstra, A.H., 2002. Geology and geochemistry of Carlin-type gold deposits in China. Miner. Deposita 37 (3), 378–392.

Hua, R.M., Li, X.F., Zhang, K.P., Qiu, D.T., Yang, F.G., 2002. Geochemical characteristics of ore-forming fluid in the Jinshan gold deposit, Jiangxi Province. J. Nanjing Univ. (Nat. Sci.) 38 (3), 408–417 (in Chinese with English abstract).

Hua, R.M., Chen, P.R., Zhang, W.L., Liu, X.D., Lu, J.J., Lin, J.F., Yao, J.M., Qi, H.W., Zhang, Z.S., Gu, S.Y., 2003. Metallogenic systems related to Mesozoic and Cenozoic granitoids in South China. Sci. China (Series D) 46 (8), 816–829.

Huang, J.Q., 1945. The Main Units of Geology and Structure of China. Geological Press, Beijing, pp. 15–67 (in Chinese with English abstract).

Huang, H.L., Yang, W.S., 1990. Geological characteristics and genesis of Jinshan gold deposit in the northeastern Jiangxi Province. Contrib. Geol. Mineral Resour. Res. 5 (2), 29–39 (in Chinese with English abstract).

Huang, C., Fan, G.M., Jiang, G.L., Luo, L., Xu, Z.L., 2012. Structural ore-controlling characteristics and electron spin resonance dating of the Yanlinsi gold deposit in northeastern Hunan Province. Geotectonica et Metallogenia 36 (1), 76–84 (in Chinese with English abstract).

Hunziker, J.C., Frey, M., Clauer, N., Dallmeyer, R.D., Friedrichsen, H., Flehmig, W., Hochstrasser, K., Roggwiler, P., Schwander, H., 1986. The evolution of the illite to muscovite: mineralogical and isotopic data from the Glarus Alps, Switzerland. Contrib. Miner. Petrol. 92, 157–180.

Jahn, B.M., Zhou, X.H., Li, J.L., 1990. Formation and tectonic evolution of southeastern China and Taiwan: isotopic and geochemical constraints. Tectonophysics 183, 145–160.

Ji, J.F., Liu, Y.J., Sun, C.Y., Qiu, D.T., Zheng, Q., 1994a. Geological characteristics of two types of ores from Jinshan shear zone-hosted gold deposit, Jiangxi-with discussion on genesis of two-stage mineralization. Geochimica 23 (3), 226–234 (in Chinese with English abstract).

Ji, J.F., Sun, C.Y., Zheng, Q., 1994b. The metallogenic characteristics of auriferous quartz veins in the Jinshan shear zone type gold deposit, Jiangxi Province. Geol. Rev. 40 (4), 361–367 (in Chinese with English abstract).

Jia, D.C., Hu, R.Z., Lu, Y., Xie, G.Q., Qiu, X.L., 2004. Characteristics of the mantle source region of sodium lamprophyres and petrogenetic tectonic setting in northeastern Hunan, China. Sci. China Series D Earth Sci. 47 (6), 559–569.

Jiang, Y.H., Jiang, S.Y., Zhao, K.D., Ling, H.F., 2006. Petrogenesis of Late Jurassic Qianlishan granites and mafic dikes, southeast China: implications for a back-arc extension setting. Geol. Mag. 143, 457–474.

Jiang, S.Y., Zhao, K.D., Jiang, Y.H., Dai, B.Z., 2008. Characteristics and genesis of Mesozoic A-type granites and associated mineral deposits in the Southern Hunan and Northern Guangxi provinces along the Shi-Hang Belt, South China. Geol. J. China Univ. 14 (4), 496–509 (in Chinese with English abstract).

Jiang, Y.H., Jiang, S.Y., Dai, B.Z., Liao, S.Y., Zhao, K.D., Ling, H.F., 2009. Middle to late Jurassic felsic and mafic magmatism in southern Hunan Province, southeast China: implications for a continental arc to rifting. Lithos 107, 185–204.

Jiang, S.H., Liang, Q.L., Bagas, L., Wang, S.H., Nie, F.J., Liu, Y.F., 2013. Geodynamic setting of the Zijinshan porphyry-epithermal Cu-Au-Mo-Ag ore system, SW Fujian Province, China: constrains from the geochronology and geochemistry of the igneous rocks. Ore Geol. Rev. 53, 287–305.

Kesler, S.E., Riciputi, L.C., Ye, Z.J., 2005. Evidence for a magmatic origin for Carlin-type gold deposits: isotopic composition of sulfur in the Betze-Post-Screamer deposit, Nevada, USA. Miner. Deposita 40 (2), 127–136.

Large, R.R., Bull, S.W., McGoldrick, J., Walters, S., Derrick, G.M., Carr, G.R., 2005. Stratiform and stratabound Zn-Pb-Ag deposits in Proterozoic sedimentary basins, northern Australia. Econ. Geol., 931–963 100th Anniversary Volume.

Lee, J.K.W., 2009. Using argon as a temporal tracer of large-scale geologic processes. Chem. Geol. 266 (2), 104–112.

Li, F.Y., 1990. Metallogenic model and prospecting direction of gold deposit zone in Huangshan. Metal. Geol. 1, 14–18 (in Chinese).

Li, J.L., 1993. Tectonic framework and evolution of southeastern China. J. SE Asian Earth Sci. 8, 219–223.

Li, Z.X., 1998. Tectonic history of the major East Asian lithospheric blocks since the mid-Proterozoic – a synthesis. Mantle dynamics and plate interactions in East Asia. Geodynamics 27, 221–243.

Li, X.H., 1999. U-Pb zircon ages of granites from the southern margin of the Yangtze Block: timing of Neoproterozoic Jinning: orogeny in SE China and implications for Rodinia Assembly. Precambr. Res. 97, 43–57.

Li, Y.K., 2009. Discussion on the Ore Genesis of Jinshan Gold Deposit and the Three Demensions Prognosis, Northeast of Jiangxi (A Dissertation Submitted to Chinese Academy of Geological Sciences for Master Degree), pp. 22–44 (in Chinese with English abstract).

Li, C.M., Chen, X.H., 2005. Metallogenic characteristic and ore prospecting direction of Shiwu gold deposit, Jiangxi. Geol. Prospect. 41 (4), 10–17 (in Chinese with English abstract).

Li, Z.X., Li, X.H., 2007. Formation of the 1300-km-wide intracontinental orogen and postorogenic magmatic province in Mesozoic South China: a flat-slab subduction model. Geology 35 (2), 179–182.

Li, Z.X., Li, X.H., Zhou, H.W., Kinny, P.D., 2002. Grenvillian continental collision in south China: New SHRIMP U-Pb zircon results and implications for the configuration of Rodinia. Geology 30, 163–166.

Li, X.F., Hua, R.M., Mao, J.W., Ji, J.F., 2003a. A study of illite Kübler Indexes and chlorite crystallinities with respect to shear deformation and alteration, Jinshan gold deposit, East China. Resour. Geol. 53 (4), 283–292.

Li, X.H., Li, Z.X., Ge, W.C., Zhou, H.W., Li, W.X., Liu, Y., Wingate, M.T.D., 2003b. Neoproterozoic granitoids in South China: crustal melting above a mantle plume at ca. 825 Ma? Precambr. Res. 122, 45–83.
Li, Z., Liu, S.F., Zhang, J.F., Wang, Q.C., 2004. Typical basin-fill sequences and basin migration in Yanshan, North China—response to Mesozoic tectonic transition. Sci. China Earth Sci. 47 (2), 181–192.
Li, P.C., Xu, D.R., Chen, G.H., Xia, B., He, Z.L., Fu, G.G., 2005a. Granites of Early Yanshanian epoch in northeastern Hunan Province—an example of intracontinental syn-collisional orogenic granite: geochemical constraint and geodynamic setting. Acta Petrol. Sin. 21 (3), 921–934 (in Chinese with English abstract).
Li, W.X., Li, X.H., Li, Z.X., 2005b. Neoproterozoic bimodal magmatism in the Cathaysia Block of South China and its tectonic significance. Precambr. Res. 136 (1), 51–66.
Li, X.F., Wang, C.Z., Yi, X.K., Feng, Z.H., Wang, Y.T., 2007a. Deformation structures at various scales and their roles during gold minerals at Jinshan gold deposit. Geol. Rev. 53 (6), 774–781 (in Chinese with English abstract).
Li, Z.L., Hu, R.Z., Yang, J.S., Peng, J.T., Li, X.M., Bi, X.W., 2007b. He, Pb and S isotopic constraints on the relationship between the A-type Qitianling granite and the Furong tin deposit, Hunan Province, China. Lithos 97, 161–193.
Li, X.H., Li, W.X., Li, Z.X., 2007c. On the genetic classification and tectonic implications of the early Yanshanian granitoids in the Nanling Range, South China. Chin. Sci. Bull. 52, 1873–1885.
Li, X.F., Watanabe, Y., Mao, J.W., Liu, S.X., Yi, X.K., 2007d. Sensitive high-resolution ion microprobe U-Pb zircon and ^{40}Ar-^{39}Ar muscovite ages of the Yinshan deposit in the northeast Jiangxi Province, South China. Resour. Geol. 57, 325–337.
Li, Z.X., Bogdanova, S.V., Collins, A.S., Davidson, A., De Waele, B., Ernst, R.E., Fitzsimons, I.C.W., Fuck, R.A., Gladkochub, D.P., Jacobs, J., Karlstrom, K.E., Lu, S., Natapov, L.M., Pease, V., Pisarevsky, S.A., Thrane, K., Vernikovsky, V., 2008a. Assembly, configuration, and break-up history of Rodinia: a synthesis. Precambr. Res. 160, 179–210.
Li, H.Q., Wang, D.H., Chen, F.W., Mei, Y.P., Cai, H., 2008b. Study on chronology of the Chanziping and Daping gold deposit in Xuefeng Mountains, Hunan Province. Acta Geol. Sin. 82 (7), 900–905 (in Chinese with English abstract).
Li, X.H., Li, W.X., Li, Z.X., Lo, Q.H., Wang, J., Ye, M.F., Yang, Y.H., 2009. Amalgamation between the Yangtze and Cathaysia Blocks in South China: constraints from SHRIMP U-Pb zircon ages, geochemistry and Nd-Hf isotopes of the Shuangxiwu volcanic rocks. Precambr. Res. 174, 117–128.
Li, X.F., Wang, C.Z., Hua, R.M., Wei, X.L., 2010a. Fluid origin and structural enhancement during mineralization of the Jinshan orogenic gold deposit, South China. Miner. Deposita 45, 583–597.
Li, Z.X., Li, X.H., Wartho, J.A., Clark, C., Li, W.X., Zhang, C.L., Bao, C., 2010b. Magmatic and metamorphic events during the early Paleozoic Wuyi-Yunkai Orogeny, southeastern South China: new age constraints and pressure-temperature conditions. GSA Bull. 122, 772–793.
Li, J., Chen, B.H., An, J.H., Tan, S.M., Zhang, X.G., Yao, Y.J., 2011. Characteristics of fluid inclusions of the Huangjindong gold deposit, Hunan Province. Geol. Mineral Resour. South China 27 (2), 163–168 (in Chinese with English abstract).
Li, J.H., Zhang, Y.Q., Dong, S.W., Li, H.L., 2012. Late Mesozoic-Early Cenozoic deformation history of the Yuanma Basin, central South China. Tectonophysics 570, 163–183.
Li, J.H., Zhang, Y.Q., Dong, S.W., Su, J.B., Li, Y., Cui, J.J., Shi, W., 2013a. The Hengshan low-angle normal fault zone: structural and geochronological constraints on the Late Mesozoic crustal extension in South China. Tectonophysics 606, 97–115.
Li, S.Z., Suo, Y.H., Santonsh, M., Dai, L.M., Liu, X., Yui, S., Zhao, S.J., Jin, C., 2013b. Mesozoic to Cenozoic intracontinental deformation and dynamics of the North China Craton. Geol. J. 48, 543–560.
Liang, Y., Wang, G.G., Liu, S.Y., Sun, Y.Z., Huang, Y.G., Hoshino, K., 2014. Study on the mineralization of the Woxi Au-Sb-W deposit, western Hunan, China. Resour. Geol. 65 (1), 27–38.
Lin, B., 1988. Geochemistry of the lead isotopes in the gold deposit zone from zhuji to longquan, Zhejiang province. Sci. Geol. Sin. 2, 128–136 (in Chinese with English abstract).
Lin, W., Wang, Q.C., Chen, K., 2008. Phanerozoic tectonics of south China block: new insights from the polyphase deformation in the Yunkai massif. Tectonics 27. TC6004.
Liu, C.Y., 1989. Geochemical signatures of the Huangjindong gold deposit. Geol. Explor. 25 (11), 43–48 (in Chinese with English abstract).
Liu, D.R., Wu, Y.Z., 1993. On the genesis of Yanlingshi gold deposit in Liling. Hunan Geol. 12 (4), 247–251 (in Chinese with English abstract).
Liu, H.C., Zhu, B.Q., 1994. Study on depositional timings of the Banxi and Lengjiaxi Groups in western Hunan Province. Chin. Sci. Bull. 39 (2), 148–150 (in Chinese).
Liu, Y.J., Sha, P., Zhu, K.J., 1989. The study on geochemistry of the gold-bearing formation of Middle Proterozoic Shuangqiaoshan Group in Dexing district, Jiangxi. J. Guilin Coll. Geol. 9 (2), 115–126 (in Chinese with English abstract).
Liu, Y.J., Ma, D.S., Ji, J.F., 1991. Metallogenic geochemistry of Jiangnan-type gold deposit. J. Guilin Coll. Geol. 11 (2), 130–138 (in Chinese with English abstract).
Liu, D.R., Wu, Y.Z., Liu, S.N., 1994a. Geochemistry of Wangu gold deposit. Hunan Geol. 13 (2), 83–90 (in Chinese with English abstract).
Liu, Y.J., Ma, D.S., Niu, H.C., 1994b. Mineralization geochemistry of gold deposits in Yiyang-Yuanling area. Geochimica 23 (1), 1–12 (in Chinese with English abstract).
Liu, L.M., Peng, S.L., Wu, Y.Z., 1997. Features of metallogenic-tectonics and mechanism of tectonic-mineralization for vein-type gold deposits in the north-eastern Hunan, China. Geotectonia et Metallognia 21 (3), 197–204 (in Chinese with English abstract).
Liu, L.M., Peng, S.L., Wu, Y.Z., 1999. Genetic features forming vein-type gold deposits in northeastern Hunan. J. Central South Univ. Technol. 30 (1), 4–7 (in Chinese with English abstract).
Liu, G., Jin, W., Zhang, L., Shen, K., 2001. Discussion of sources of metallogenetic meterials of porphyry-type and hydrothemal copper deposits in northeastern Hunan Province. Geol. Mineral Resour. South China, 40–47 (in Chinese with English abstract).
Liu, Z.Y., Jin, C.Z., Wang, R.H., Liang, J.H., Zhang, K.P., 2005a. Significance and geochemical characteristics of rare earth elements of Jinshan gold deposit, Jiangxi Province. Geol. Resour. 14 (1), 12–17 (in Chinese with English abstract).
Liu, Z.Y., Jin, C.Z., Wang, R.H., 2005b. Geochemical feature of fluid inclusion in Jinshan gold deposit, Jiangxi Province. Mineral Resour. Geol. 19 (108), 127–133 (in Chinese with English abstract).
Liu, X., Fan, H.R., Santosh, M., Hu, F.F., Yang, K.F., Li, Q.L., Yang, Y.H., Liu, Y.S., 2012. Remelting of Neoproterozoic relict island arcs in the Middle Jurassic: implication for the formation of the Dexing porphyry copper deposit, Southeastern China. Lithos 150, 85–100.
Liu, X., Fan, H.R., Hu, F.F., Yang, K.F., Wen, B.J., 2016. Nature and evolution of the ore-forming fluids in the giant Dexing porphyry Cu-Mo-Au deposit, Southeastern China. J. Geochem. Explor. 171, 83–95.
Long, C.X., Qin, Q., Zhou, L.L., 2015. Guizhou Jinping County Pingqiu Bize Metallogenic fluid hydrogen and oxygen isotope geochemistry. Nonferrous Metals Abstract 30 (3), 18–19 (in Chinese with English abstract).
Lu, H.Z., Wang, Z.G., Chen, W.Y., Wu, X.Y., Zhu, X.Q., Hu, R.Z., 2006. Turbidite hosted gold deposits in southeast Guizhou: their structural control, mineralization characteristics, and some genetic constrains. Mineral Deposits 25 (4), 369–387 (in Chinese with English abstract).
Luo, X.L., 1988. On the genesis and metallogenic model of the Huangjidong gold deposit from Hunan. J. Guilin Coll. Geol. 3, 225–239 (in Chinese with English abstract).
Luo, X.L., 1989. On the epoch of the formation of Precambrian gold deposits in Hunan province. J. Guilin Coll. Geol. 9 (1), 25–34 (in Chinese with English abstract).
Luo, X.L., 1990. Discussion on the material sources of gold deposits in Precambrian strata in Hunan. J. Guilin Inst. Met. Geol. 10 (1), 13–25 (in Chinese with English abstract).
Luo, X.L., 1991. Main characteristics and genetic types of gold ore deposits in Hunan. J. Guilin Coll. Geol. 11 (1), 23–33 (in Chinese with English abstract).
Luo, G.Y., 1994a. Geologic features of granite-porphyry dykes in Liaojiaping district and the relationship with W, Sb, Au mineralization. Hunan Geol. 13 (1), 7–10 (in Chinese with English abstract).
Luo, X.L., 1994b. The geochemical features of the Banxi Sb ore deposit in Hunan Province and its prospecting effect. Mineral Resour. Geol. 8 (3), 169–177 (in Chinese).
Luo, X.L., 1994c. Geological characteristics of Precambrian antimony metallogeny in Hunan. J. Guilin Coll. Geol. 14 (4), 335–349 (in Chinese with English abstract).
Luo, X.Q., 1996. Mineralization and prospecting guide of Chanziping gold deposit in Hunan. Hunan Geol. 15 (1), 33–38 (in Chinese with English abstract).
Luo, Q.Z., Chen, D.K., 1995. Metallogenic regularity and prospecting progression of gold deposit in north Guangxi. Gold Geol. 1 (2), 14–20 (in Chinese with English abstract).
Luo, X.L., Yi, S.J., Liang, J.C., 1984. The genesis of Xiangxi Au-Sb-W-deposit. Geol. Prospect. 7, 1–10 (in Chinese).
Luo, X.L., Zhong, D.Q., Li, G.S., 1996. Geology of Woxi-type Stratabound Gold Deposits in Hunan Province. Seismal Press, Beijing, pp. 1–300 (in Chinese).
Luo, M., Huang, H.G., Zhang, P., Wu, Q.B., Chen, D.F., 2014. Origins of gas discharging from the Qiangtang Basin in the northern Qinghai-Tibet Plateau, China: evidence from gas compositions, helium, and carbon isotopes. J. Geochem. Explor. 146, 119–126.
Ma, D.S., Liu, Y.J., 1991. Study on the geochemical characteristics of stratum-controlled gold mines in Jiangnan gold metallogenic belt and its genesis. Sci. China (series B) 4, 424–433 (in Chinese).
Ma, C.Q., Li, Z.C., Ehlers, C., Yang, K.G., Wang, R.J., 1998. A post-collisional magmatic plumbing system: Mesozoic granitoid plutons from the Dabieshan high-pressure and ultrahigh-pressure metamorphic zone, east-central China. Lithos 45, 431–456.
Mao, D.H., 1998. A discussion on the geological characteristics and genesis of Hamoshi gold deposit in Jiangxi. Jiangxi Geol. 12 (2), 116–122 (in Chinese with English abstract).
Mao, J.W., Du, D.A., 2001. The 982 Ma Re-Os isotopic age of Cu-Ni sulfide ores in Baotan area, Guangxi Province and its geological significance. Sci. China (series D) 31 (12), 992–998.
Mao, J.W., Li, Y.H., 1997. Research on genesis of the gold deposits in the Jiangnan terrain. Geochemica 26 (5), 71–81 (in Chinese with English abstract).
Mao, J.W., Wang, Z.L., 2000. A preliminary study on time limits and geodynamic setting of large-scale metallogeny in east China. Mineral Deposits 19 (4), 289–296 (in Chinese with English abstract).
Mao, J.W., Kerrich, R., Li, H.Y., Li, Y.H., 2002. High ^{3}He/^{4}He ratios in the Wangu gold depoit, Hunan province, China: implications for mantle fluids along the Tanlu deep fault zone. Geochem. J. 36, 197–208.
Mao, G.Z., Hua, R.M., Gao, J.F., Zhao, K.D., Long, G.M., Lu, H.J., Yao, J.M., 2005. REE composition and trace element features of gold-bearing pyrite in Jinshan gold deposit, Jiangxi Province. Minerals Deposits 25 (4), 412–426 (in Chinese with English abstract).

Mao, G.Z., Hua, R.M., Long, G.M., Lu, H.J., 2008. Discussion on the mineralogenetic epoch of the Jinshan gold deposit, Jiangxi Province—based on the quartz fluid inclusion Rb-Sr dating. Acta Geol. Sinica 82 (4), 532–539 (in Chinese with English abstract).
Mao, J.W., Pirajno, F., Cook, N., 2011a. Mesozoic metallogeny in East China and corresponding geodynamic settings——an introduction to the special issue. Ore Geol. Rev. 43, 1–7.
Mao, J.W., Zhang, J.D., Pirajno, F., Ishiyama, D., Su, H.M., Guo, C.L., Chen, Y.C., 2011b. Porphyry Cu-Au-Mo-epithermal Ag-Pb-Zn-distal hydrothermal Au deposits in the Dexing area, Jiangxi province, East China—a linked ore system. Ore Geol. Rev. 43, 203–216.
Mao, J.W., Cheng, Y.B., Chen, M.H., Pirajno, F., 2013a. Major types and time-space distribution of Mesozoic ore deposits in South China and their geodynamic settings. Miner. Deposita 48, 267–294.
Mao, G.Z., Hua, R.M., Long, G.M., Lu, H.J., 2013b. Rb-Sr dating of pyrite and quartz fluid inclusions and origin of ore froming materials of Jinshan dold deposit. Acta Geol. Sin. (English edition) 87 (6), 1658–1667.
Mao, J.R., Li, Z.L., Ye, H.M., 2014. Mesozoic tectono-magmatic activities in South China: retrospect and prospect. Sci. China (Earth Sci.) 57 (12), 2853–2877.
McCuaig, T.C., Kerrich, R., 1998. P-T-t deformation-fluid characteristics of lode gold deposits: evidence from alteration systematics. Ore Geol. Rev. 12, 381–453.
Meng, Q.X., 2014. Ages of the Lengjiaxi and Banxi Groups in the Middle Jiangnan Orogenic Belt: Implications on the Neoproterozoic Tectonic Evolution of the Jiangnan Orogenic Belt (A Dissertation Submitted to Chengdu University of Technology for Master Degree), pp. 1–40 (in Chinese with English abstract).
Muntean, J.L., Cline, J.S., Simon, A.C., Longo, A.A., 2011. Magmatic-hydrothermal origin of Nevada's Carlin-type gold deposits. Nat. Geosci. 4, 122–127.
Nägler, Th.F., Pettke, Th., Marshall, D., 1995. Initial isotopic heterogeneity and secondary disturbance of the Sm-Nd system in fluorites and fluid inclusions: a study on mesothermal veins from the central and western Swiss Alps. Chem. Geol. (Isot. Geosci. Section) 125, 241–248.
Ni, P., Wang, G.G., Chen, H., Xu, Y.F., Guan, S.J., Pan, J.Y., Li, L., 2015. An Early Paleozoic orogenic gold belt along the Jiangshao Fault, South China: evidence from fluid inclusions and Rb-Sr dating of quartz in the Huangshan and Pingshui deposits. J. Asian Earth Sci. 103, 87–102.
Niu, H.C., Ma, D.S., 1991. Fluid inclusion studies of Jiangnan-type gold deposits in western Hunan Province. Acta Mineral. Sin. 11 (4), 386–394 (in Chinese with English abstract).
Ohmoto, H., 1999. Stable isotope geochemistry of ore deposits. In: Valley, J.W., Taylore, H.P., O'Neil, J.R. (Eds.), Stable Isotopes in High Temperature Geological Processes, Reviews in Mineralogy, vol. 16, pp. 491–561.
Pan, C.J., Bao, Z.X., Bao, J.M., 2015. Geological characteristics and metallogenesis of the Fuzhuxi gold deposit in the west Hunan Province. Contrib. Geol. Mineral Resour. Res. 30 (1), 53–59 (in Chinese with English abstract).
Peng, B., Frei, R., 2004. Nd-Sr-Pb isotopic constraints on metal and fluid sources in W-Sb-Au mineralization at Woxi and Liaojiaping (Western Hunan, China). Miner. Deposita 39, 313–327.
Peng, J.T., Hu, R.Z., 1999. Geochemical characteristics and ore genesis of gold deposits in southwestern Hunan Province. Geochimica 28 (5), 464–472 (in Chinese with English abstract).
Peng, J.T., Hu, R.Z., Zhao, J.H., Fu, Y.Z., Lin, Y.X., 2003. Scheelite Sm-Nd dating and quartz Ar-Ar dating for Woxi Au-Sb-W deposits, western Hunan. Chin. Sci. Bull. 48 (23), 2640–2646.
Peng, T.P., Xi, X.W., Wang, Y.J., Peng, B.X., Jiang, Z.M., 2004. Geochemical characteristics of the Early Mesozoic granodiorites and their tectonic implications. Geotectonica et Metallogenia 28 (3), 287–296 (in Chinese with English Abstract).
Peters, S.G., 2004. Syn-deformational features of Carlin-type Au deposits. J. Struct. Geol. 26, 1007–1023.
Pettke, Th., Diamond, L., 1995. Rb-Sr isotopic analysis of fluid inclusions in quartz: evaluation of bulk extraction procedures and geochronometer systematics using synthetic fluid inclusions. Geochim. Cosmochim. Acta 59 (19), 4009–4027.
Pirajno, F., Bagas, L., 2002. Gold and silver metallogeny of the South China Fold Belt: a consequence of multiple mineralizing events? Ore Geol. Rev. 20, 109–126.
Pirajno, F., Ernst, R.E., Borisenko, A.S., Fedoseev, G., Naumov, E.A., 2009. Intraplate magmatism in central Asia and China and associated metallogeny. Ore Geol. Rev. 35, 114–136.
Qin, Y.J., Du, Y.S., Mou, J., Lu, D.B., Long, J.X., Wang, A.H., Zhang, H.S., Zemg, C.X., 2015. Geochronology of Neoproterozoic Xiajiang Group in southeast Guizhou, South China, and its geological implications. Earth Sci. J. China Univ. Geosci. 40 (7), 1107–1120 (in Chinese with English abstract).
Ren, J.-Sh., 1991. The basic characteristics of the tectonic evolution of the continental lithosphere in China. Geol. Bull. China 4, 289–293 (in Chinese with English abstract).
Rye, R.O., 1993. The evolution of magmatic fluids in the epithermal environment: the stable isotope perspective. Econ. Geol. 88, 733–753.
Shi, W., Dong, S.W., Zhang, Y.Q., Huang, S.Q., 2015. The typical large-scale superposed folds in the central South China: implications for Mesozoic intracontinental deformation of the South China Block. Tectonophysics 664, 50–66.
Shu, L.S., Charvet, J., 1996. Kinematic and geochronology of the Proterozoic Dongxiang-Shexian ductile shear zone (Jiangnan region, South China). Tectonophysics 267 (1), 291–302.
Shu, L.S., Wang, D.Z., 2006. A comparison study of basin and range tectonics in the western North America and woutheastern China. Geol. J. China Univ. 12 (1), 1–13 (in Chinese with English Abstract).
Shu, L.S., Shi, Y.S., Guo, L.Z., 1995. Plate-Terrane Tectonics and Collisional Orogeny. Nanjing University Press, Nanjing. 94-120 (in Chinese).
Shu, L.S., Lu, H.F., Jia, D., Charvet, J., Faure, M., 1999. Study of the $^{40}Ar/^{39}Ar$ isotopic age for the early Paleozoic tectonothermal event in the Wuyishan region, south China. J. Nanjing Univ. (Nat. Sci.) 35 (6), 668–674 (in Chinese with English abstract).
Shu, L.S., Zhou, X.M., Deng, P., Zhu, W.B., 2007. Mesozoic-Cenozoic basin features and evolution of southeast China. Acta Gelol. Sin. 81 (4), 573–586.
Shu, L., Zhou, X., Deng, P., Wang, B., Jiang, S.Y., Yu, J., Zhao, X., 2009. Mesozoic tectonic evolution of the Southeast China Block: new insights from basin analysis. J. Asian Earth Sci. 34, 376–391.
Shu, L.S., Faure, M., Yu, J.H., Jahn, B.M., 2011. Geochronological and geochemical features of the Cathaysia block (South China): new evidence for the Neoproterozoic breakup of Rodinia. Precambr. Res. 187, 263–276.
Shu, L.S., Jahn, B.M., Charvet, J., Santosh, M., Wang, B., Xu, X.S., Jiang, S.Y., 2014. Early Paleozoic depositional environment and intraplate tectono-magmatism in the Cathaysia Block (South China): evidence from stratigraphic, structural, geochemical and geochronological investigations. Am. J. Sci. 314, 154–186.
Simmons, S.F., White, N.C., John, D.A., 2005. Geological characteristics of epithermal precious and base metal deposits. Econ. Geol., 485–522 100th anniversary volume 29.
Simpson, M.P., Palinkas, S.S., Mauk, J.L., Bodnar, R.J., 2015. Fluid inclusion chemistry of adularia-sericite epithermal Au-Ag deposits of the southern Hauraki Goldfield, New Zealand. Econ. Geol. 110, 763–786.
Su, W.C., Heinrich, C.A., Pettke, T., Zhang, X.C., Hu, R.Z., Xia, B., 2009a. Sediment-hosted gold deposits in Guizhou, China: products of wall-rock sulfidation by deep crustal fluids. Econ. Geol. 104 (1), 73–93.
Su, W.B., Huff, W.D., Ettensohn, F.R., Liu, X.M., Zhang, J.E., Li, Z.M., 2009b. K-bentonite, black-shale and flysch successions at the Ordovician-Silurian transition, South China: possible sedimentary responses to the accretion of Cathaysia to the Yangtze Block and its implications for the evolution of Gondwana. Gondwana Res. 15, 111–130.
Su, W.C., Zhang, H.T., Hu, R.Z., Ge, X., Xia, B., Chen, Y.Y., Zhu, C., 2012. Mineralogy and geochemistry of gold-bearing arsenian pyrite from the Shuiyindong Carlin-type gold deposit, Guizhou, China: implications for gold depositional processes. Miner. Deposita 47 (6), 653–662.
Sun, M.C., 2011. Study on the geological and ore mineralogy characteristics of the Gubang gold deposit in the southeastern Guizhou. China Univ. Geosci., 46–49 (in Chinese with English abstract)
Sun, W.D., Ding, X., Hu, Y.H., Li, X.H., 2007. The golden transformation of the Cretaceous plate subduction in the west Pacific. Earth Planet. Sci. Lett. 262, 533–542.
Taylor, S.R., McLennan, S.M., 1985. The Continental Crust: Its Composition and Evolution. Blackwell, Oxford, pp. 1–312.
Tian, H.D., Huang, D.G., Yu, Q.P., 2011. Analyses on geologic characters and genesis of Kengtou gold deposit in Tianzhu, southeast Guizhou. Guizhou Geol. 28 (4), 265–271 (in Chinese with English abstract).
Tong, X.F., 2014. Determination and significance of Huangshan orogenic gold deposits in Zhejiang Province. J. Geol. 38 (3), 347–351 (in Chinese with English abstract).
Wan, J.M., 1986. Geochemical studies of the Xi'an tungsten ore deposit, west Hunan, China. Geochimica 15 (2), 183–192 (in Chinese with English abstract).
Wang, M., 2012. The Neoproterozoic Magmatism and Tectonic Implications, The Fanjingshan Mt., Northeast Guizhou Province (A Dissertation Submitted to China University of Geosciences for Doctoral Degree), pp. 1–154 (in Chinese with English abstract).
Wang, R.H., Zhang, Q.H., 1997. Geological features and geneses of geothermal fluid leaching type gold deposits in northern Guangxi. Guangxi Geol. 10 (2), 25–35 (in Chinese with English abstract).
Wang, W., Zhou, M.F., 2012. Sedimentary records of the Yangtze Block (South China) and their correlation with equivalent Neoproterozoic sequences on adjacent continents. Sed. Geol. 265–266, 126–142.
Wang, P.R., Quan, Y.Y., Hu, N.Y., 1993. Forming condition for rock-gold deposits in Hunan province and their disciplinarians of distribution and enrichment. Hunan Geol. 12 (3), 163–170 (in Chinese with English abstract).
Wang, X.Z., Liang, H.Y., Shan, Q., Cheng, J.P., Xia, P., 1999. Metallogenic age of the Jinshan gold deposit and Caledonian gold mineralization in South China. Geol. Rev. 45 (1), 19–25 (in Chinese with English abstract).
Wang, Q., Zhao, Z.H., Jian, P., Xu, J.F., Bao, Z.W., Ma, J.L., 2004. SHRIMP zircon geochronology and Nd-Sr isotopic geochemistry of the Dexing granodiorite porphyries. Acta Petrol. Sin. 20 (2), 315–324 (in Chinese with English abstract).
Wang, X.L., Zhou, J.C., Qiu, J.S., Zhang, W.L., Liu, X.M., Zhang, G.L., 2006. LA-ICP-MS U-Pb zircon geochronology of the Neoproterozoic igneous rocks from Northern Guangxi, South China: implications for tectonic evolution. Precambr. Res. 145, 111–130.
Wang, J.S., Wen, H.J., Li, C., Ding, W., Zhang, J.R., 2011a. Re-Os isotope dating of Arsenopyrite from the quartz vein type gold deposit southeastern Guizhou province and its geological implications. Acta Geol. Sin. 85 (6), 955–962 (in Chinese with English abstract).
Wang, T., Zheng, Y.D., Zhang, J.J., Zeng, L.S., Donskaya, T., Guo, L., Li, J.B., 2011b. Pattern and kinematicpolarity of late Mesozoic extension in continental NE Asia: perspectives from metamorphic core complexes. Tectonics 30. TC6007.
Wang, X.L., Shu, L.S., Xing, G.F., Zhou, J.C., Tang, M., Shu, X.J., Qi, L., Hu, Y.H., 2012a. Post-orogenic extension in the eastern part of the Jiangnan Orogen: evidence from ca 800–760 Ma volcanic rocks. Precambr. Res. 222–223, 404–423.

Wang, X.L., Shu, X.J., Xing, G.F., Xie, S.W., Zhang, C.H., Xia, H., 2012b. LA-ICP-MS zircon U-Pb ages of the Shijiao-Huangshan intrusive rocks in Zhuji area, Zhejiang Province. Implications for the petrogenesis of the ultramafic orbicular rocks. Geol. Bull. China 31, 75–81 (in Chinese with English abstract).

Wang, Y.J., Fan, W.M., Zhang, G.W., Zhang, Y., 2013a. Phanerozoic tectonics of the South China Block: key observations and controversies. Gondwana Res. 23 (4), 1273–1305.

Wang, Y., Zhou, L.Y., Zhao, L.J., 2013b. Cratonic reactivation and orogeny: an example from the northern margin of the North China Craton. Gondwana Res. 24, 1203–1222.

Wang, G.G., Ni, P., Yao, J., Wang, X.L., Zhao, K.D., Zhu, R.Z., Xu, Y.F., Pan, J.Y., Li, Li., Zhang, Y.H., 2015. The link between subduction-modified lithosphere and the giant Dexing porphyry copper deposit, South China: constraints from high-Mg adakitic rocks. Ore Geol. Rev. 67, 109–126.

Wei, D.F., 1993. Source of ore-forming materials in Chanziping gold deposit and the geologic study of its mechanism of formation. Hunan Geol. 12 (1), 29–34 (in Chinese with English abstract).

Wei, X.L., 1995. Geological characteristics and gold mineralization of the Jinshan gold deposit. Mineral Resour. Geol. 9, 471–478 (in Chinese).

Wen, Z.L., Deng, T., Dong, G.J., Zou, F.H., Xu, D.R., Wang, Z.L., Lin, G., Chen, G.W., 2016. Study on the characters and rules of the ore-controlling structures of the Wangu gold deposit in northeastern Hunan Province. Geotectonica et Metallogenia 40 (2), 281–294 (in Chinese with English abstract).

Wong, W.H., 1927. Crustal movements and igneous activities in eastern China since Mesozoic time. Acta Geol. Sinica 6, 9–37.

Wu, W.M., 2009. Study on the Major Characteristics of the Fluid Inclusions of the main Gold Deposit in Jinping County, Guizhou (A Dissertation submitted to Guizhou University for Master Degree), pp. 21–44 (in Chinese with English abstract).

Wu, P., Ye, J., Yu, D.L., 2005. Geochemistry of metallogenic fluid in Tonggu gold deposit, eastern Guizhou Province. Gold 26 (10), 7–10 (in Chinese with English abstract).

Wu, R.X., Zheng, Y.F., Wu, Y.B., Zhao, Z.F., Zhang, S.B., Liu, X.M., Wu, F.Y., 2006. Reworking of juvenile crust: element and isotope evidence from Neoproterozoic granodioritic in South China. Precambr. Res. 146, 179–212.

Wu, R.H., Pang, B.C., Tan, J., Zhang, M., 2012. Preliminary analysis of distribution regularity and prospecting direction of gold deposits in Guangxi. Mineral Resour. Geol. 26 (4), 291–298 (in Chinese with English abstract).

Xiang, X.K., Yin, Q.Q., Sun, K.K., Chen, B., 2015. Origin of the Dahutang syncollisional granite-porphyry in the middle segment of the Jiangnan Orogen: zircon U-Pb geochronologic, geochemical and Nd-Hf isotopic constraints. Acta Petrol. Mineral. 34 (5), 581–600 (in Chinese with English abstract).

Xu, D.R., Chen, G.-H., Xia, B., Li, P.C., He, Z.L., 2006. The Caledonian adakite-like granodiorites in Banshanpu area, eastern Hunan Province, South China: petrogenesis and geological significance. Geol. J. China Univ. 12 (4), 507–552 (in Chinese with English abstract).

Xu, D.R., Xia, B., Li, P.C., Chen, G.H., Ma, C., Zhang, Y.Q., 2007. Protolith natures and U-Pb sensitive high mass-resolution ion microprobe (SHRIMP) zircon ages of the metabasites in Hainan Island, South China: implications for geodynamic evolution since the late Precambrian. Island Arc 16, 575–597.

Xu, D.R., Wang, L., Li, P.C., Chen, G.H., He, Z.L., Fu, G.G., Wu, J., 2009. Petrogenesis of the Lianyunshan granites in northeastern Hunan Province, South China, and its geodynamic implications. Acta Petrol. Sin. 25 (01), 1056–1078 (in Chinese with English abstract).

Yan, M., Ma, D.S., Liu, Y.J., 1994. Ore-forming fluid geochemistry and genesis of the Taojinchong gold deposit. Mineral Deposits 13 (2), 156–162 (in Chinese with English abstract).

Yang, K.G., Li, X.G., Dai, C.G., Zhang, H., Zhou, Q., 2012. Analysis of the origin of trough-like folds in southeast Guizhou. Earth Sci. Front. 9 (5), 53–60 (in Chinese with English abstract).

Yang, J.H., Wang, L., Zhang, J.D., Yang, S.F., 2013. Characteristics of gravity and magnetic anomlies and gold anpmalies in southeast Guizhou and their ore-prosepcting significance. Geophys. Geochem. Expor. 37 (5), 794–799 (in Chinese with English abstract).

Yang, L.Q., Deng, J., Goldfarb, R.J., Zhang, J., Gao, B.F., Wang, Z.L., 2014. $^{40}Ar/^{39}Ar$ geochronological constraints on the formation of the Dayingezhuang gold deposit: new implications for timing and duration of hydrothermal activity in the Jiaodong gold province, China. Gondwana Res. 25 (4), 1469–1483.

Yang, C., Li, X.H., Wang, X.C., Lan, Z.W., 2015. Mid-Neoproterozoic angular unconformity in the Yangtze Block revisited: Insights from detrital zircon U-Pb age and Hf-O isotopes. Precambr. Res. 266, 165–178.

Yang, L.Q., Guo, L.N., Wang, Z.L., Zhao, R.X., Song, M.C., Zheng, X.L., 2017. Timing and mechanism of gold mineralization at the Wang'ershan gold deposit, Jiaodong Peninsula, eastern China. Ore Geol. Rev. 88, 491–510.

Yao, Z.K., Zhu, R.B., 1993. Polygenetic compound model for the Fuzhuxi gold deposit of Hunan province and its prospecting. Geotectonica et Metellogenia 17 (3), 199–209 (in Chinese with English abstract).

Yao, J.L., Shu, L.S., Santosh, M., Zhao, G.C., 2014. Neoproterozoic arc-related mafic-ultramafic rocks and syn-collision granite from the western segment of the Jiangnan Orogen, South China: constraints on the Neoproterozoic assembly of the Yangtze and Cathaysia Blocks. Precambr. Res. 243, 39–62.

Ye, H., Shedlock, K.M., Hellinger, S.J., Sclater, J.G., 1985. The North China basin: an example of a Cenozoic rifted intraplate basin. Tectonics 4 (2), 153–169.

Ye, C.Q., Dai, W.J., Liu, Y.C., Han, X.J., 1988. Discussion on genesis of the Huangjindong gold deposit and its prospecting significance. Gold Geol. 02, 24–36 (in Chinese with English abstract).

Ye, Y.Z., Ye, G.S., Zhao, G.L., Bai, Q.R., 1993. Discussion on mineralization period of gold (silver) deposits in Huangshan district of Zhuji, Zhejiang province. Geol. Zhejiang 9 (2), 10–14 (in Chinese with English abstract).

Ye, G.S., Ye, Y.Z., Zhao, G.L., Bai, Q.R., 1994. Fluid inclusions features of gold (silver) deposit hosted in ductile shear zone in Huangshan region, Zhejiang Province. Geoscience 8 (3), 291–298 (in Chinese with English abstract).

Ye, M.F., Li, X.H., Li, W.X., Liu, Y., Li, Z.X., 2007. SHRIMP zircon U-Pb geochronological and whole-rock geochemical evidence for an early Neoproterozoic Sibaoan magmatic arc along the southeastern margin of the Yangtze Block. Gondwana Res. 12, 144–156.

Yin, H.F., Wu, S.B., Du, Y.S., Peng, Y.Q., 1999. South China defined as part of Tethyan archipelagic ocean system. Earth Sci. J. China Univ. Geosci. 24 (1), 1–12 (in Chinese with English abstract).

Yu, D.L., 1990. Inclusion studies of gold ores from Mobin. Geochimica 1, 72–80 (in Chinese with English abstract).

Yu, D.L., 1997. A study on the geological and geochemical characteristics of bake gold deposit, east Guizhou. Geol. Geochem. 1, 12–17 (in Chinese with English abstract).

Yu, C., Yu, D.L., 2011. Fluid inclusion features and genesis of the Loli gold deposit in southeastern Guizhou Province. Geol. Explor. 47 (5), 856–864 (in Chinese with English abstract).

Yuan, X.Y., 1992. Geochemical characteristics and origin of gold deposits in the Suichang-Longquan district, Zhejianng Province. Contrib. Geol. Mineral Resour. Res. 7 (1), 22–36 (in Chinese with English abstract).

Zachariáš, J., Morávek, P., Gadas, P., Pertoldová, J., 2014. The Mokrsko-West gold deposit, Bohemian Massif, Czech Republic: mineralogy, deposit setting and classification. Ore Geol. Rev. 58, 238–263.

Zartman, R., Doe, B., 1981. Plumbotectonics—the model. Tectonophysics 75, 135–162.

Zaw, K., Peters, S.G., Cromie, P., Burrett, C., Hou, Z.Q., 2007. Nature, diversity of deposit types and metallogenic relations of South China. Ore Geol. Rev. 31, 3–47.

Zeng, J.N., Fan, Y.X., Lin, W.B., 2002a. The lead and sulfur isotopic tracing of the source of ore-forming material in Jinshan gold deposit in Jiangxi Province. Geoscience 16 (2), 170–176 (in Chinese with English abstract).

Zeng, J.N., Lin, W.B., Fan, Y.X., 2002b. A study of metallogeno-geochemical characteristics of Jinshan gold deposit, Jiangxi Province. Geol. Geochem. 30 (4), 26–33 (in Chinese with English abstract).

Zhai, M.G., Yang, J.H., Liu, W.J., 2001. Large clusters of gold deposits and large-scale metallogenesis in the Jiaodong Peninsula, Eastern China. Sci. China (Series D) 44 (8), 758–768.

Zhai, W., Sun, X.M., Sun, W.D., Su, L.W., He, X.P., Wu, Y.L., 2009. Geology, geochemistry, and genesis of Axi: A Paleozoic low-sulfidation type epithermal gold deposit in Xinjiang, China. Ore Geol. Rev. 36, 265–281.

Zhang, L.G., 1985. Stable isotopic geology of W-Sb-Au ore deposits developed along the Xuefeng uplift in western Hunan. Geol. Explor. 21, 24–28 (in Chinese).

Zhang, H.X., 1991. The gold concentration zone in Guangxi and the distribution feature of its major lode gold deposits. Gold 12 (6), 4–9 (in Chinese with English abstract).

Zhang, H., 2015. Chronology and Structural Properties of Late Precambrian Stratigraphic in the Southern Margin of the eastern Jiangnan Orogenic Belt (A Dissertation Submitted to Chinese Academy of Geological Sciences for Doctoral Degree), pp. 1–117 (in Chinese with English abstract).

Zhang, J.R., Luo, X.L., 1989. Metallogenetic epochs of endogenic gold deposits in south china. J. Guilin Coll. Geol. 9 (4), 369–379 (in Chinese with English abstract).

Zhang, J., Yu, D.L., Li, M.Q., Zhang, X.Y., Yang, Y.J., 1997. Geochemical characteristics and metallogenesis of Moshan-Youma'ao gold mineralized zone in Tianzhu, Guizhou. Bull. Mineral. Petrol. Geochem. 16 (3), 186–190 (in Chinese with English abstract).

Zhang, J., Yu, D.L., Zhang, X.Y., Yang, Y.J., 1998. Petrological, mineralogical and geochemical study of the Moshan-Youma'ao gold mineralized zone in Guizhou Province. Geol. Prospect. 34 (2), 30–36 (in Chinese with English abstract).

Zhang, H.Y., Hou, Q.L., Cao, D.Y., 2007. Study of thrust and nappe tectonics in the eastern Jiaodong Peninsula, China. Sci. China Earth Sci. 50 (2), 161–171.

Zhang, C.H., Li, C.M., Deng, H.L., Liu, Y., Liu, L., Wei, B., Li, H.B., Liu, Z., 2011. Mesozoic contraction deformation in the Yanshan and northern Taihang mountains and its implications to the destruction of the North China Craton. Sci. China Earth Sci. 54 (6), 798–822.

Zhang, B.L., Zhu, G., Jiang, D.Z., Li, C.C., Chen, Y., 2012. Evolution of the Yiwulushan metamorphic core complex from distributed to localized deformation and its tectonic implications. Tectonics 31. TC4018.

Zhang, L.S., Peng, J.T., Hu, A.X., Lin, F.M., Zhang, T., 2014. Re-Os dating of molybdenite from Darongxi tungsten deposit in Western Hunan and its geological implications. Mineral Deposits 33 (1), 181–189 (in Chinese with English abstract).

Zhang, C.Y., Xing, C., Chen, C.J., 2015. Metallogenic model and prospecting potential of gold deposits in southeastern Guizhou Province. Geol. Explor. 51 (4), 690–698 (in Chinese with English abstract).

Zhao, J.G., 2001. Geological characteristics of Au-deposit and its prosecting foreground at Daping gold mine, Hongjiang. Hunan Geol. 20 (3), 171–176 (in Chinese with English abstract).

Zhao, G.C., 2015. Jiangnan Orogen in South China: developing from divergent double subduction. Gondwana Res. 27, 1173–1180.

Zhao, G.C., Cawood, P.A., 2012. Precambrian geology of China. Precambr. Res. 222–223, 13–54.
Zhao, Z.H., Tu, G.Z., 2003. The Superlarge Ore Deposits in China. Science Publishing House, Beijing, pp. 1–619 (in Chinese).
Zhao, C., Ni, P., Wang, G.G., Ding, J.Y., Chen, H., Zhao, K.D., Cai, Y.T., Xu, Y.F., 2013a. Geology, fluid inclusion, and isotope constraints on ore genesis of the Neoproterozoic Jinshan orogenic gold deposit, South China. Geofluids 13, 506–527.
Zhao, J.H., Zhou, M.F., Zheng, J.P., 2013b. Constraints from zircon U-Pb ages, O and Hf isotopic compositions on the origin of Neoproterozoic peraluminous granitoids from the Jiangnan Fold Belt, South China. Contrib. Miner. Petrol. 166, 1505–1519.
Zheng, J.J., Jia, B.H., Liu, Y.R., Cao, J.H., 2001. Age, magma source and formation environment of mafic-ultramafic rocks in the Anjiang area, western Hunan. Reg. Geol. China 20 (2), 164–169 (in Chinese with English abstract).
Zheng, Y.F., Zhang, S.B., Zhao, Z.F., Wu, Y.B., Li, X., Li, Z., Wu, F.Y., 2007. Contrasting zircon Hf and O isotopes in the two episodes of Neoproterozoic granitoids in South China: implications for growth and reworking of continental crust. Lithos 96, 127–150.
Zheng, Y.F., Wu, R.X., Wu, Y.B., Zhang, S.B., Yuan, H., Wu, F.Y., 2008. Rift melting of juvenile arc-derived crust: geochemical evidence from Neoproterozoic volcanic and granitic rocks in the Jiangnan Orogen, South China. Precambr. Res. 163, 351–383.
Zhou, X.M., Li, W.X., 2000. Origin of Late Mesozoic igneous rocks in Southeastern China: implications for lithosphere subduction and underplating of mafic magmas. Tectonophysics 326, 269–287.
Zhou, D.Z., Ye, D.Y., Yu, D.L., 1989. A preliminary discussion on the genesis of the Mobin quartz vein-type gold deposit in Hunan Province. Mineral Deposits 8 (1), 51–64 (in Chinese with English abstract).
Zhou, X.H., Chen, H., Chen, H.H., 1992. Sm-Nd dating of mafic-ultramafic rocks from Qiyang area, western Hunan. Sci. Geol. Sin. 4, 391–393 (in Chinese with English abstract).
Zhou, M.F., Yan, D., Kennedy, A.K., Li, Y., Ding, J., 2002. SHRIMP U-Pb zircon geochronological and geochemical evidence for Neoproterozoic arc-magmatism along the western margin of the Yangtze Block, South China. Earth Planet. Sci. Lett. 196, 51–67.
Zhou, X., Sun, T., Shen, W., Shu, L., Niu, Y., 2006. Petrogenesis of Mesozoic granitoids and volcanic rocks in South China: a response to tectonic evolution. Episodes 29, 26–33.
Zhou, J.C., Wang, X.L., Qiu, J.S., 2009. Geochronology of Neoproterozoic mafic rocks and sandstones from northeastern Guizhou, South China: coeval arc magmatism and sedimentation. Precambr. Res. 170, 27–42.
Zhou, Q., Jiang, Y.H., Peng, Z., Liao, S.Y., 2012a. Origin of the Dexing Cu-bearing porphyries, SE China: elemental and Sr-Nd-Pb-Hf isotopic constraints. Int. Geol. Rev. 54, 572–592.
Zhou, Q., Jiang, Y.H., Liao, S.Y., Zhao, P., Jin, G.D., Jia, R.Y., Liu, Z., Xu, S.M., 2012b. SHRIMP zircon U-Pb dating and Hf isotope studies of the diorite porphyrite from the Dexing copper deposit. Acta Geol. Sin. 86 (11), 1726–1734 (in Chinese with English abstract).
Zhou, Q., Jiang, Y.H., Zhang, H.H., Liao, S.Y., Jin, G.D., Zhao, P., Jia, R.Y., Liu, Z., 2013. Mantle origin of the Dexing porphyry copper deposit, SE China. Int. Geol. Rev. 55, 337–349.
Zhou, J., Jiang, Y.H., Ge, W.Y., 2014. High Sr/Y Jingde plution in the eastern Jiangnan Orogen, South China: formation mechanism and tectonic implications. Acta Geol. Sinica 88 (1), 53–62 (in Chinese with English abstract).
Zhou, J., Ge, W.Y., Jiang, Y.H., 2015. Geochemical characteristic of tungsten-bearing pluton in the eastern Jiangnan orogen. Contrib. Geol. Mineral Resour. Res. 30 (2), 157–166 (in Chinese with English abstract).
Zhu, K.J., Fan, H.R., 1991. Geological and geochemical evidences for stratabound genesis of Jinshan gold deposit in Jiangxi Province. Geol. Explor. Forum 6 (4), 18–27 (in Chinese with English abstract).
Zhu, Y.N., Peng, J.T., 2015. Infrared microthermometric and noble gas isotope study of fluid inclusions in ore minerals at the Woxi orogenic Au-Sb-W deposit, western Hunan, South China. Ore Geol. Rev. 65, 55–69.
Zhu, X., Huang, C.K., Rui, Z.Y., 1983. Dexing Porphyry Copper Deposit. Geology Publishing House, Beijing, pp. 1–336 (in Chinese).
Zhu, J.C., Chen, J., Wang, R.C., Lu, J.J., Xie, L., 2008. Early Yanshanian NE trending Sn/W-bearing A-type granites in the western-middle part of the Nanling Mts Region. Geol. J. China Univ. 14 (4), 474–484 (in Chinese with English abstract).
Zhu, R.X., Xu, Y.G., Zhu, G., Zhang, H.F., Xia, Q.K., Zheng, T.Y., 2012. Destruction of the North China Craton. Sci. China Earth Sci. 55, 1565–1587.
Zhu, K.Y., Li, Z.X., Xu, X.S., Wilde, S.A., 2014. A Mesozoic Andean-type orogenic cycle in southeastern China as recorded by granitoid evolution. Am. J. Sci. 314, 187–234.
Zhu, R.X., Fan, H.R., Li, J.W., Meng, Q.R., Li, S.R., Zeng, Q.D., 2015. Decratonic gold deposits. Sci. China Earth Sci. 58 (9), 1523–1537.